Mon. Not. R. Astron. Soc. **393,** 911–948 (2009) doi:10.1111/j.1365-2966.2008.14156.x

Is H_3^+ cooling ever important in primordial gas?

S. C. O. Glover[1,2⋆] and D. W. Savin[3]

[1]*Astrophysikalisches Institut Potsdam, An der Sternwarte 16, D-14482 Potsdam, Germany*
[2]*Institut für Theoretische Astrophysik, Albert-Ueberle-Str. 2, 69120 Heidelberg, Germany*
[3]*Columbia Astrophysics Laboratory, Columbia University, 550 West 120th Street, New York, NY 10027-6601, USA*

Accepted 2008 October 23. Received 2008 September 3

ABSTRACT

Studies of the formation of metal-free Population III stars usually focus primarily on the role played by H_2 cooling, on account of its large chemical abundance relative to other possible molecular or ionic coolants. However, while H_2 is generally the most important coolant at low gas densities, it is not an effective coolant at high gas densities, owing to the low critical density at which it reaches local thermodynamic equilibrium (LTE) and to the large opacities that develop in its emission lines. It is therefore possible that emission from other chemical species may play an important role in cooling high-density primordial gas.

A particularly interesting candidate is the H_3^+ molecular ion. This ion has an LTE cooling rate that is roughly a billion times larger than that of H_2, and unlike other primordial molecular ions such as H_2^+ or HeH^+, it is not easily removed from the gas by collisions with H or H_2. It is already known to be an important coolant in at least one astrophysical context – the upper atmospheres of gas giants – but its role in the cooling of primordial gas has received little previous study.

In this paper, we investigate the potential importance of H_3^+ cooling in primordial gas using a newly developed H_3^+ cooling function and the most detailed model of primordial chemistry published to date. We show that although H_3^+ is, in most circumstances, the third most important coolant in dense primordial gas (after H_2 and HD), it is nevertheless unimportant, as it contributes no more than a few per cent of the total cooling. We also show that in gas irradiated by a sufficiently strong flux of cosmic rays or X-rays, H_3^+ can become the dominant coolant in the gas, although the size of the flux required renders this scenario unlikely to occur.

Key words: astrochemistry – molecular data – molecular processes – stars: formation – cosmology: theory.

1 INTRODUCTION

Over the past decade, we have made substantial progress in understanding how the very first stars in the Universe formed. We know that in cosmological models based on cold dark matter (CDM), the first stars will form in small protogalaxies, with total masses of the order of 10^5–10^6 $M_\odot$, and that by a redshift $z \sim 30$ we expect to find at least one such star-forming system per comoving Mpc^3 (Yoshida et al. 2003). We also know that although molecular hydrogen formation is inefficient, owing to the absence of dust, it is nevertheless the most abundant molecule in primordial gas, and is the main source of cooling at low densities, for temperatures between ∼200 and 8000 K.

Furthermore, simple semi-analytical estimates (e.g. Tegmark et al. 1997), later confirmed by detailed simulations (e.g. Yoshida et al. 2003), demonstrate that H_2 provides enough cooling in these small protogalaxies to allow the gas to collapse under the influence of gravity on a time-scale comparable to its gravitational free-fall time-scale, thereby allowing star formation to occur. High-resolution, adaptive mesh simulations performed by Abel, Bryan & Norman (2000, 2002) have taught us much about the dynamics of the gas in these first protogalaxies. They consider gas cooled only by H_2, and find that gravitational fragmentation of the collapsing gas is inefficient and that therefore only a single, massive star will form during the collapse. This will then suppress further star formation through a variety of feedbacks (see the recent review by Ciardi & Ferrara 2005). Other simulations, making simplifying assumptions such as the adoption of spherical symmetry, have allowed us to examine the importance of various aspects of the physics of the gas which are currently difficult to treat in the high-resolution adaptive mesh simulations (e.g. the development of large optical depths in the rotational and vibrational lines of H_2 at high densities; see e.g. Omukai & Nishi 1998; Ripamonti et al. 2002).

Much of the theoretical uncertainty that remains concerns the behaviour of dense gas during the later stages of gravitational

⋆E-mail: sglover@ita.uni-heidelberg.de

collapse, and during the period of accretion that follows the formation of the first protostar. There is much that is still unknown here – for instance, a complete understanding of the mechanism by which the collapsing gas loses much of its initial angular momentum still eludes us – but in this paper we intend to focus on one relatively simple aspect: the identification of the dominant coolant(s) in the dense gas.

As previously noted, H_2 cooling has long been known to dominate at low densities, and it is frequently assumed that it also dominates at high densities. However, it is not at all obvious that this is actually the case. Two factors dramatically reduce the effectiveness of H_2 as a coolant in high-density gas. The first is the fact that the excited rotational and vibrational levels of H_2 have small radiative transition probabilities, and hence long radiative lifetimes ($\tau \gtrsim 10^6$ s; Wolniewicz, Simbotin & Dalgarno 1998). This means that collisional de-excitation of excited H_2 becomes competitive with radiative de-excitation at fairly low gas densities ($n \sim 10^4$ cm^{-3}), and so as the number density n increases, the cooling rate of H_2 quickly reaches its local thermodynamic equilibrium (LTE) value, given by

$$\Lambda_{\rm H_2,LTE} = \sum_{i,j>i} A_{\rm ji} E_{\rm ji} n_j, \quad (1)$$

where $A_{\rm ji}$ is the transition probability for a transition from $j \rightarrow$ i, $E_{\rm ji}$ is the energy of this transition, n_j is the number density of H_2 molecules in level j, computed assuming LTE, and where we sum over all bound levels i and over all bound levels j with energies greater than i. In the LTE limit, the cooling rate per H_2 molecule is independent of the gas density, and is largely determined by the size of the transition probabilities. Since these are small, the LTE cooling rate is also small. Consequently, at high gas densities, a molecular species whose excited states have much shorter radiative lifetimes than those of H_2 will provide far more cooling *per molecule* than H_2.

The second factor reducing the effectiveness of H_2 cooling at very large n is the fact that the gas eventually becomes optically thick in the cores of the main ro-vibrational lines of H_2. The effects of this cannot currently be treated fully in three-dimensional simulations, due to the high computational cost of solving the resulting radiative transfer problem, but it has been modelled accurately in simple spherically symmetric, one-dimensional simulations (Omukai & Nishi 1998; Ripamonti et al. 2002; Ripamonti & Abel 2004) and in an approximate fashion in three dimensions (Yoshida et al. 2006). These studies confirm that at densities $n \gtrsim 10^{10}$ cm^{-3}, optical depth effects significantly suppress H_2 cooling.

Together, these factors combine to render H_2 a fairly ineffective coolant in high-density gas, despite the fact that at $n > 10^{10}$ cm^{-3}, several three-body H_2 formation reactions:

$$\rm H + H + H \rightarrow H_2 + H, \quad (2)$$

$$\rm H + H + He \rightarrow H_2 + He, \quad (3)$$

$$\rm H + H + H_2 \rightarrow H_2 + H_2, \quad (4)$$

rapidly convert almost all of the hydrogen in the gas to H_2 (Palla, Salpeter & Stahler 1983). It is therefore reasonable to ask whether cooling from any of the other molecular species present in the gas will become competitive with H_2 cooling at these densities.

One obvious possibility is deuterated hydrogen, HD. Its excited rotational and vibrational levels have radiative lifetimes that are about a factor of 100 shorter than those of H_2, and so the HD cooling rate does not reach its LTE limit until $n \sim 10^6$ cm^{-3}. It is also a far more effective coolant than H_2 at low temperatures ($T \lesssim 200$ K; see e.g. Flower et al. 2000). This is due primarily to the fact that radiative transitions can occur between rotational levels with odd and even values of J, allowing cooling to occur through the $J = 1 \rightarrow 0$ transition. The corresponding odd $\rightarrow$ even transitions in the case of H_2 represent conversions from ortho-H_2 to para-H_2 or vice versa, and are highly forbidden. Furthermore, at low temperatures the ratio of HD to H_2 can be significantly enhanced with respect to the cosmological D:H ratio by chemical fractionation (see e.g. Glover 2008).

The role of HD cooling in early protogalaxies has been investigated by a number of authors. In the case of the earliest generation of protogalaxies, which form from very cold neutral gas that is never heated to more than a few thousand kelvin during the course of the galaxy formation process, HD cooling appears to be unimportant, as the collapsed gas does not become cold enough for sufficient fractionation to occur to make HD cooling dominant (Bromm, Coppi & Larson 2002).

The situation is rather different, however, in primordial gas cooling from an initially ionized state. In that case more H_2 is formed, allowing the gas to cool to a lower temperature, at which point fractionation becomes effective and HD cooling rapidly becomes dominant (see e.g. Nakamura & Umemura 2002; Nagakura & Omukai 2005; Johnson & Bromm 2006; Shchekinov & Vasiliev 2006). However, the initial ionization required is much larger than that expected to be present in the earliest protogalaxies.

Another molecule to have attracted considerable attention is lithium hydride, LiH. This molecule has a very large dipole moment, $\mu = 5.888$ debyes (Zemke & Stwalley 1980), and consequently its excited levels have very short radiative lifetimes. Therefore, despite the very low lithium abundance in primordial gas ($x_{\rm Li} = 4.3 \times 10^{-10}$, by number; see Cyburt 2004), it was thought for a time that LiH would dominate the cooling at very high densities (see e.g. Lepp & Shull 1984). However, accurate quantal calculations of the rate of formation of LiH by radiative association (Dalgarno, Kirby & Stancil 1996; Gianturco & Gori Giorgi 1996; Bennett et al. 2003),

$$\rm Li + H \rightarrow LiH + \gamma, \quad (5)$$

have shown that the rate is much smaller than was initially assumed, while recent work by Defazio et al. (2005) has shown that the reaction,

$$\rm LiH + H \rightarrow Li + H_2, \quad (6)$$

has no activation energy and so will be an efficient destruction mechanism for LiH for as long as some atomic hydrogen remains in the gas. Consequently, the amount of lithium hydride present in the gas is predicted to be very small, even at very high densities, and so LiH cooling is no longer believed to be important (Mizusawa, Omukai & Nishi 2005).

In contrast to HD or LiH, the various molecular ions present in the gas, such as H_2^+, H_3^+ or HeH^+, have attracted little attention. Some early work on H_2^+ cooling in ionized primordial gas can be found in Suchkov & Shchekinov (1977, 1978), and its possible importance in hot, highly ionized conditions has recently been re-emphasized by Yoshida et al. (2007), but aside from this, there has been little exploration of the role that cooling from these species might play in the evolution of primordial gas, presumably because the abundances of these species are expected to be small. It is this absence that this paper attempts to rectify.

We present here the results of a set of simulations of the chemical and thermal evolution of gravitationally collapsing primordial gas. These simulations use a very simple one-zone dynamical model for the gas, but couple this with a detailed chemical network and a

comprehensive model of the various heating and cooling processes at work. Besides the coolants considered above, we include the effects of cooling from (in no particular order) H_2^+, HD^+, D_2^+, H_3^+, H_2D^+, HD_2^+, D_3^+, HeH^+, HeD^+, He_2^+, LiH^+, LiD^+, LiD and LiH_2^+. We focus in particular on the possible role of H_3^+. This ion has a very large number of excited rotational and vibrational levels that are energetically accessible at the temperatures of interest in primordial gas, and its vibrational levels have much shorter radiative lifetimes than those of H_2 or HD. In LTE, its cooling rate per molecule is roughly 10^9 times larger than that of H_2. It is known to be an important coolant in planetary atmospheres (Miller et al. 2000) and may also be an effective coolant in high-density primordial gas (Glover & Savin 2006). Unlike ions such as H_2^+ or HeH^+, it does not react with H_2, and is not easily destroyed by collisions with H, and so its abundance in high-density gas should be large compared to the other molecular ions included in our model.

The layout of this paper is as follows. In Section 2 we outline the numerical method used to simulate the thermal and chemical evolution of the protostellar gas. The chemical reactions included in the model are discussed in Section 3, and the thermal processes, in particular H_3^+ cooling, are discussed in Section 4. We present the results of our simulations in Section 5 and close with a brief discussion in Section 6.

2 NUMERICAL METHOD

We treat the thermal and chemical evolution of the gas using a one-zone model, in which the density is assumed to evolve as

$$\frac{\mathrm{d}\rho}{\mathrm{d}t} = \eta \frac{\rho}{t_{\rm ff}}, \tag{7}$$

where $t_{\rm ff} = \sqrt{3\pi/32G\rho}$ is the free-fall time-scale of the gas and where η is an adjustable constant. In most of our simulations, we set $\eta = 1$, corresponding to free-fall collapse, but in a few runs we examine the effect of slowing down the collapse by setting $\eta < 1$ (see Section 5.7 for details).

To follow the temperature evolution, we solve the energy equation

$$\frac{\mathrm{d}e}{\mathrm{d}t} = \frac{p}{\rho^2}\frac{\mathrm{d}\rho}{\mathrm{d}t} - \Lambda + \Gamma, \tag{8}$$

where e is the internal energy density, p is the thermal pressure, Λ is the total cooling rate (which includes contributions from both radiative and chemical cooling, as outlined in Section 4) and Γ is the total heating rate. Since the temperature evolution is strongly coupled to the chemical evolution, we solve equation (8) simultaneously with the chemical rate equations using the DVODE implicit ordinary differential equation solver (Brown, Byrne & Hindmarsh 1989). To model the chemistry we use an extensive chemical network consisting of 392 reactions among 30 atomic and molecular species. Table 1 lists all 30 species considered. Tables A1–A14 in Appendix A list the reactions included in this network, broken down by the type of process involved. These tables also give details of the rate coefficient or rate adopted for each reaction and the source of the data. In these tables and elsewhere in the paper, T is the gas temperature in K, $T_3 = T/1000\,\mathrm{K}$, and $T_{\rm e}$ is the temperature in units of eV. (Note that we assume, both here and throughout, that the kinetic temperature of the electrons is the same as that of the atoms and molecules.)

For many of these species, we followed the full time-dependent, non-equilibrium chemistry, but in some cases – the ions H^-, D^-, Li^-, H_2^+, HD^+, D_2^+, HeH^+, HeD^+, He_2^+, LiD^+ and LiH_2^+ – chemical equilibrium is reached very rapidly, on a time-scale of the order of $t_{\rm eq} = 1/(k_{\rm dest}n) \sim 10^9\, n^{-1}$ s, where $k_{\rm dest} \sim 10^{-9}\,\mathrm{cm^3\,s^{-1}}$ is a characteristic destruction rate coefficient and n is the number density of hydrogen nuclei. At the gas densities considered in this paper ($1 < n < 3 \times 10^{13}\,\mathrm{cm^{-3}}$ in the majority of our simulations), this chemical equilibrium time-scale for these rapidly reacting ions is orders of magnitude smaller than the free-fall time-scale of the gas, which is approximately $1.5 \times 10^{15}\, n^{-1/2}\,\mathrm{s^{-1}}$. It is therefore sufficient to use the equilibrium abundances for these ions. Some of the species remaining in our non-equilibrium model may also be close to chemical equilibrium during a large portion of the collapse, but are included in the non-equilibrium treatment because we cannot be sure that they always remain in equilibrium. Further details of our chemical network are given in Section 3.

We assume elemental abundances relative to hydrogen of 0.083, 2.6×10^{-5} and 4.3×10^{-10} for helium, deuterium and lithium, respectively (Cyburt 2004). In Section 5.5 we explore the effects of reducing the deuterium and/or the lithium abundance to zero, in order to asses the impact of the deuterium and lithium chemistry on the evolution of the gas. The initial abundances of the various molecular and ionic species in our standard model are summarized in Table 1. The values used for the initial H^+, He^+ and H_2 abundances, and the ratio of ionized to neutral lithium are taken from the calculations of Stancil, Lepp & Dalgarno (1998) – specifically their model V. Deuterated species are assumed to have abundances that are a factor of $(2.6 \times 10^{-5})^{N_{\rm D}}$ smaller than the abundances of the undeuterated equivalents, where $N_{\rm D}$ is the number of deuterium nuclei in the species in question. The electron abundance is computed assuming charge conservation. To assess our sensitivity to these initial values, we have also run several simulations with

Table 1. Initial fractional abundances in our reference calculation.

Species	Initial abundance	Species	Initial abundance	Species	Initial abundance
e^-	2.2×10^{-4}	HD^+	–	HeD^+	–
H^+	2.2×10^{-4}	HD	6.2×10^{-11}	He_2^+	–
H	0.999 78	D_2^+	–	Li^+	2.2×10^{-10}
H^-	–	D_2	1.6×10^{-15}	Li	2.1×10^{-10}
H_2^+	–	H_2D^+	0.0	Li^-	–
H_2	2.4×10^{-6}	HD_2^+	0.0	LiH^+	0.0
H_3^+	0.0	D_3^+	0.0	LiH	0.0
D^+	5.7×10^{-9}	He^+	2.8×10^{-26}	LiD^+	–
D	2.6×10^{-5}	He	8.3×10^{-2}	LiD	0.0
D^-	–	HeH^+	–	LiH_2^+	–

Note: The quoted values are fractional abundances relative to the number density of hydrogen nuclei. Chemical species listed without initial abundances are assumed to be in chemical equilibrium, as described in the text.

different initial abundances; the results of these runs are discussed in Section 5.5.

For most simulations, we adopt an initial density $n_i = 1\,\mathrm{cm}^{-3}$ and an initial temperature $T_i = 1000\,\mathrm{K}$. The effects of altering n_i and T_i are examined in Section 5.5. All of the simulations are run until the density exceeds $n_f = 3 \times 10^{13}\,\mathrm{cm}^{-3}$. At higher densities, collision-induced emission (CIE) from H_2 quickly comes to dominate the cooling, and the minor species considered here are unlikely to be important coolants in this very high-density regime.

Finally, we ran all of our simulations starting at a redshift $z = 20$. However, the main influence of the redshift is to set a minimum temperature for the gas (since the gas cannot cool radiatively to below the cosmic microwave background (CMB) temperature, T_{CMB}). As the gas temperature $T \gg T_{\mathrm{CMB}}$ at the densities of interest in this paper, we do not anticipate that changing z by a moderate amount will significantly affect our results.

3 CHEMISTRY

The chemical evolution of the gas is modelled using a chemical network consisting of 392 reactions amongst 30 neutral and ionized species. A list of all of the reactions included can be found in Tables A1–A14. This network, which to the best of our knowledge is the largest used to date for the study of primordial gas chemistry, is based in part on previous compilations by Abel et al. (1997), Stancil et al. (1998), Galli & Palla (1998, 2002), Lepp, Stancil & Dalgarno (2002), Wang & Stancil (2002) and Walmsley, Flower & Pineau des Forêts (2004), supplemented with additional reactions drawn directly from the chemical literature, as well as some whose rates have not (to our knowledge) been previously discussed. These latter are generally rates involving one or more deuterium nuclei in place of hydrogen nuclei; and in estimating rates for these reactions, we have generally followed the same procedure as in Stancil et al. (1998): for a non-deuterated reaction with a reaction rate coefficient that has a power-law temperature dependence $k \propto T^m$, we have estimated a rate coefficient for the deuterated reaction by multiplying this rate coefficient by a scaling factor of $(\mu_{\mathrm{H}}/\mu_{\mathrm{D}})^m$, where μ_{H} and μ_{D} are the reduced masses of the reactants in the non-deuterated and deuterated reactions, respectively. Some notable exceptions to this strategy are discussed in more detail in Section 3.1 below.

For reactions where the presence of a deuteron increases the number of distinguishable outcomes and where no good information exists on the branching ratio of the reaction, we have assumed that each outcome is equally likely. An example of this is the dissociative attachment of HD with e^- (reactions AD6–AD7), which can produce either H and D^- or H^- and D, in contrast to the dissociative attachment of H_2 with e^- (reaction AD5) which can only produce H^- and H. For this particular example, this assumption gives branching ratios of 50 per cent for reactions AD6 and AD7, respectively.

In spite of the size of our chemical network, there remain a number of chemical processes that are not included. These are discussed in Section 3.4, along with our justifications for omitting them.

3.1 Discussion of selected reactions

3.1.1 Photorecombination of H and He (reactions PR1 and PR3, Table A2)

We assume that the ionizing photons produced by the recombination of H^+ to ground state H are immediately consumed by the ionization of atomic hydrogen (the on-the-spot approximation), and so we use the case B rate coefficient for hydrogen recombination (Ferland et al. 1992). We note that although the fractional abundance of atomic hydrogen becomes small at densities greater than $10^{10}\,\mathrm{cm}^{-3}$, the number density of atomic hydrogen remains considerable, and so case B remains a good approximation.

We also use the on-the-spot approximation to treat He^+ recombination, but in this case the net recombination rate is larger than the case B rate, as some of the photons produced by recombination directly into the $n = 1$ ground state are lost through photoionization of H rather than He. For He^+ recombinations directly into the ground state, occurring in primordial gas with a low fractional ionization and low molecular abundance, approximately 68 per cent of the resulting photons are absorbed by H, with the remaining 32 per cent being absorbed by He (Osterbrock 1989). Therefore, the effective He^+ recombination rate coefficient in these conditions is given by

$$k_{\mathrm{PR3}} = 0.68 k_{\mathrm{PR3,rr,A}} + 0.32 k_{\mathrm{PR3,rr,B}} + k_{\mathrm{PR3,di}}\ \mathrm{cm}^3\ \mathrm{s}^{-1}, \quad (9)$$

where $k_{\mathrm{PR3,rr,A}}$ and $k_{\mathrm{PR3,rr,B}}$ are the case A and case B rate coefficients, and $k_{\mathrm{PR3,di}}$ is the dielectronic recombination rate coefficient. This formula becomes incorrect once the H_2 fraction of the gas becomes large, but as this occurs only at densities $n \gtrsim 10^{10}\,\mathrm{cm}^{-3}$ at which the He^+ fractional abundance is negligible, the error that is introduced by using this prescription for k_{PR3} throughout the simulation is unimportant.

It is also necessary to take account of the photoionization of H caused by the He^+ recombination emission. In addition to the contribution coming from He^+ recombination into the $n = 1$ ground state, there is an additional contribution made by photons produced during transitions from $n = 2$ to $n = 1$ in He; in other words, even pure case B recombination of He^+ produces H-ionizing photons. The proportion of case B recombinations that yield photons capable of ionizing hydrogen depends upon the relative populations of the $n = 2$ singlet and triplet states, and hence upon the electron density, but in the low-density limit, 96 per cent of all recombinations to excited states produce photons that will ionize hydrogen (Osterbrock 1989). To model the effects of these photons, along with those produced by recombination direct to the $n = 1$ ground state and by dielectronic recombination, we include in our chemical network a local H ionization rate per unit volume R_{pi}, with a value

$$\begin{aligned} R_{\mathrm{pi}} &= \left[0.68(k_{\mathrm{PR3,rr,A}} - k_{\mathrm{PR3,rr,B}}) + 0.96 k_{\mathrm{PR3,rr,B}} + 2 k_{\mathrm{PR3,di}}\right] \\ &\quad \times n_{\mathrm{e}} n_{\mathrm{He^+}}\ \mathrm{cm}^{-3}\ \mathrm{s}^{-1}, \\ &= \left[0.68 k_{\mathrm{PR3,rr,A}} + 0.28 k_{\mathrm{PR3,rr,B}} + 2 k_{\mathrm{PR3,di}}\right] n_{\mathrm{e}} n_{\mathrm{He^+}}\ \mathrm{cm}^{-3}\ \mathrm{s}^{-1}, \end{aligned} \quad (10)$$

where the three terms in brackets on the first line correspond to the contributions from recombination direct to the $n = 1$ ground state, pure case B recombination (i.e. recombination to all states $n \geq 2$), and dielectronic recombination, respectively. (Note that every dielectric recombination produces two photons capable of ionizing hydrogen: one due to the radiative stabilization of the process, and one as the captured electron cascades to the 1s level.) If the electron density is large ($n_{\mathrm{e}} \gtrsim 10^3\,\mathrm{cm}^{-3}$; Clegg 1987), then more helium recombinations will result in two-photon transitions from $2^1\mathrm{S}$–$1^1\mathrm{S}$, reducing the number of photons produced that are capable of ionizing hydrogen (Osterbrock 1989). However, the effect on R_{pi} is relatively small, and in any case, we do not expect to encounter large abundances of He^+ in dense gas in the particular scenario that we are investigating. Therefore, adopting this simplified treatment at all n should be sufficient for our purposes.

3.1.2 Dissociative recombination of H_3^+ (reactions DR4 and DR5, Table A3)

For a long time, considerable disagreement has existed on the subject of the H_3^+ dissociative recombination rate. Measurements of the rate in merged beam experiments (e.g. Sundström et al. 1994) typically give values of the order of 10^{-7} cm^3 s^{-1} for the rate coefficient at temperatures near room temperature, while measurements made in flowing afterglow experiments (e.g. Smith & Španel (1993a,b)) often give values of the order of 10^{-8} cm^3 s^{-1}, an order of magnitude smaller. At the same time, most theoretical calculations have indicated a smaller rate still, of the order of 10^{-11} cm^3 s^{-1} (see Orel, Schneider & Suzor-Weiner 2000, and references therein), which is in complete disagreement with the experimental measurements.

However, it has recently become clear that three-body effects play a highly important role in the recombination of H_3^+ in flowing afterglow experiments (see e.g. Glosík et al. 2005). When proper allowance is made for these effects, the inferred two-body recombination rate is in good agreement with the results of the merged beam experiments (see the discussion in Glosík et al. 2008). Moreover, recent theoretical calculations of the rate coefficient by Kokoouline & Greene (2003) that account for the effects of Jahn–Teller coupling between the electronic and vibrational degrees of freedom produce a result that is in good agreement with the experimental measurements, although disagreement at the level of a factor of 2 or so is still present at some energies.

In our calculations, we therefore take our value for the total H_3^+ dissociative recombination rate coefficient from the recent ion storage ring measurements of McCall et al. (2004). To convert this total rate coefficient – the sum of the rate coefficients for reactions DR4 and DR5 – into a rate coefficient for each individual reaction, we adopt a branching ratio of 0.25 for reaction DR4 and 0.75 for reaction DR5, based on the measurements of Datz et al. (1995). Strictly speaking, these values are only appropriate for temperatures $T < 3000$ K, but in practice the behaviour of the gas is not particularly sensitive to the values chosen.

3.1.3 H_3^+ formation by radiative association (reaction RA18, Table A5)

The rate coefficient we quote for reaction RA18, the radiative association of H_2 and H^+ to form H_3^+, was taken from the study of Gerlich & Horning (1992), and was the rate coefficient quoted by Galli & Palla (1998) for this reaction. However, Stancil et al. (1998) prefer a much smaller rate coefficient of 10^{-20} cm^3 s^{-1} for this reaction. In Section 5.6, we examine the effect of adopting this smaller rate coefficient.

3.1.4 H_2 formation by associative detachment of H^- (reaction AD1, Table A6)

The rate of this reaction is quite uncertain, and we have shown in previous work that this uncertainty can lead in some cases to a substantial uncertainty in the amount of H_2 formed in the gas (Glover, Savin & Jappsen 2006). However, we do not expect this uncertainty to significantly affect the results in this paper. At the high densities at which H_3^+ cooling is potentially important, the dominant H_2 formation pathway is three-body formation. This can produce a much larger molecular fraction than is possible via two-body reactions, and so uncertainty in the amount of H_2 produced via the H^- ion has a negligible impact on the evolution of the gas at high densities. In our simulations, we adopt a default value for the rate coefficient for reaction AD1 of $k_{\rm AD1} = 1.5 \times 10^{-9} T_3^{-0.1}$ cm^3 s^{-1}, where $T_3 = T/300$ K, taken from Launay, Le Dourneuf & Zeippen (1991). In Section 5.6 we demonstrate that our results are insensitive to this choice.

We note also that the other reaction discussed in Glover et al. (2006), the mutual neutralization of H^- by H^+ (reaction MN1, Table A8), is no longer a source of significant uncertainty in chemical models of primordial gas. Recent measurements of the cross-section for this reaction at astrophysically relevant energies made by X. Urbain (private communication) yield values in good agreement with those obtained by Fussen & Kubach (1986) and used as a basis for the rate coefficient of Croft, Dickinson & Gadea (1999). These measurements strongly suggest that the earlier measurements of the mutual neutralization cross-section made by Moseley, Aberth & Peterson (1970) were somehow in error, and that rate coefficients based on them (see e.g. Dalgarno & Lepp 1987; Galli & Palla 1998) are incorrect. The error in the rate coefficient for this reaction has thus been reduced from the order of magnitude discussed in Glover et al. (2006) to an uncertainty of about 50 per cent (X. Urbain, private communication).

3.1.5 Collisional dissociation of H_2 (reactions CD9–CD12, Table A7)

The rate coefficients for the collisional dissociation of H_2 by H (CD9), H_2 (CD10), He (CD11) and e^- (CD12) are represented by functions of the form

$$\log k_{\rm i} = \left(\frac{n/n_{\rm cr}}{1 + n/n_{\rm cr}} \right) \log k_{\rm i,LTE} + \left(\frac{1}{1 + n/n_{\rm cr}} \right) \log k_{\rm i,v=0}, \quad (11)$$

where n is the number density of hydrogen nuclei, $k_{\rm i}$ is the collisional dissociation rate for collisions with species i, and $k_{\rm v=0,i}$ and $k_{\rm LTE,i}$ are the rate coefficients for this reaction in the limits in which all of the H_2 molecules are in the vibrational ground state (appropriate in low-density gas), or have their LTE level populations (appropriate for high-density gas). The critical density, $n_{\rm cr}$, for H_2 collisional dissociation in a gas containing a mix of H, H_2, He and electrons is not well determined. For simplicity, we therefore assume that it is given by a weighted harmonic mean of the (better known) critical densities corresponding to reactions CD9, CD10 and CD11 considered individually, i.e.

$$\frac{1}{n_{\rm cr}} = \frac{1}{1 + x_{\rm He}} \left[\frac{x_{\rm H}}{n_{\rm cr,H}} + \frac{2x_{\rm H_2}}{n_{\rm cr,H_2}} + \frac{x_{\rm He}}{n_{\rm cr,He}} \right], \quad (12)$$

where $x_{\rm H}$, $x_{\rm H_2}$ and $x_{\rm He}$ are the fractional abundances of H, H_2 and He relative to the total number of hydrogen nuclei, we use the approximation that $x_{\rm H} + 2x_{\rm H_2} = 1$, and where

$$n_{\rm cr,H} = {\rm dex}\left[3.0 - 0.416 \log T_4 - 0.327 (\log T_4)^2\right] \ {\rm cm}^{-3}, \quad (13)$$

$$n_{\rm cr,H_2} = {\rm dex}\left[4.845 - 1.3 \log T_4 + 1.62 (\log T_4)^2\right] \ {\rm cm}^{-3}, \quad (14)$$

$$n_{\rm cr,He} = {\rm dex}\left[5.0792 \left\{1.0 - 1.23 \times 10^{-5} (T - 2000)\right\}\right] \ {\rm cm}^{-3}, \quad (15)$$

with $T_4 = T/10\,000$ K. The expression for $n_{\rm cr,H}$ is from Lepp & Shull (1983), but has been decreased by an order of magnitude, as recommended by Martin, Schwarz & Mandy (1996). The expression for $n_{\rm cr,H_2}$ comes from Shapiro & Kang (1987), and the expression for $n_{\rm cr,He}$ comes from Dove et al. (1987). Note that this expression for the critical density assumes that in high-density gas, $n_{\rm e} \ll n_{\rm H}$, so that electron excitation of H_2 does not significantly affect the value of $n_{\rm cr}$. Other forms of averaging to obtain $n_{\rm cr}$ are

possible, of course, but we would not expect our results to be sensitive to our particular choice here, as any differences will only be seen for densities $n \sim n_{\rm cr}$, and in our simulations, gas at these densities is always far too cold for collisional dissociation of H_2 to be important.

To ensure that our adopted collisional dissociation rate coefficients and three-body H_2 formation rate coefficients are consistent, we used the fact that in LTE, the equilibrium constant K obeys

$$K = k_{\rm TB1}/k_{\rm CD9} = k_{\rm TB2}/k_{\rm CD10} = k_{\rm TB3}/k_{\rm CD11} \quad (16)$$

and varies with temperature as (Flower & Harris 2007)

$$K = 1.05 \times 10^{-22} T^{-0.515} \exp\left(\frac{52\,000}{T}\right), \quad (17)$$

to determine values for the rate coefficients of reactions CD9, CD10 and CD11 in the LTE limit. However, we also ran some test simulations where we used rate coefficients from Lepp & Shull (1983) and Shapiro & Kang (1987) for reactions CD9 and CD10, regardless of the value of $k_{\rm TB1}$ or $k_{\rm TB2}$. These simulations produced almost identical results, demonstrating that our results here are insensitive to our treatment of H_2 collisional dissociation.

3.1.6 Collisional dissociation of HD and D_2 (reactions CD13–CD20, Table A7)

For collisions with electrons, accurate rate coefficients are available from Trevisan & Tennyson (2002a) and Trevisan & Tennyson (2002b). For collisions with H, H_2, or He, however, we are unaware of a treatment in the literature. We have therefore assumed that the rate coefficients of these reactions in the $v = 0$ and LTE limits are the same as for the corresponding H reactions (CD9)–(CD11). For D_2, we have also adopted the same value for the critical density, while for HD, we have increased it by a factor of 100 to account for the larger radiative transition probabilities. Note that although these rate coefficients are highly approximate, this probably does not introduce much uncertainty into the chemical model, as reactions IX18 and IX20 (Table A10) become effective at much lower temperatures and therefore dominate the destruction of HD and D_2 in warm gas.

3.1.7 Three-body H_2 formation (reactions TB1–TB3, Table A9)

Although unimportant at low densities, three-body reactions are the dominant source of H_2 in high-density primordial gas, and so these reactions represent an important part of our chemical network. Unfortunately, rate coefficients for these reactions are, in general, not known to a high degree of accuracy. For three-body collisions in which atomic hydrogen is the third body (reaction TB1), the situation is particularly bad. One commonly adopted rate coefficient is that of Palla et al. (1983), who quote a rate coefficient

$$k_{\rm TB1,PSS} = 5.5 \times 10^{-29} T^{-1} \ {\rm cm^6 \ s^{-1}} \quad (18)$$

for this reaction, based on experimental work by Jacobs, Giedt & Cohen (1967). Also in common usage is the rate coefficient adopted by Abel et al. (2002), which is

$$\begin{aligned} k_{\rm TB1,ABN} &= 1.14 \times 10^{-31} T^{-0.38} \ {\rm cm^6 \ s^{-1}} \quad T \leq 300 \ {\rm K} \\ &= 3.90 \times 10^{-30} T^{-1.00} \ {\rm cm^6 \ s^{-1}} \quad T > 300 \ {\rm K}. \end{aligned} \quad (19)$$

The low-temperature portion of this rate coefficient is based on Orel (1987), while the high-temperature portion is an extrapolation by Abel et al. (2002). This reaction is also discussed by Cohen & Westberg (1983) in their large compilation and review of chemical kinetic data. They summarize a large number of different experimental measurements and argue that the precision of the data does not justify anything more elaborate than a constant rate coefficient

$$k_{\rm TB1,CW} = 8.8 \times 10^{-33} \ {\rm cm^6 \ s^{-1}}. \quad (20)$$

Another possibility is found in Schwenke (1990), who gives calculated values at $T = 3000$ K and $T = 5000$ K of 1.4×10^{-32} cm^6 s^{-1} and 8.2×10^{-33} cm^6 s^{-1}, respectively. These values are roughly an order of magnitude larger than those given by the Abel et al. (2002) rate coefficient, and about 30 per cent lower than the values given by the Palla et al. (1983) rate coefficient.

More recently, Flower & Harris (2007) have argued in favour of a rate coefficient

$$k_{\rm TB1,FH} = 1.44 \times 10^{-26} T^{-1.54} \ {\rm cm^6 \ s^{-1}}, \quad (21)$$

which they derived from the rate coefficient of the inverse process (H_2 collisional dissociation by atomic hydrogen, reaction CD9) by using the principle of detailed balance. This rate coefficient is approximately six times larger than the Palla et al. (1983) rate coefficient at $T = 1000$ K, or approximately 90 times larger than the Abel et al. (2002) rate coefficient. Unfortunately, the accuracy of a rate coefficient derived using detailed balance depends upon the accuracy with which the rate coefficient of the inverse process is known. In this case, that accuracy is poor, as the H_2 collisional dissociation rate coefficient is not well constrained by experiment at low temperatures (i.e. $T < 2000$ K) owing to its small size at these temperatures. Flower & Harris (2007) used the Jacobs et al. (1967) fit to the collisional dissociation rate coefficient, but if we instead use the calculated rate coefficient from Martin et al. (1996), then a much smaller three-body H_2 formation rate coefficient is obtained, which can be fitted to within ∼20 per cent by (Glover 2008)

$$k_{\rm TB1,GL} = 7.7 \times 10^{-31} T^{-0.464} \ {\rm cm^6 \ s^{-1}}. \quad (22)$$

There is thus an uncertainty of almost two orders of magnitude in the rate coefficient for reaction TB1. In our simulations, we adopt the Abel et al. (2002) rate coefficient as our default value, but in Section 5.6 we examine the effect of using a different rate coefficient.

The rate coefficient for three-body H_2 formation in collisions where H_2 is the third body (reaction TB2) is known with greater precision, but nevertheless substantial uncertainty remains. Palla et al. (1983) quote a rate coefficient

$$k_{\rm TB2,PSS} = 6.9 \times 10^{-30} T^{-1.0} \ {\rm cm^6 \ s^{-1}} \quad (23)$$

for this reaction, again taken from Jacobs et al. (1967), while Cohen & Westberg (1983) recommend instead

$$k_{\rm TB2,CW} = 2.8 \times 10^{-31} T^{-0.6} \ {\rm cm^6 \ s^{-1}}. \quad (24)$$

Flower & Harris (2007) assume that the ratio of $k_{\rm TB2}$ to $k_{\rm TB1}$ is the same as that measured by Jacobs et al. (1967), i.e. one-eighth. Therefore, their rate coefficient for reaction TB2 is

$$k_{\rm TB2,FH} = 1.8 \times 10^{-27} T^{-1.54} \ {\rm cm^6 \ s^{-1}}. \quad (25)$$

The same assumption applied to the rate coefficient from Glover (2008) gives

$$k_{\rm TB2,GL} = 9.625 \times 10^{-32} T^{-0.464} \ {\rm cm^6 \ s^{-1}}. \quad (26)$$

Finally, calculations by Schwenke (1988) using orbital resonance theory find a rate coefficient that is about a factor of 2 lower than the Cohen & Westberg (1983) values, but Schwenke (1990) shows that one of the assumptions underlying his own orbital resonance

calculations is invalid, and provides revised values, obtained from a master equation approach, that agree well with the Cohen & Westberg (1983) recommendation.

These rate coefficients agree to within a factor of a few at $T = 3000$ K, consistent with the scatter in experimental determinations of the rate coefficient at this temperature (Cohen & Westberg 1983), but differ more by more than an order of magnitude at low temperatures. In our simulations, we use the Palla et al. (1983) rate coefficient as our default value, but we examine in Section 5.6 the effect of altering $k_{\rm TB2}$.

We also included three-body formation of H_2 via collisions with He (reaction TB3), using a rate coefficient from Walkauskas & Kaufman (1975). This reaction has not been included in previous treatments of the evolution of dense primordial gas and so we wished to assess its effects. We found that reaction TB3 could be responsible for anywhere between 0.1 and 10 per cent of the total three-body H_2 formation rate, depending on the temperature, the H_2 abundance and the choice of rate coefficients for reactions TB1 and TB2. Moreover, this estimate does not take into account the uncertainty in the rate of reaction TB3, which we have been unable to quantify, but which should probably be assumed to be comparable to the uncertainty in the other three-body rates. Thus, although it probably never dominates, reaction TB3 should be included if accurate modelling of H_2 formation in dense gas is desired.

3.1.8 Deuterated three-body reactions (TB4–TB9, TB11–TB13, TB17–TB31 and TB34–TB35, Table A9)

In view of the large uncertainties present in the rate coefficients of many of the three-body reaction rates (particularly for reactions TB1 and TB2, as discussed above), we consider that the most prudent course of action when estimating rates for the deuterated forms of these reactions is simply to adopt the same values as for the non-deuterated reactions. Any uncertainty introduced by this assumption is likely dwarfed by the uncertainties arising from our poor knowledge of the non-deuterated reaction rates. We note that Flower & Harris (2007) follow a similar course of action in their study of three-body H_2 and HD formation in primordial gas.

3.1.9 Destruction of D_2 by collision with H (reaction IX20, Table A10)

Our fit to the data collated by Mielke et al. (2003) for this reaction is accurate to within a few per cent over the temperature range of the tabulated data, $200 \leq T \leq 2200$ K. Outside of this range, our fit may be significantly inaccurate (although at low temperatures, the reaction rate is small enough that any inaccuracy is unlikely to be important).

3.1.10 Photodissociation of H_2 and HD (reactions BP7 and BP8, Table A12)

Table A12 lists the rates of these reactions in optically thin gas, given our assumed incident ultraviolet (UV) spectrum (see Section 3.2). In optically thick gas, however, self-shielding of H_2 by H_2 and HD by HD can significantly reduce both of these rates, by factors $f_{\rm sh,H_2}$ and $f_{\rm sh,HD}$, respectively. In static, isothermal gas, these self-shielding factors can be calculated approximately using the prescription of Draine & Bertoldi (1996) together with an appropriate set of molecular data, provided that one knows the H_2 and HD column densities. In gas which is in motion, with internal velocities comparable to or larger than the thermal velocity of the gas, the Draine & Bertoldi (1996) treatment breaks down, and one must use approaches that are either less accurate or more computationally expensive, as discussed in Glover & Jappsen (2007). However, in the one-zone calculations presented here, we know neither the H_2 and HD column densities, nor the velocity structure of the gas, and so including even a highly approximate treatment of the effects of self-shielding is problematic. In our runs with a non-zero UV background, we therefore consider two limiting cases: one in which self-shielding is highly efficient and $f_{\rm sh,H_2} = f_{\rm sh,HD} = 0$ throughout the run, and one in which it is ineffective, and we remain in the optically thin limit throughout (i.e. $f_{\rm sh,H_2} = f_{\rm sh,HD} = 1$). These two limiting cases bracket the true behaviour of the gas.

3.1.11 Formation and destruction of LiH_2^+ (reactions RA20, DR19, DR20, DR21 and CD26)

To date, the LiH_2^+ ion has attracted little attention in the astrochemical literature. Kirby & Dalgarno (1978) considered the reaction chain

$$\mathrm{Li^+ + H_2 \rightarrow LiH_2^+ + \gamma}, \tag{27}$$

$$\mathrm{LiH_2^+ + e^- \rightarrow LiH + H} \tag{28}$$

(reactions RA20 and DR20 in our chemical model) as a possible source of LiH in the interstellar medium (ISM), but showed that even if the rate coefficient for the radiative association were assumed to be very large ($k_{\rm RA20} \sim 10^{-16}\,{\rm cm^3\,s^{-1}}$), the resulting LiH abundance would be far too small to be observable. More recently, Stancil, Lepp & Dalgarno (1996) considered the LiH_2^+ ion in their comprehensive study of the lithium chemistry of the primordial intergalactic medium, but again reached the conclusion that its abundance would be very small, and so chose not to include it in their chemical model. However, to the best of our knowledge, there has been no previous investigation of the role that this ion may play in regulating the fractional ionization of very dense primordial gas.

Previous work focusing on modelling the fractional ionization at high densities (Maki & Susa 2004, 2007), in the context of the study of ambipolar diffusion in dense Population III pre-stellar cores, has shown that once the free electron fraction falls below $x \sim 10^{-10}$, ionized lithium takes over from ionized hydrogen as the primary positive ion in the gas. It is therefore important to ensure that all of the major loss routes for Li^+ are represented in the chemical model. In addition to photorecombination (reaction PR4), Li^+ can be removed from the gas by a number of reactions with atomic or molecular hydrogen:

$$\mathrm{Li^+ + H \rightarrow Li + H^+}, \tag{29}$$

$$\mathrm{Li^+ + H \rightarrow LiH^+ + \gamma}, \tag{30}$$

$$\mathrm{Li^+ + H_2 \rightarrow Li + H_2^+}, \tag{31}$$

$$\mathrm{Li^+ + H_2 \rightarrow LiH^+ + H}, \tag{32}$$

$$\mathrm{Li^+ + H_2 \rightarrow LiH + H^+}, \tag{33}$$

$$\mathrm{Li^+ + H_2 \rightarrow LiH_2^+ + \gamma}. \tag{34}$$

Most of these processes are highly endothermic, and so are not competitive with photorecombination even when x is small. However, the two radiative association reactions are exothermic and deserve

closer scrutiny. Radiative association with atomic hydrogen (reaction RA10) has been included in a number of previous models of primordial gas chemistry (e.g. Stancil et al. 1996; Galli & Palla 1998), and accurate quantal calculations of the rate coefficient for this reaction are available (Dalgarno et al. 1996; Gianturco & Gori Giorgi 1996). However, at the densities of interest in the present case, efficient three-body formation of H_2 ensures that the hydrogen is primarily molecular rather than atomic, and so renders radiative association with H_2 (reaction RA20) the more important reaction. Unfortunately, we have been unable to locate any calculation of the rate coefficient of this reaction. Kirby & Dalgarno (1978) quote an upper limit of $k_{\rm RA20} = 10^{-16}\,{\rm cm^3\,s^{-1}}$, while Stancil et al. (1996) quote an upper limit of $k_{\rm RA20} = 10^{-17}\,{\rm cm^3\,s^{-1}}$, but the true rate coefficient could be orders of magnitude smaller. In our reference model, we make the conservative assumption that the rate coefficient is of the same order of magnitude as that for reaction RA10, and hence adopt a value $k_{\rm RA20} = 10^{-22}\,{\rm cm^3\,s^{-1}}$. We investigate the effects of adopting a larger value in Section 5.6.4.

The inclusion of reaction RA20 in our chemical network necessitates the inclusion of additional reactions: the dominant destruction mechanisms for LiH_2^+. Unfortunately, there has been very little theoretical or experimental study of any reactions involving LiH_2^+ and so it is not even clear which processes dominate. The best studied destruction process is dissociative recombination (reactions DR19, DR20 and DR21):

$$LiH_2^+ + e^- \rightarrow Li + H_2, \tag{35}$$

$$\rightarrow LiH + H, \tag{36}$$

$$\rightarrow Li + H + H. \tag{37}$$

Thomas et al. (2006) have studied this process experimentally using the CRYRING heavy ion storage ring, and have reported preliminary results regarding the branching ratio of the reaction, but have not yet reported any value for the total rate. C. Greene and collaborators are currently involved in a theoretical calculation of the total rate coefficient, but again have yet to publish any results. However, their preliminary findings suggest a total rate coefficient that is about 2.5–3 times larger than that for the dissociative recombination of H_3^+. (C. Greene, private communication). We therefore adopt a total rate coefficient $2 \times 10^{-7}\,(T/300)^{-1/2}\ {\rm cm^3\ s^{-1}}$ for the dissociative recombination of LiH_2^+, and use the values quoted by Thomas et al. (2006) for the branching ratios.

Other reactions that could be important destruction mechanisms for LiH_2^+ include

$$LiH_2^+ + H \rightarrow LiH^+ + H_2, \tag{38}$$

$$LiH_2^+ + H \rightarrow Li^+ + H_2 + H, \tag{39}$$

$$LiH_2^+ + H_2 \rightarrow Li^+ + H_2 + H_2, \tag{40}$$

$$LiH_2^+ + He \rightarrow LiHe^+ + H_2. \tag{41}$$

None of these reactions appears to have previously been studied in the astrochemical literature, and so their rates are unknown. For simplicity, therefore, we include only a single representative example from this set of reactions, namely the collisional dissociation of LiH_2^+ by H_2 (reaction CD26). As we are primarily interested in the role of LiH_2^+ within the highly molecular dense core, it is likely that this reaction will dominate, unless its rate coefficient is unusually small. In our reference model, we adopt a rate coefficient of $k_{\rm CD26} = 1.0 \times 10^{-9} \exp(-3250/T)\ {\rm cm^3\ s^{-1}}$ for this reaction; however, in Section 5.6.4 we examine the effect of adopting a smaller value.

3.2 Photochemistry

To compute rates for the photochemical reactions listed in Table A12, we assume that the gas is illuminated by an external background radiation field with the spectral shape of a 10^5 K blackbody at energies $h\nu < 13.6\,{\rm eV}$, and which is zero at higher energies. This choice of spectrum is motivated by the fact that the brightest Population III stars are expected to have high effective temperatures, $T_{\rm eff} \simeq 10^5$ K (Cojazzi et al. 2000), while the cut-off at the Lyman limit is intended to account for the effects of absorption by neutral hydrogen in the intergalactic medium. We quantify the strength of this background radiation field in terms of the flux at the Lyman limit, $J(\nu_\alpha) = 10^{-21}\ J_{21}\ {\rm erg\,s^{-1}\,cm^{-2}\,Hz^{-1}\,sr^{-1}}$. The rates listed in Table A12 are computed assuming that $J_{21} = 1.0$, but scale linearly with J_{21} and so can easily be rescaled for other values of the background radiation field strength.

3.3 Cosmic rays

If cosmic rays are present, then they will directly ionize some species and indirectly photoionize and photodissociate others. Direct ionization is simple to treat, and the appropriate rates are listed in Table A13, normalized by the cosmic ray ionization rate of atomic hydrogen, $\zeta_{\rm H}$, which we treat as a free parameter. However, the indirect effects of the cosmic rays are harder to model accurately.

The basic physics is straightforward, and was first discussed by Prasad & Tarafdar (1983). They noted that the secondary electrons produced by cosmic ray ionizations are energetic enough to excite the electronic states of H_2, and that the subsequent radiative decay of these excited states would produce UV photons. In the Galactic context, the mean free path of these photons is small, and so the cosmic ray induced photochemistry can be modelled as a purely local process (see e.g. Gredel et al. 1989).

In the Population III star formation context in which we are interested, however, there are two main factors that complicate matters. First, the H_2 fraction in the gas is small at densities $n \ll 10^{10}\,{\rm cm^{-3}}$, and so most of the secondary electrons produced by the cosmic rays lose energy by exciting and ionizing atomic hydrogen, rather than molecular hydrogen. Secondly, an accurate treatment of the propagation of the photons produced by excited H and H_2 is far more involved than in the Galactic case. The continuum opacity of metal-free gas is very small at most densities of interest (Lenzuni, Chernoff & Salpeter 1991), owing to the absence of dust absorption, and so the majority of the photons produced by cosmic ray induced excitation of H_2 have large mean free paths. On the other hand, Lyα photons produced by the excitation of atomic hydrogen have small mean free paths, but scatter many, many times before escaping the gas (see e.g. Dijkstra, Haiman & Spaans 2006). In neither case is it a good approximation to assume that all of the photons are absorbed locally in the gas, and so the simple local treatment developed for Galactic dark clouds no longer applies.

If we consider only the effects of emission from H_2, then to compute $R_{\rm X}$, the photoionization (or photodissociation) rate per unit volume of species X, one must use an equation of the form

$$R_{\rm X}(\boldsymbol{x}) = \frac{1}{4\pi} \int_0^\infty \sigma_{\rm X}(\nu) \int_V \frac{\epsilon(\nu, \boldsymbol{x}') {\rm e}^{-\tau(\nu, \boldsymbol{x}', \boldsymbol{x})}}{|\boldsymbol{x}' - \boldsymbol{x}|^2}\, {\rm d}\boldsymbol{x}'\, {\rm d}\nu, \tag{42}$$

where the volume V that we integrate over corresponds to the entirety of the protogalactic core, and where $\tau(\nu, \boldsymbol{x}', \boldsymbol{x})$ is the optical depth of the gas between point $\boldsymbol{x}$ and point $\boldsymbol{x}'$ at a frequency ν. The photon emissivity $\epsilon(\nu, \boldsymbol{x}')$ is given in this case by

$$\epsilon(\nu, \boldsymbol{x}') = P_{\rm H_2}(\nu)\zeta_{\rm H_2} n_{\rm H_2}, \tag{43}$$

where $P_{\rm H_2}(\nu)\,{\rm d}\nu$ is the probability that the cosmic ray ionization of H_2 leads to the production of a photon with a frequency in the range $\nu \rightarrow \nu + {\rm d}\nu$, and $\zeta_{\rm H_2}$ is the cosmic ray ionization rate of H_2.

For gas at the centre of a spherically symmetric protogalactic core, we can simplify equation (42) to

$$R_{\rm X} = \int_0^\infty \sigma_{\rm X}(\nu) \int_0^R \epsilon(\nu, r) {\rm e}^{-\tau(\nu,r)}\,{\rm d}r\,{\rm d}\nu, \tag{44}$$

where $\tau(\nu, r)$ is the optical depth between the centre of the halo and gas at a radius r, $\epsilon(\nu, r)$ is the emissivity at r, and R is the core radius. However, even after making this simplification, calculation of $R_{\rm X}$ still requires more information than we have available in our one-zone calculation, namely the radial profiles of density, temperature and chemical abundances, which determine both $\tau(\nu, r)$ and $\epsilon(\nu, r)$. In their absence, we are forced to approximate.

If we assume that the protogalactic core has a density structure with a 'core plus halo' form, i.e.

$$n(r) = \begin{cases} n_{\rm c}, & r < r_{\rm c}, \\ n_{\rm c}(r_c/r)^\alpha, & r > r_{\rm c}, \end{cases} \tag{45}$$

then provided that $\alpha > 1$, the integral in equation (42) will be dominated by the contribution from the core of the density profile. If we further assume that the core is chemically homogeneous, and that $\tau(\nu, r) \sim 0$, then we can approximate equation (42) as

$$R_{\rm X} \simeq \int_0^\infty \sigma_{\rm X}(\nu) r_{\rm c} P_{\rm H_2}(\nu)\zeta_{\rm H_2} n_{\rm c,H_2}\,{\rm d}\nu, \tag{46}$$

where $n_{\rm c,H_2}$ is the number density of H_2 within the core. Note that even if the point we are considering is not directly at the centre of the core, equation (46) remains a reasonable approximation to $R_{\rm X}$, provided that we are considering a point within $r_{\rm c}$, and that $r_{\rm c} \ll R$. Provided that our approximations hold, equation (46) allows us to reduce what is formally a non-local problem into one that can be treated as if it were local.

To properly include the effects of hydrogen excitation, one would have to solve for the radiative transfer of the Lyα photons within the collapsing protostellar core. However, as the outcome would be highly sensitive to the assumed density and velocity profiles of the gas, which are not available from our one-zone calculation, the wisdom of performing such a detailed calculation for each of our simulations that include cosmic rays is questionable; we run the risk of getting an answer that is completely determined by our assumptions, and that therefore is not robust. Instead, we have chosen a more conservative course, and have attempted to put limits on the effects of the Lyα photons by considering two limiting cases: one in which they do not propagate significantly into the core of the protogalaxy, and do not contribute to $R_{\rm X}$ (which is thus given in this case by equation 46 above), and another in which the optical depth of the gas to the Lyα photons is negligible, and $R_{\rm X}$ is given by a generalization of equation (46):

$$R_{\rm X} \simeq \int_0^\infty \sigma_{\rm X}(\nu) r_{\rm c} \left(P_{\rm H_2}(\nu)\zeta_{\rm H_2} n_{\rm c,H_2} + P_{\rm H}(\nu)\zeta_{\rm H} n_{\rm c,H}\right)\,{\rm d}\nu, \tag{47}$$

where $P_{\rm H}(\nu)\,{\rm d}\nu$ is the probability that the cosmic ray ionization of H leads to the production of a photon with a frequency in the range $\nu \rightarrow \nu + {\rm d}\nu$, $\zeta_{\rm H}$ is the cosmic ray ionization rate of H, and $n_{\rm c,H}$ is the number density of atomic hydrogen in the core.

To evaluate $R_{\rm X}$, it remains necessary to specify $r_{\rm c}$. In our calculations, we assume, following Omukai (2000) and Omukai et al. (2005), that $r_{\rm c}$ is given by the current Jeans length.

In Table A14, we list estimated values for $\sigma_{\rm X,eff,H_2} = \int_0^\infty \sigma_{\rm X}(\nu) P_{\rm H_2}(\nu)\,{\rm d}\nu$ and $\sigma_{\rm X,eff,H} = \int_0^\infty \sigma_{\rm X}(\nu) P_{\rm H}(\nu)\,{\rm d}\nu$ for both photoionization and photodissociation for a number of different chemical species. To compute these values, we assumed that all of the photons produced by excited hydrogen are emitted in the Lyα line, implying that $P_{\rm H} = \delta(\nu_\alpha - \nu)$, where ν_α is the frequency of Lyα and δ is the Dirac delta function. For $P_{\rm H_2}$, we used estimated values based on the emission spectra given in Sternberg, Dalgarno & Lepp (1987); note that these are likely accurate only to within a factor of a few. Given these values, the rates for the cosmic ray induced photoionization and photodissociation of these species in our model cores can be calculated using equation (46) or (47), as appropriate.

3.4 Neglected processes

Although the chemical network presented in this paper is, to the best of our knowledge, the most comprehensive network used to date to simulate primordial gas chemistry, there remain a large number of possible reactions that we have not included. Below, we discuss which types of processes have been omitted, and why.

(i) We do not include the formation of H_2 or D_2 by the radiative association of ground state atomic hydrogen or deuterium, respectively, on the grounds that the rate coefficients for these processes are negligible.

(ii) We have not included reactions that involve electronically excited atomic hydrogen (as considered in Latter & Black 1991 or Rawlings, Drew & Barlow 1993, for instance). We justify this omission by noting that the population of the $n = 2$ electronic level of atomic hydrogen will be very small at the densities and temperatures considered in this paper, on account of the large Einstein coefficient associated with the Lyα transition and the large energy separation of the $n = 1$ and $n = 2$ levels. For similar reasons, we have not included any reactions that require electronically excited deuterium, helium or lithium.

(iii) We have restricted the range of chemical species considered to those with three or fewer atoms. In principle, the formation of larger species is possible – for instance, H_5^+ can be formed from H_3^+ by the radiative association reaction (Paul et al. 1995)

$$H_3^+ + H_2 \rightarrow H_5^+ + \gamma. \tag{48}$$

However, the chemical abundances of the three-atom species in our model are very small, and we expect the abundance of even larger species to be much smaller still. It therefore seems unlikely that they will play any significant role in the cooling or chemistry of the gas.

(iv) We have omitted any photochemical reactions that require photons with energies greater than 13.6 eV, under the assumption that any such photons emitted by external sources of radiation will be absorbed in the intergalactic medium, or in the ISM of the protogalaxy, before reaching the particular collapsing core under study. Moreover, since we consider only the initial collapse of the core, internal sources of radiation, such as a central protostar, fall outside the scope of this paper.

(v) We do not include processes that have negligible reaction rates at all temperatures treated in this paper. This includes the production of doubly ionized helium, He^{2+}, or doubly or triply ionized lithium, Li^{2+} and Li^{3+} by collisional ionization (see e.g. Lepp et al. 2002), which are therefore omitted from the chemical model.

(vi) We have ignored the effects of stimulated radiative association and stimulated radiative attachment, i.e. reactions of the form

$$\mathrm{X} + \mathrm{Y} + \gamma_\mathrm{b} \rightarrow \mathrm{XY} + \gamma + \gamma_\mathrm{b}, \tag{49}$$

$$\mathrm{X} + \mathrm{e}^- + \gamma_\mathrm{b} \rightarrow \mathrm{X}^- + \gamma + \gamma_\mathrm{b}, \tag{50}$$

where γ_b represents a background photon. The influence of stimulated radiative association or attachment on the production of various molecules in primordial gas (LiH, HD, H^-, Li^- and HeH^+) has been investigated (Stancil & Dalgarno 1997a,b, 1998; Zygelman, Stancil & Dalgarno 1998), generally for the case of a blackbody radiation field. However, significant effects are found only for radiation temperatures $T_\mathrm{rad} > 500\,\mathrm{K}$, much larger than the CMB temperature at the redshifts of interest in this study. The background radiation fields considered in Section 5.4 have the same shape below $h\nu = 13.6\,\mathrm{eV}$ as a $10^5\,\mathrm{K}$ blackbody, but have intensities that are orders of magnitude weaker than a true blackbody radiation field with this temperature, and so are also unimportant in this context. Therefore, it is clear that the influence of these simulated processes will be negligible.

(vii) We have omitted collisional processes such as

$$\mathrm{H}_2 + \mathrm{H}_2 \rightarrow \mathrm{H} + \mathrm{H} + \mathrm{H} + \mathrm{H} \tag{51}$$

or

$$\mathrm{H} + \mathrm{H} \rightarrow \mathrm{H}^+ + \mathrm{H}^+ + \mathrm{e}^- + \mathrm{e}^- \tag{52}$$

that have energy thresholds corresponding to temperatures significantly higher than those considered in this paper, as we do not expect these processes to play an important role in low-temperature gas.

(viii) We do not include dissociative charge transfer reactions involving H_2^+ or its isotopologues, e.g.

$$\mathrm{H} + \mathrm{H}_2^+ \rightarrow \mathrm{H} + \mathrm{H} + \mathrm{H}^+, \tag{53}$$

$$\mathrm{H} + \mathrm{HD}^+ \rightarrow \mathrm{H} + \mathrm{D} + \mathrm{H}^+, \tag{54}$$

because at the temperature of interest in this study, the cross-sections for these processes are far smaller than those for the equivalent non-dissociative charge transfer reactions (Krstić 2002; Krstić & Janev 2003)

$$\mathrm{H} + \mathrm{H}_2^+ \rightarrow \mathrm{H}_2 + \mathrm{H}^+, \tag{55}$$

$$\mathrm{H} + \mathrm{HD}^+ \rightarrow \mathrm{HD} + \mathrm{H}^+. \tag{56}$$

(ix) We have not included charge transfer from He^+ to Li:

$$\mathrm{He}^+ + \mathrm{Li} \rightarrow \mathrm{He} + \mathrm{Li}^+, \tag{57}$$

or its inverse

$$\mathrm{He} + \mathrm{Li}^+ \rightarrow \mathrm{He}^+ + \mathrm{Li}. \tag{58}$$

The first of these reactions is unimportant in comparison to charge transfer from H^+ owing to the low He^+ abundances we find in our simulations. The second reaction is negligible at $T < 10\,000\,\mathrm{K}$ due to its large endothermicity.

(x) We have omitted all collisional dissociation reactions caused by minor molecules or ions, e.g. HD, Li, LiH, etc. Collisional dissociation reactions involving HD, such as

$$\mathrm{H}_2 + \mathrm{HD} \rightarrow \mathrm{H} + \mathrm{H} + \mathrm{HD}, \tag{59}$$

will be unimportant compared to the analogous reactions involving H_2, while reactions of the form

$$\mathrm{XY} + \mathrm{Li} \rightarrow \mathrm{X} + \mathrm{Y} + \mathrm{Li}, \tag{60}$$

will be unimportant due to the very small abundance of lithium relative to hydrogen.

(xi) We have ignored a large number of possible three-body processes: specifically, every process that involves any species other than H, H_2 or He as the third body. At the densities at which three-body reactions become significant, the abundances of these three species are orders of magnitude higher than the abundances of any other species, and so it is easy to justify the omission of these minor contributions.

(xii) We do not include transfer reactions involving two ions of the same charge, e.g.

$$\mathrm{H}_2^+ + \mathrm{H}_2^+ \rightarrow \mathrm{H}_3^+ + \mathrm{H}^+, \tag{61}$$

as the mutual Coulomb repulsion of the ions renders these reactions ineffective at the temperatures considered in this paper.

(xiii) We do not include the double ionization of H_2 or He by cosmic rays, i.e.

$$\mathrm{H}_2 + \mathrm{CR} \rightarrow \mathrm{H}^+ + \mathrm{H}^+ + \mathrm{e}^- + \mathrm{e}^-, \tag{62}$$

$$\mathrm{He} + \mathrm{CR} \rightarrow \mathrm{He}^{++} + \mathrm{e}^- + \mathrm{e}^-, \tag{63}$$

as the fraction of cosmic ray ionization events leading to these outcomes is expected to be very small (Glassgold & Langer 1973).

(xiv) We assume that in mutual neutralization reactions involving H_3^+ or one of its isotopologues, complete break-up of the ion is unlikely to occur; this is in line with e.g. the detailed chemical network of Le Teuff, Millar & Markwick (2000), which includes the processes

$$\mathrm{H}_3^+ + \mathrm{H}^- \rightarrow \mathrm{H}_2 + \mathrm{H}_2 \tag{64}$$

and

$$\mathrm{H}_3^+ + \mathrm{H}^- \rightarrow \mathrm{H}_2 + \mathrm{H} + \mathrm{H}, \tag{65}$$

but not

$$\mathrm{H}_3^+ + \mathrm{H}^- \rightarrow \mathrm{H} + \mathrm{H} + \mathrm{H} + \mathrm{H}. \tag{66}$$

(xv) A number of possible reactions involving LiH_2^+ have been omitted, as have any reactions involving LiHD^+ or LiD_2^+. As we have already discussed in Section 3.1.11, we know very little regarding the values of the rate coefficients for many of the most important formation and destruction processes for LiH_2^+, rendering its abundance highly uncertain. In view of this large uncertainty, there is little to be gained by adding in additional, equally uncertain but less important processes involving LiH_2^+, or by considering the chemistry of the deuterated forms of the molecular ion.

4 THERMAL PROCESSES

Our model of the thermal behaviour of the gas includes the effects of heating and cooling from a large number of different radiative and chemical processes. A full list of the processes included is given in Table 2, while a more detailed discussion is given below.

4.1 H_2 cooling

In our treatment of H_2 ro-vibrational cooling at low densities, we include the effects of collisions between H_2 and H, H_2, He, H^+ and e^-, using fitting formulae from Glover & Abel (2008). At high densities, we use the standard LTE cooling function (see e.g. Hollenbach & Mckee 1979). We assumed the usual value of 3:1 for the H_2 ortho–para ratio, which Glover & Abel (2008) have demonstrated is a good approximation for all temperatures in the range in

Table 2. Processes included in our thermal model.

Species	Process	Collision partner(s)	References
Cooling			
H_2	Ro-vibrational lines	H, H_2, He, H^+, e^-	1, 2
H_2	Collision-induced emission	H_2	2
HD	Ro-vibrational lines	H	3
LiH	Ro-vibrational lines	H, H_2	4
H_3^+	Ro-vibrational lines	H, H_2, He, e^-	5
H	Resonance lines	e^-	6
CMB photons	Compton scattering	e^-	6
H_2^+, HD^+, D_2^+	Ro-vibrational lines	H, e^-	7
Minor species	Ro-vibrational lines	H, H_2, He, e^-	8
H^+	Recombination	e^-	9
He^+	Recombination	e^-	10
H	Collisional ionization	e^-	11
H_2	Collisional dissociation	H, H_2, He, e^-	12
H^+	Charge transfer (reaction CT19)	H_2	13
Heating			
H_2	Formation	–	12
H_2	Photodissociation	–	14
H_2	Ultraviolet pumping	–	15
Cosmic rays	Ionization/excitation	–	16

Note: See the appropriate subsections in Section 4 for details of how we have decided which collision partners to include.

References: 1 – Wrathmall & Flower (2007); 2 – Ripamonti & Abel (2004); 3 – Lipovka et al. (2005); 4 – Galli & Palla (1998); 5 – Neale et al. (1996), Oka & Epp (2004); 6 – Black (1981), Cen (1992); 7 – See Section 4.5; 8 – See Section 4.6; 9 – Ferland et al. (1992); 10 – Hummer & Storey (1998); 11 – Janev et al. (1987); 12 – See Section 3 and Section 4.9; 13 – Savin et al. (2004); 14 – Black & Dalgarno (1977); 15 – Burton et al. (1990); 16 – Goldsmith & Langer (1978).

which H_2 cooling is important. Although the revised treatment of H_2 cooling presented by Glover & Abel (2008) can make a significant difference to the thermal evolution of the gas in some circumstances – notably, in gas with a substantial fractional ionization – we do not expect it to have a significant impact on our current results, as at the densities of greatest interest in this paper, H_2 is well within the LTE cooling regime.

An important source of inaccuracy at high densities is the treatment of the opacity of the H_2 emission lines. In our models, we follow Ripamonti & Abel (2004) and model optically thick H_2 cooling with the expression

$$\Lambda_{\rm H_2,thick} = \Lambda_{\rm H_2,thin} \times \min[1, (n/n_0)^{-\beta}], \tag{67}$$

where $\Lambda_{\rm H_2,thick}$ and $\Lambda_{\rm H_2,thin}$ are the optically thick and optically thin cooling rates, respectively, n is the number density of hydrogen nuclei, and where $n_0 = 8 \times 10^9\,{\rm cm^{-3}}$ and $\beta = 0.45$. This approximation works well for modelling gas at the centre of a collapsing core, but is less accurate when used to treat H_2 cooling in the surrounding envelope (N. Yoshida, private communication). Yoshida et al. (2006) present a more accurate approach based on the computation of escape probabilities for each individual H_2 line using the Sobolev approximation. However, this treatment requires dynamical information, in the form of the local velocity gradient, that is not available in any meaningful form in our simple models, and so for our current study we must be content with the Ripamonti & Abel (2004) approach.

At very high densities ($n > 10^{14}\,{\rm cm^{-3}}$), cooling from H_2 becomes dominated by CIE. When an H_2 molecule collides with a hydrogen or helium atom, or another H_2 molecule, the particles involved briefly act as a 'supermolecule' with a non-zero electric dipole, which has a high probability of emitting a photon. Because the collision time is very short, the resulting CIE lines are very broad, and typically merge into a continuum. In our model, we model the CIE cooling rate with a power-law approximation taken from Ripamonti & Abel (2004), valid for gas in which $x_{\rm H_2} > 0.5$:

$$\Lambda_{\rm CIE} = 4.578 \times 10^{-49} T^4 n_{\rm H_2} n\ {\rm erg\ s^{-1}\ cm^{-3}}. \tag{68}$$

Although cooling from CIE contributes only 12 per cent of the total cooling at the density reached at the end of our simulation, $n_{\rm f} = 3 \times 10^{13}\,{\rm cm^{-3}}$, we have verified in test runs that at higher densities it very rapidly becomes the dominant form of cooling, justifying our decision to end our simulations at this point.

4.2 H_3^+ cooling

In the LTE limit, it is straightforward to calculate the H_3^+ cooling rate using the data presented by Neale, Miller & Tennyson (1996). In our simulations, we use tabulated values computed directly from the Neale et al. (1996) line list. However, for the convenience of readers, we also provide an analytical fit of the form

$$\log\left[\frac{\Lambda_{\rm H_3^+,LTE}}{n_{\rm H_3^+}}\right] = \sum_{i=0}^{8} a_i (\log T)^i, \tag{69}$$

where $\Lambda_{\rm H_3^+,LTE}$ is the H_3^+ cooling rate per unit volume in the LTE limit, and where the values of the a_i coefficients are listed in Table 3. This fit is accurate to within 25 per cent for temperatures in the range $20 < T < 400\,{\rm K}$ and to within a few per cent for temperatures in the range $400 < T < 10\,000\,{\rm K}$. At high temperatures, the Neale et al. (1996) line list is known to be incomplete, and so for $T > 3000\,{\rm K}$, we may systematically underestimate the cooling due to H_3^+. However, as we shall see in Section 5, we never find gas at

Table 3. Numerical coefficients used in our analytical fit to the H_3^+ cooling rate.

	LTE $20 < T < 400$ K	LTE $400 < T < 10\,000$ K	$n \rightarrow 0$ $20 < T < 10\,000$ K
a_0	$-1.658\,3133 \times 10^4$	$9.503\,3824 \times 10^3$	$-7.919\,2725$
a_1	$5.080\,8831 \times 10^4$	$-1.783\,2745 \times 10^4$	$-43.505\,799$
a_2	$-5.947\,5456 \times 10^4$	$1.284\,7118 \times 10^4$	$41.100\,652$
a_3	$2.845\,9331 \times 10^4$	$-3.907\,9919 \times 10^3$	$-17.327\,161$
a_4	$1.998\,8968 \times 10^3$	$-2.828\,6326 \times 10^1$	$3.389\,5649$
a_5	$-8.637\,0305 \times 10^3$	$3.739\,4515 \times 10^2$	$-0.249\,312\,87$
a_6	$4.042\,9912 \times 10^3$	$-1.113\,0317 \times 10^2$	0.0
a_7	$-8.286\,3818 \times 10^2$	$1.418\,7579 \times 10^1$	0.0
a_8	$6.597\,5582 \times 10^1$	$-6.996\,9136 \times 10^{-1}$	0.0

these temperatures in the regime where H_3^+ is potentially important, and so this incompleteness will not affect our results.

At densities where H_3^+ is not in LTE, the calculation of the H_3^+ cooling rate presents more of a problem. A commonly used approximation for dealing with the cooling from molecular species (see e.g. Hollenbach & Mckee 1979) is to compute the cooling at a density n using the expression

$$\Lambda = \frac{\Lambda_{\rm LTE}}{1 + (n_{\rm cr}/n)}, \tag{70}$$

where $\Lambda_{\rm LTE}$ is the LTE cooling rate per unit volume, and where the critical density $n_{\rm cr}$ is given by $n_{\rm cr}/n = \Lambda_{\rm LTE}/\Lambda_{n\rightarrow 0}$, where $\Lambda_{n\rightarrow 0}$ is the cooling rate per unit volume in the $n \rightarrow 0$ limit. For $n \ll n_{\rm cr}$ and $n \gg n_{\rm cr}$, this expression is highly accurate, while for $n \sim n_{\rm cr}$ it does a reasonable job of capturing the basic behaviour, at a far smaller computational cost than a full level population calculation would require. We adopt this approximation in our treatment of H_3^+ cooling, reducing the problem of calculating $\Lambda_{H_3^+}$ to one of calculating $\Lambda_{H_3^+,n\rightarrow 0}$. Here, however, we hit a problem. To compute $\Lambda_{H_3^+,n\rightarrow 0}$, we must evaluate

$$\Lambda_{H_3^+,n\rightarrow 0} = n_{H_3^+} \sum_j C_{0j} E_{0j}, \tag{71}$$

where C_{0j} is the rate of collisional excitation from the H_3^+ ground state,[1] here denoted as level 0, to an excited level j, and E_{0j} is the energy difference between level 0 and level j. The collisional excitation rate for transitions from $0 \rightarrow j$ is simply

$$C_{0j} = q_{0j,\rm H} n_{\rm H} + q_{0j,\rm H_2} n_{\rm H_2} + q_{0j,\rm He} n_{\rm He} + q_{0j,\rm e^-} n_{\rm e^-}, \tag{72}$$

where $q_{0j,\rm H}$, $q_{0j,\rm H_2}$, $q_{0j,\rm He}$ and $q_{0j,\rm e^-}$ are the collisional excitation rate coefficients for collisions with H, H_2, He and e^-, respectively; $n_{\rm H}$, $n_{\rm H_2}$, $n_{\rm He}$ and $n_{\rm e^-}$ are the corresponding particle number densities; and where we have ignored the effect of collisions with protons (which are unimportant in the case of a positively charged ion such as H_3^+) or with minor ionic or molecular species such as H^- or HD. The difficulty in computing the collisional terms, and hence the low-density limit of the H_3^+ cooling rate, arises because most of the required collisional excitation rate coefficients are unknown. Faure & Tennyson (2003) give rate coefficients for the collisional excitation of a number of low-lying rotational states by collisions with electrons, but in the high-density, low-ionization conditions of interest in this study, collisions with electrons are unimportant, and analogous data sets for collisions with H, He or H_2 are not available.

To deal with this problem, we have used an approach introduced by Oka & Epp (2004). They computed rate coefficients for rotational transitions in H_3^+ caused by collisions with H_2 by making use of the principle of detailed balance and by assuming that the collisional transitions are completely random (i.e. that they obey no selection rules). These assumptions led them to suggest rate coefficients of the form

$$q_{\rm ij} = K_{\rm ij} \sqrt{\frac{g_j}{g_i}} \exp\left(-\frac{E_j - E_i}{2kT}\right) \tag{73}$$

for transitions between an initial level i and final level j, where g_i and g_j, are the statistical weights of levels i and j, respectively, E_i and E_j are the corresponding level energies, and $K_{\rm ij}$ is a normalizing factor given by

$$K_{\rm ij} = C \left\{ 1 + \sum_m \left(\frac{g_m}{\sqrt{g_j g_i}} \right)^{1/2} \times \exp\left[-\frac{E_m - (1/2)(E_j + E_i)}{2kT} \right] \right\}^{-1}, \tag{74}$$

where C is the total collision rate, which is independent of i and j, and where the summation does not include levels i or j. Although Oka & Epp (2004) consider only pure rotational transitions, the same scheme can be used to treat ro-vibrational transitions.

In our treatment, we assume that the Oka–Epp scheme can be used to treat collisions with atomic hydrogen and helium as well as H_2, and hence are able to determine the temperature dependence of the set of collisional excitation rate coefficients for each collider ($q_{0j,\rm H}$, $q_{0j,\rm H_2}$ and $q_{0j,\rm He}$); we ignore collisions with electrons, on the grounds of the very small electron abundance that exists at the densities where H_3^+ cooling is potentially important. Using these collisional excitation rate coefficients, we can then construct C_{0j} via equation (72), from which $\Lambda_{H_3^+,n\rightarrow 0}$ follows via equation (71). The overall normalization of the cooling rate remains uncertain, as it depends on the H_3^+ number density, and on the total collision rates with each of H, H_2 and He, which we can write as $C_{\rm H}$, $C_{\rm H_2}$ and $C_{\rm He}$. If we define the total collision rate C to be the sum of these three unknowns:

$$C = C_{\rm H} + C_{\rm H_2} + C_{\rm He}, \tag{75}$$

and write the low-density H_3^+ cooling rate as

$$\Lambda_{H_3^+,n\rightarrow 0} = L_{H_3^+,n\rightarrow 0} n_{H_3^+}, \tag{76}$$

then it is easy to show that the combination $L_{H_3^+,n\rightarrow 0}/C$ is completely determined. We have computed an analytical fit to this quantity, using a fit of the form of equation (69). The fitting coefficients are listed in Table 3. This fit is accurate to within 1 per cent over the temperature range $20 < T < 10\,000$ K. To convert from $L_{H_3^+,n\rightarrow 0}/C$ to $L_{H_3^+,n\rightarrow 0}$, we must fix the size of our remaining free parameter, the total collision rate C. In most of our simulations, we assume that C is given by

$$C = 2.2 \times 10^{-9} n_{\rm H} + 1.9 \times 10^{-9} n_{\rm H_2} + 8.1 \times 10^{-10} n_{\rm He}\ {\rm s}^{-1} \tag{77}$$

which is the sum of the Langevin rates for collisions between H_3^+ and H, H_2 and He, respectively. These Langevin rates were computed using polarizabilities for He and H_2 taken from Huiszoon & Briels (1993); the exact value was used for H. The true value of C is unlikely to be very much larger than this, but could be considerably smaller, and so in Section 5.2 we examine the sensitivity of our results to our choice of value for C. Finally, we note that as

[1] The $(J, K) = (1, 1)$ rotational level of the vibrational ground state; occupation of the $(J, K) = (0, 0)$ level is forbidden by the Pauli exclusion principle.

both $\Lambda_{H_3^+,\rm LTE}$ and $\Lambda_{H_3^+,n\rightarrow 0}$ are directly proportional to $n_{H_3^+}$, the H_3^+ critical density is independent of $n_{H_3^+}$. Thus, once C is specified, $n_{\rm cr}$ can be trivially computed using our numerical fits.

We assume that the H_3^+ emission remains optically thin throughout our simulations. For a subsonic collapse in which the effect of large-scale velocity gradients are unimportant compared to the local Doppler broadening of the emission lines, the optical depth at line centre corresponding to a given emission line can be written as (Mihalas & Mihalas 1984)

$$\tau_{\rm ji} = \frac{g_j}{g_i}\frac{c^2}{8\pi\nu_{\rm ij}^2}A_{\rm ji}\frac{N_i}{\pi^{1/2}\Delta\nu_{\rm D}}, \tag{78}$$

where g_j and g_i are the statistical weights of levels i and j, $\nu_{\rm ij}$ is the frequency of the transition from level j to level i, $A_{\rm ij}$ is the corresponding spontaneous radiative transition rate, N_i is the column density of absorbers in level i and $\Delta\ \nu_{\rm D} = (\nu_{\rm ij}/c)\ (2kT/m)^{1/2}$ is the Doppler width of the line, where m is the mass of the H_3^+ ion. For simplicity, we have neglected the effects of stimulated emission. Illustrative values for $\nu_{\rm ij}$ and $A_{\rm ij}$ for a strong vibrational transition are $\nu_{\rm ij} \simeq 8.46 \times 10^{13}$ Hz and $A_{\rm ij} \simeq 94\,{\rm s}^{-1}$ (Neale et al. 1996), and so for this transition

$$\tau_{\rm ji} \sim 10^{-15} N_i, \tag{79}$$

where we have assumed a gas temperature of 1000 K. Therefore, in this example, the line becomes optically thick only once $N_i \gtrsim 10^{15}\,{\rm cm}^{-2}$. As many of the H_3^+ emission lines are considerably weaker than this example, and as the column density of H_3^+ ions in any particular level i can clearly be no larger than the total H_3^+ column density, $N_{H_3^+}$, it is safe to conclude from this analysis that optical depth effects are unlikely to significantly affect the H_3^+ cooling rate until $N_{H_3^+} > 10^{15}\,{\rm cm}^{-2}$.

We now investigate whether we expect our models to reach this column density in H_3^+. Our one-zone dynamical model does not contain any information about the overall structure of the collapsing core and so does not predict $N_{H_3^+}$ directly. However, based on the results of more detailed numerical simulations (Abel et al. 2002; Yoshida et al. 2006), we assume that the protostellar core has a density profile that is well approximated by a power law $n(r) \propto r^{-2.2}$, and that it is collapsing subsonically. With this assumed density profile, the column density of hydrogen nuclei along a radial ray from a point r to the edge of the core is given by

$$N_{\rm H,tot}(r) = \int_r^{r_{\rm core}} n(r'){\rm d}r', \tag{80}$$

$$= \frac{5}{6} r n(r) \left[1 - \left(\frac{r}{r_{\rm core}}\right)^{1.2}\right], \tag{81}$$

where $n(r)$ is the number density of hydrogen nuclei at r and $r_{\rm core}$ is the radius of the core. As we shall see in Section 5, the H_3^+ abundance in the collapsing gas typically varies only slightly with density below some threshold density $n_{\rm thr}$ and then declines sharply for $n > n_{\rm thr}$. The value of $n_{\rm thr}$ depends on factors such as the cosmic ray ionization rate and the speed of the collapse, but even in the most extreme models (e.g. run CR5; see Section 5.3) $n_{\rm thr} = 10^{11}\,{\rm cm}^{-3}$, while in general it is much smaller. Therefore, almost all of the contribution to $N_{H_3^+}$ comes from gas at densities $n < n_{\rm thr}$, and hence at radii $r > r_{\rm thr}$, where $r_{\rm thr}$ is the radius such that $n(r_{\rm thr}) = n_{\rm thr}$. If we assume that $r_{\rm thr} \ll r_{\rm core}$, or in other words that the density distribution of the collapsing core extends to densities $n \ll n_{\rm thr}$, then equation (81) tells us that the column density of hydrogen nuclei between $r_{\rm thr}$ and the edge of the core is approximately

$$N_{\rm tot}(r_{\rm thr}) \simeq \frac{5}{6} r_{\rm thr} n_{\rm thr}. \tag{82}$$

Denoting the fractional abundance of H_3^+ at $r_{\rm thr}$ as $x_{H_3^+}(r_{\rm thr})$, and assuming that it remains constant for $r > r_{\rm thr}$, we can therefore write the H_3^+ column density between $r_{\rm thr}$ and the edge of the core as

$$N_{H_3^+}(r_{\rm thr}) \simeq \frac{5}{6} x_{H_3^+}(r_{\rm thr}) r_{\rm thr} n_{\rm thr}. \tag{83}$$

For a typical protogalactic core, simulations have shown that a density $n_{\rm thr} = 10^{11}\,{\rm cm}^{-3}$ corresponds to a radius $r_{\rm thr} \simeq 10^{15}$ cm (see e.g. Abel et al. 2002; Yoshida et al. 2006). Furthermore, the results presented in Section 5.3 demonstrate that in run CR5, $x_{H_3^+}(r_{\rm thr}) \simeq 4.4 \times 10^{-11}$. We therefore obtain $N_{H_3^+}(r_{\rm thr}) \simeq 4 \times 10^{15}\,{\rm cm}^{-2}$. At $r > r_{\rm thr}$, the H_3^+ column density is smaller, but at $r < r_{\rm thr}$, it does not grow significantly larger. In this particular case, the core may be marginally optically thick, albeit only in the strongest lines. However, in most of our models, $n_{\rm thr}$ is significantly smaller, and $x_{H_3^+}(r_{\rm thr})$ is orders of magnitude smaller. In these runs, it is clear that the core remains optically thin.

4.3 HD cooling

To model HD cooling, we use the cooling function of Lipovka, Núñez-López & Avila-Reese (2005). Although formally valid only in the temperature range $100 < T < 2 \times 10^4$ K, we have compared its behaviour at lower temperatures with an explicit calculation of the cooling rate made using radiative de-excitation rates from Abgrall, Roueff & Viala (1982) and collisional rates extrapolated from those computed by Wrathmall, Gusdorf & Flower (2007). We find that the Lipovka et al. (2005) rate remains reasonably accurate down to temperatures as low as 50 K, with errors no greater than 20 per cent, and that even at $T = 30$ K it remains accurate to within a factor of 2. At temperatures $T \gg 100$ K, the Lipovka et al. (2005) cooling rate slightly underestimates the effects of HD cooling compared to the newer calculations of Wrathmall et al. (2007), presumably owing to the more accurate vibrational excitation rates used in the latter study, but the differences are never greater than about 50 per cent, and in any case occur in the temperature regime in which H_2 cooling dominates. The breakdown of the Lipovka et al. (2005) fit at very high temperatures ($T > 20\,000$ K) is unimportant, as the gas in our models never reaches this temperature.

To correctly model the effects of HD cooling at low temperatures, it is necessary to take the effects of the CMB into account. We do this approximately, by using a modified HD cooling rate, $\Lambda'_{\rm HD}$, defined as

$$\Lambda'_{\rm HD} = \Lambda_{\rm HD}(T) - \Lambda_{\rm HD}(T_{\rm CMB}), \tag{84}$$

where $\Lambda_{\rm HD}(T)$ and $\Lambda_{\rm HD}(T_{\rm CMB})$ are the unmodified HD cooling rates at the gas temperature T and the CMB temperature $T_{\rm CMB}$, respectively.

The quoted range of densities for which the Lipovka et al. (2005) cooling function is valid is $1 < n < 10^8\,{\rm cm}^{-3}$. To extend the range of the cooling function to densities $n < 1\,{\rm cm}^{-3}$, we assume that at these densities the HD cooling rate scales proportionately to the number density of HD times the number density of colliders (i.e. as n^2), and hence that

$$\Lambda_{\rm HD}(n = n') = (n')^2 \Lambda_{\rm HD}(n = 1) \tag{85}$$

for $n' \leq 1\,{\rm cm}^{-3}$, where $\Lambda_{\rm HD}(n)$ is the HD cooling rate per unit volume (with units erg cm^{-3} s^{-1}) at gas number density n. To extend

the cooling function to high densities, $n > 10^8\,\mathrm{cm}^{-3}$, we assume that the HD molecule is in LTE and hence that the HD cooling rate per unit volume is independent of the number density of colliders and scales linearly with n; or in other words, that $\Lambda_{\mathrm{HD}}/n_{\mathrm{HD}}$ is independent of n. In view of the fact that $1 \ll n_{\mathrm{cr,HD}} \ll 10^8\,\mathrm{cm}^{-3}$, where $n_{\mathrm{cr,HD}}$ is the HD critical density, both of these assumptions appear well justified.

The Lipovka et al. (2005) cooling function only includes the effects of collisions between HD and H. However, Flower et al. (2000) have shown that the influence of the H_2/H ratio on the HD cooling rate is very small, and so the Lipovka et al. (2005) cooling function should remain reasonably accurate even after the molecular fraction becomes large. Moreover, collisions between HD and other species (electrons, H^+, etc.) can be neglected compared to collisions with H on account of the much larger abundance of the latter at the gas densities of interest.

Finally, we assume that the HD ro-vibrational lines remain optically thin throughout all of our runs. In practice, this is probably not the case: the strongest HD lines will become saturated once the HD column density exceeds $N_{\mathrm{HD}} = 10^{22}\,\mathrm{cm}^{-2}$, and an analysis similar to that performed for H_3^+ in the previous section suggests that this will occur in our model cores once $n \gtrsim 3 \times 10^{13}\,\mathrm{cm}^{-3}$. However, HD is only a minor coolant at these high densities, and so we can safely neglect optical depth effects on HD cooling without significantly affecting the thermal evolution of the gas in our models.

4.4 LiH cooling

To treat cooling from LiH, we use the cooling function given in Galli & Palla (1998). This is the low-density limit of the LiH cooling rate and so is strictly valid only for gas densities significantly below the LiH critical density, $n_{\mathrm{cr,LiH}}$. However, the transition probabilities for the rotational and vibrational transitions of LiH are very large, on account of the molecule's large dipole moment. This means that the LiH critical density is large, $n_{\mathrm{cr,LiH}} \simeq 10^{12}\,\mathrm{cm}^{-3}$ (Lepp & Shull 1984), and so the Galli & Palla (1998) cooling function is a reasonable choice over most of the range of densities covered by our simulations. At very high densities, we would expect LiH to begin to reach LTE, and our approximation to break down; at these densities, our continued use of the Galli & Palla (1998) cooling function means that we will overestimate the effectiveness of LiH cooling. Despite this, we find LiH cooling to be ineffective at all densities (see Section 5.1 below), suggesting that if we were to use a more accurate treatment of LiH cooling at high densities it would not significantly alter our conclusions.

In principle, we should adjust the LiH cooling rate to account for the effects of the CMB, just as we do for the HD cooling rate. However, as LiH cooling proves to be unimportant at all densities, this correction is also unimportant and its omission does not significantly affect the thermal evolution of the gas.

We assume that the LiD cooling rate is the same as the LiH cooling rate. While this is a crude approximation, in practice the LiD abundance is so small that its contribution is always negligible and thus the choice of LiD cooling rate is unimportant.

4.5 H_2^+, HD^+ and D_2^+ cooling

To treat cooling from these molecular ions, we use the same approach as in Glover & Abel (2008). At low densities, most H_2^+ cooling occurs due to collisions with free electrons and neutral hydrogen atoms; collisions with He and H_2 excite H_2^+ at comparable rates to collisions with H (Roberge & Dalgarno 1982), but are unimportant due to the low abundances of these species relative to atomic hydrogen. To model the cooling due to collisions with electrons, we use the vibrational excitation rate coefficients of Sarpal & Tennyson (1993), while for collisions with neutral hydrogen, we use a fit to the Suchkov & Shchekinov (1978) rate coefficient provided to us by D. Galli (private communication); note that this is a factor of 10 smaller than the rate coefficient given in Galli & Palla (1998), owing to a normalization error in the latter paper.

At high densities, the vibrational levels of H_2^+ will be in LTE. In this regime, the cooling rate is given approximately by

$$\Lambda_{\mathrm{H}_2^+,\mathrm{LTE}} = 2.0 \times 10^{-19} T^{0.1} \exp\left(-\frac{3125}{T}\right) n_{\mathrm{H}_2^+}. \quad (86)$$

This fit is from Glover & Abel (2008) and includes contributions from all vibrational states $v \leq 8$ (higher vibrational states are not expected to contribute significantly at the temperatures of interest in this paper). It was computed using level energies from Karr & Hilico (2006) and radiative transition rates from Posen, Dalgarno & Peek (1983). The effects of rotational excitation were not included, but are unlikely to change this expression by a large amount, owing to the very small Einstein coefficients associated with pure rotational transitions in H_2^+.

At intermediate densities, we assume that the H_2^+ vibrational cooling rate is given approximately by the function

$$\Lambda_{\mathrm{H}_2^+} = \frac{\Lambda_{\mathrm{H}_2^+,\mathrm{LTE}}}{1 + n_{\mathrm{cr}}/n}, \quad (87)$$

where $n_{\mathrm{cr}}/n = \Lambda_{\mathrm{H}_2^+,\mathrm{LTE}}/\Lambda_{\mathrm{H}_2^+,\mathrm{n}\rightarrow 0}$ is the H_2^+ critical density, and where $\Lambda_{\mathrm{H}_2^+,\mathrm{n}\rightarrow 0}$ is the H_2^+ cooling rate in the low-density limit. This is given by

$$\Lambda_{\mathrm{H}_2^+,\mathrm{n}\rightarrow 0} = \left[L_{\mathrm{H}_2^+,\mathrm{e}} n_{\mathrm{e}^-} + L_{\mathrm{H}_2^+,\mathrm{H}} n_{\mathrm{H}}\right] n_{\mathrm{H}_2^+}, \quad (88)$$

where $L_{\mathrm{H}_2^+,\mathrm{e}}$ and $L_{\mathrm{H}_2^+,\mathrm{H}}$ are the cooling rates per H_2^+ ion per unit collider density for collisions with electrons and atomic hydrogen, respectively, taken from Sarpal & Tennyson (1993) and Suchkov & Shchekinov (1978) as noted above.

To model cooling from vibrational transitions in HD^+, we assume, in the absence of better information, that the low-density cooling rate is the same as that used for H_2^+. However, since HD^+ has much larger radiative transition rates than H_2^+, the LTE cooling rate for HD^+ is much larger than that for H_2^+. Accordingly, we use the following functional fit for the HD^+ LTE cooling rate

$$\Lambda_{\mathrm{HD}^+,\mathrm{LTE}} = 1.09 \times 10^{-11} T^{0.03} \exp\left(-\frac{2750}{T}\right) n_{\mathrm{HD}^+} \quad (89)$$

at temperatures $T \leq 1000\,\mathrm{K}$ and

$$\Lambda_{\mathrm{HD}^+,\mathrm{LTE}} = 5.07 \times 10^{-12} T^{0.14} \exp\left(-\frac{2750}{T}\right) n_{\mathrm{HD}^+} \quad (90)$$

at $T > 1000\,\mathrm{K}$. These fits are from Glover & Abel (2008) and were calculated using HD^+ level energies from Karr & Hilico (2006) and radiative transition rates from Peek, Hashemi-Attar & Beckel (1979). For densities between the low-density and LTE limits, we again use a function of the form of equation (87) to compute the cooling rate.

Finally, to model D_2^+ cooling, we simply assume that the same rates apply as for H_2^+ cooling. In practice, the very small size of the typical D_2^+ abundance renders this process completely unimportant.

4.6 Other radiative coolants

In addition to the coolants discussed above, we also include a treatment of cooling from a number of other minor molecular ions that are present in the gas. Specifically, we include the effects of cooling from H_2D^+, HD_2^+, D_3^+, HeH^+, HeD^+, He_2^+, LiH^+, LiD^+ and LiH_2^+. Since appropriate collisional data are not available for most of these species, we treat their contribution to the cooling rate in an extremely simple fashion. We assume that the contribution to the cooling rate made by a species i with number density n_i can be written as

$$\Lambda_i = kT \left(\sum_c C_{\rm ic} n_c \right) n_i, \tag{91}$$

where n_c is the number density of a collider c, $C_{\rm ic}$ is the rate coefficient for inelastic collisions between i and c, and where we sum over all possible colliders. For collisions with H, H_2 or He, we assume that $C_{\rm ic}$ is given by the Langevin rate, while for collisions with electrons we conservatively assume that $C_{\rm ic} = 10^{-6}\,{\rm cm^3\,s^{-1}}$, which is comparable to the total rate coefficients found for other molecules, such as H_3^+ (Faure & Tennyson 2003). Collisions with all other species can be and are neglected.

In constructing this approximation we have assumed that each collision with i transfers an amount of energy kT, all of which is subsequently radiated. In practice, this procedure is likely to significantly overestimate the cooling provided by i, for several reasons. For one thing, it is not clear that the mean amount of energy transferred in a collision will always be $\sim kT$, since collisions that transfer $\Delta E \ll kT$ are possible while collisions that transfer $\Delta E \gg kT$ are highly unlikely. More importantly, this procedure neglects effects such as the collisional de-excitation of excited levels that will significantly limit cooling at high densities. However, these simplifications are unlikely to significantly affect our results, since even when we use these overestimates for the cooling rates, we find that the contribution of these minor species to the total cooling rate is negligible (see Section 5).

As well as these minor coolants, we also include two forms of cooling that are of great importance in hot, ionized gas. The first is cooling from electron impact excitation of atomic hydrogen (Lyα cooling). We treat this using a rate from Cen (1992), which is itself based on a rate in Black (1981). However, we note that for temperatures $T < 8000\,{\rm K}$, Lyα cooling is completely negligible, and so it does not significantly affect the outcome of the simulations presented in this paper.

The second process is cooling due to the Compton scattering of CMB photons by free electrons. This is also treated using a rate from Cen (1992), but again plays very little role in the thermal evolution of the gas, since it is important primarily at low densities ($n \lesssim 1\,{\rm cm^{-3}}$), even when the gas is initially highly ionized.

Finally, we note that we do not include the effects of cooling from D_2. As D_2 is a homonuclear molecule, it suffers from the same drawbacks that H_2 does with regard to low-temperature cooling. However, as the results in Section 5.1 demonstrate, it generally has a chemical abundance that is many orders of magnitude smaller than H_2. Thus, in contrast to HD, it appears highly unlikely that D_2 cooling is ever significant.

4.7 Radiative heating

We include two forms of radiative heating that can be significant if a strong UV background is present. The first is the photodissociation of H_2. We calculate the H_2 photodissociation rate as discussed in Section 3, and then, following Black & Dalgarno (1977), we assume that each photodissociation deposits 0.4 eV of heat into the gas. Note that although the photodissociation of other ionic and molecular species (e.g. H_2^+, HD) will also heat the gas, they are unimportant when compared to H_2 photodissociation owing to the low abundances of the other species relative to H_2.

The second form of radiative heating included in our thermal model arises due to the population of excited vibrational states of H_2 produced by radiative pumping by the UV field. At high densities, this leads to heating of the gas, as most of the excited molecules undergo collisional de-excitation. We adopt a radiative pumping rate that is 8.5 times larger than the photodissociation rate (Draine & Bertoldi 1996), and assume that each excitation transfers an average of $2(1 + n_{\rm cr}/n)^{-1}\,{\rm eV}$ to the gas (Burton, Hollenbach & Tielens 1990), where $n_{\rm cr}$ is the H_2 critical density, calculated as discussed in Section 3 above.

4.8 Cosmic ray heating

Following Goldsmith & Langer (1978), we assume that each primary ionization deposits 20 eV of energy into the gas, giving us a heating rate

$$\Gamma_{\rm cr} = 3.2 \times 10^{-28} \left(\frac{\zeta}{10^{-17}\,{\rm s^{-1}}} \right) n\ {\rm ergs\,s^{-1}\,cm^{-3}}, \tag{92}$$

where $\zeta = \sum_i \zeta_i$ and we sum over all species listed in Table A13.

4.9 Chemical heating and cooling

Any exothermic chemical reaction will potentially heat the gas, while any endothermic reaction will cool it. In practice, however, the effect of most reactions on the gas temperature is small, and only in a few cases do we need to take chemical heating or cooling into account.

In highly ionized gas, cooling due to the recombination of hydrogen and helium can be a significant effect, particularly at temperatures which are too low for Lyα cooling to be effective. However, recombination cooling becomes ineffective once the fractional ionization of the gas falls below $x \sim 0.01$, and it therefore plays no role at the high gas densities of interest in this study.

Other forms of chemical cooling included in our model occur due to the collisional dissociation of H_2 (reactions CD9, CD10, CD11 and CD12), the destruction of H_2 by charge transfer with H^+ (reaction CT2), and the collisional ionization of hydrogen and helium (reactions CI1 and CI2). Cooling from these processes may be of some importance at very early times in simulations starting at high temperatures ($T \gtrsim 10^4\,{\rm K}$), but in general the gas temperature is too low for these sources of cooling to be significant.

As far as chemical heating is concerned, the most significant process is H_2 formation heating. When H_2 is formed by reaction AD1 or reaction CT1, it preferentially forms in an excited vibrational state, with an energy comparable to the exothermicity of the reaction (3.73 eV for reaction AD1, 1.83 eV for reaction CT1). In low-density gas, this energy is simply radiated away, but for $n > 10^4\,{\rm cm^{-3}}$, most is instead converted into thermal energy by collisional de-excitation of the newly formed H_2. H_2 formation via H^- or H_2^+ therefore acts as a minor heat source in gas with $n > 10^4\,{\rm cm^{-3}}$.

Three-body formation of H_2 also heats the gas, since the third body in the collision generally carries away additional energy equal to the binding energy of the new H_2 molecule, 4.48 eV. In our

Table 4. List of simulations run.

Run	$n_{\rm i}$(cm^{-3})	$T_{\rm i}$ (K)	$x_{\rm H^+}$	J_{21}	$\zeta_{\rm H}$ (s^{-1})	$C/C_{\rm ref}$	η	Notes
REF	1.0	1000	2.2×10^{-4}	0.0	0.0	1.0	1.0	
C1	1.0	1000	2.2×10^{-4}	0.0	0.0	0.1	1.0	
C2	1.0	1000	2.2×10^{-4}	0.0	0.0	10.0	1.0	
CR1	1.0	1000	2.2×10^{-4}	0.0	10^{-20}	1.0	1.0	
CR2	1.0	1000	2.2×10^{-4}	0.0	10^{-19}	1.0	1.0	
CR3	1.0	1000	2.2×10^{-4}	0.0	10^{-18}	1.0	1.0	
CR4	1.0	1000	2.2×10^{-4}	0.0	10^{-17}	1.0	1.0	
CR5	1.0	1000	2.2×10^{-4}	0.0	10^{-16}	1.0	1.0	
CR6	1.0	1000	2.2×10^{-4}	0.0	10^{-16}	1.0	1.0	No H_3^+ cooling
CR7	1.0	1000	2.2×10^{-4}	0.0	10^{-20}	1.0	1.0	No PT mechanism
CR8	1.0	1000	2.2×10^{-4}	0.0	10^{-18}	1.0	1.0	No PT mechanism
CR9	1.0	1000	2.2×10^{-4}	0.0	10^{-16}	1.0	1.0	No PT mechanism
CR10	1.0	1000	2.2×10^{-4}	0.0	10^{-20}	1.0	1.0	'Maximal' PT mechanism
CR11	1.0	1000	2.2×10^{-4}	0.0	10^{-18}	1.0	1.0	'Maximal' PT mechanism
CR12	1.0	1000	2.2×10^{-4}	0.0	10^{-16}	1.0	1.0	'Maximal' PT mechanism
UV1	1.0	1000	2.2×10^{-4}	10^{-4}	0.0	1.0	1.0	Optically thin
UV2	1.0	1000	2.2×10^{-4}	10^{-2}	0.0	1.0	1.0	Optically thin
UV3	1.0	1000	2.2×10^{-4}	1.0	0.0	1.0	1.0	Optically thin
UV4	1.0	1000	2.2×10^{-4}	10^{-4}	0.0	1.0	1.0	$f_{\rm sh,H_2} = f_{\rm sh,HD} = 0$
UV5	1.0	1000	2.2×10^{-4}	10^{-2}	0.0	1.0	1.0	$f_{\rm sh,H_2} = f_{\rm sh,HD} = 0$
UV6	1.0	1000	2.2×10^{-4}	1.0	0.0	1.0	1.0	$f_{\rm sh,H_2} = f_{\rm sh,HD} = 0$
N1	0.03	1000	2.2×10^{-4}	0.0	0.0	1.0	1.0	
N2	30	1000	2.2×10^{-4}	0.0	0.0	1.0	1.0	
T1	1.0	100	2.2×10^{-4}	0.0	0.0	1.0	1.0	
T2	1.0	10 000	2.2×10^{-4}	0.0	0.0	1.0	1.0	
X1	1.0	1000	10^{-6}	0.0	0.0	1.0	1.0	
X2	1.0	1000	10^{-2}	0.0	0.0	1.0	1.0	
X3	1.0	1000	1.0	0.0	0.0	1.0	1.0	
EL1	1.0	1000	2.2×10^{-4}	0.0	0.0	1.0	1.0	No D
EL2	1.0	1000	2.2×10^{-4}	0.0	0.0	1.0	1.0	No Li
EL3	1.0	1000	2.2×10^{-4}	0.0	0.0	1.0	1.0	No D or Li
RA	1.0	1000	2.2×10^{-4}	0.0	0.0	1.0	1.0	$k_{\rm RA18}$ from reference 1
AR1	1.0	1000	2.2×10^{-4}	0.0	0.0	1.0	1.0	See Section 5.6.3
AR2	1.0	1000	2.2×10^{-4}	0.0	0.0	1.0	1.0	See Section 5.6.3
3B1	1.0	1000	2.2×10^{-4}	0.0	0.0	1.0	1.0	$k_{\rm TB1}$ from reference 2
3B2	1.0	1000	2.2×10^{-4}	0.0	0.0	1.0	1.0	$k_{\rm TB1}$ from reference 3
3B3	1.0	1000	2.2×10^{-4}	0.0	0.0	1.0	1.0	$k_{\rm TB2}$ from reference 4
3B4	1.0	1000	2.2×10^{-4}	0.0	0.0	1.0	1.0	$k_{\rm TB2}$ from reference 3
LP1	1.0	1000	2.2×10^{-4}	0.0	0.0	1.0	1.0	See Section 5.6.4
LP2	1.0	1000	2.2×10^{-4}	0.0	0.0	1.0	1.0	See Section 5.6.4
LP3	1.0	1000	2.2×10^{-4}	0.0	0.0	1.0	1.0	See Section 5.6.4
DYN1	1.0	1000	2.2×10^{-4}	0.0	0.0	1.0	0.6	
DYN2	1.0	1000	2.2×10^{-4}	0.0	0.0	1.0	0.3	
DYN3	1.0	1000	2.2×10^{-4}	0.0	0.0	1.0	0.1	

References: 1 – Stancil et al. (1998); 2 – Palla et al. (1983); 3 – Flower & Harris (2007); 4 – Cohen & Westberg (1983).

reference simulation, this is the dominant heat source for densities $5 \times 10^{10} < n < 2 \times 10^{12}$ cm^{-3}.

5 RESULTS

Our simple one-zone dynamical model of gravitationally collapsing primordial gas contains a number of free parameters. To fully explore the role of H_3^+ cooling and its sensitivity to these free parameters, it is necessary to perform a large number of calculations. However, discussion of the results of all of these calculations to the same level of detail would not only be extremely tedious, but would also run the risk of obscuring our main results. Therefore, we proceed by first discussing in detail in Section 5.1 the results of a single calculation – our reference model, hereafter denoted as computational run REF – before highlighting in the subsequent sections the differences in outcome (if any) that result from alterations in our free parameters. Full details of all of the runs discussed here can be found in Table 4.

5.1 The role of H_3^+ cooling

We begin our study by investigating the outcome of our reference calculation, run REF, whose parameters are indicated in Table 4. In Fig. 1 we show how the fractional abundances of 28 of our 30 chemical species vary with density during the course of the collapse. For clarity, we have divided these species into four sets on the basis of the elements that they contain, and illustrate the evolution of each set separately in Figs 1(a)–(d). The two species that are not plotted – He^+ and He_2^+ – have abundances that remain negligibly small throughout the calculation.

Fig. 1 demonstrates that the evolution of the H_3^+ abundance passes through four distinct phases. In the first phase, at $n \lesssim 10^8$ cm^{-3}, the

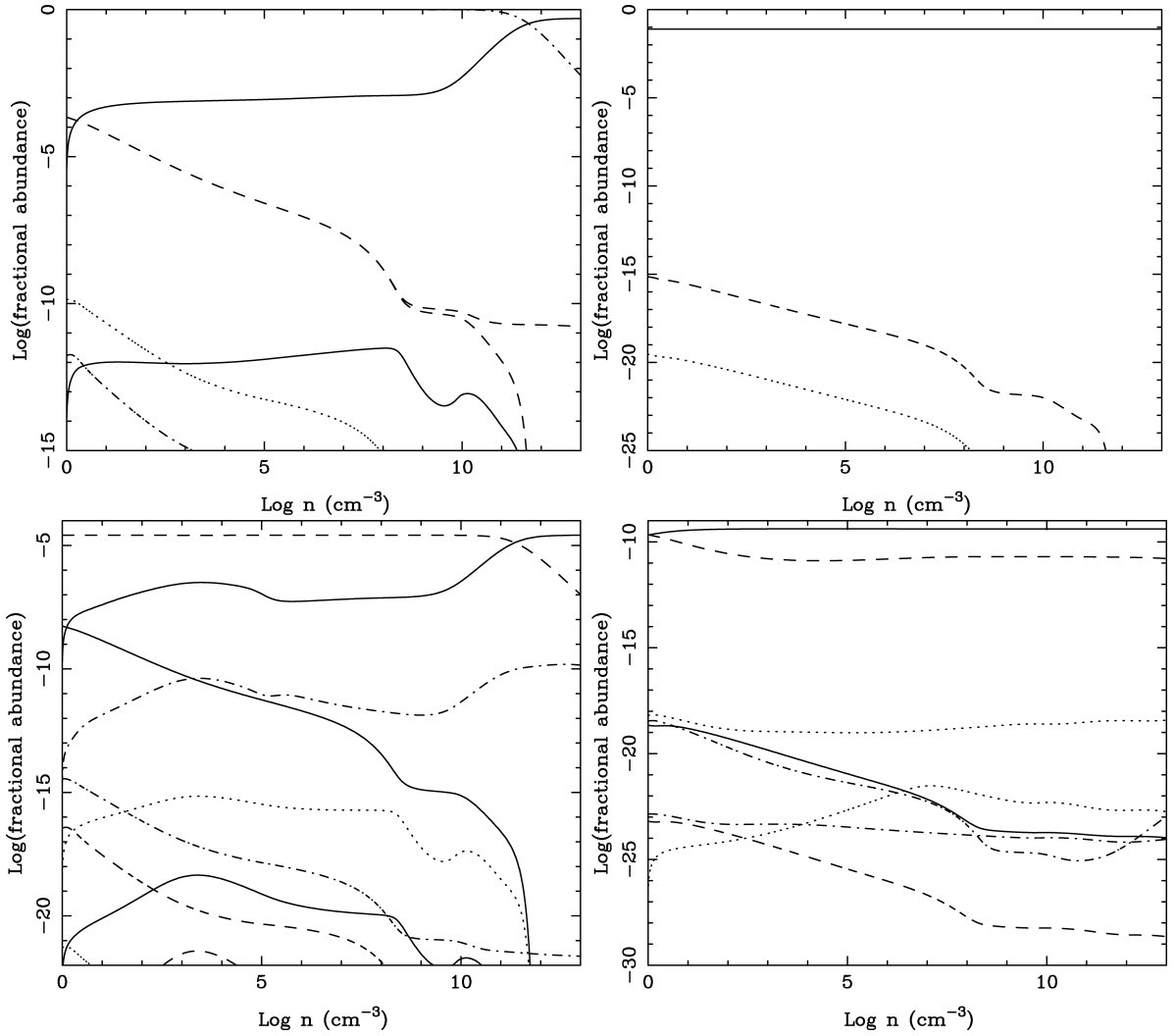

Figure 1. (a) Chemical evolution of the gas in our reference calculation. Fractional abundances are plotted for H_2 (upper solid line), H_3^+ (lower solid line), e^- (upper dashed line), H^+ (lower dashed line), H (upper dash–dotted line), H_2^+ (lower dash–dotted line) and H^- (dotted line). (b) As (a), but showing the fractional abundances of He (solid line), HeH^+ (dashed line) and HeD^+ (dotted line). The abundances of He^+ and He_2^+ remained negligibly small throughout the simulation and are not plotted here. (c) As (a), but for the fractional abundances of HD (upper solid line), D (upper dashed line), D_2 (upper dash–dotted line), D^+ (central solid line), H_2D^+ (upper dotted line), D^- (lower dash–dotted line), HD_2^+ (lower solid line), HD^+ (central dashed line), D_2^+ (lower dotted line) and D_3^+ (lower dashed line). (d) As (a), but for the fractional abundances of Li (upper solid line), Li^+ (upper dashed line), LiH (upper dotted line), Li^- (upper dash–dotted line), LiH_2^+ (lower dotted line), LiH^+ (lower solid line), LiD (lower dash–dotted line) and LiD^+ (lower dashed line).

ratio of H_3^+ to H_2 remains approximately constant: $x_{H_3^+}/x_{H_2} \sim 10^{-9}$. This is a consequence of the balance between two main processes: the formation of H_3^+ by the radiative association of H_2 and H^+ (reaction RA18) and its destruction by dissociative recombination (reactions DR4 and DR5). If we assume that these reactions dominate the formation and destruction of H_3^+, then the corresponding equilibrium abundance of H_3^+ is given by

$$x_{H_3^+} = \frac{k_{RA18} n_{H^+} x_{H_2}}{(k_{DR4} + k_{DR5}) n_e}, \tag{93}$$

which reduces to

$$x_{H_3^+} = \frac{k_{RA18}}{(k_{DR4} + k_{DR5})} x_{H_2} \simeq 10^{-9} x_{H_2} \tag{94}$$

if $x_e = x_{H^+}$, which is a very good approximation at these densities, as Fig. 1(a) demonstrates.

The second phase in the evolution of the H_3^+ abundance begins at a density of around $10^8\,cm^{-3}$, when there is a sudden decrease in the H_3^+ abundance. This decline is caused by the fact that at these densities, dissociative recombination is no longer the only significant destruction mechanism. Increasingly, H_3^+ is also destroyed by reaction TR17:

$$H_3^+ + H \rightarrow H_2^+ + H_2. \tag{95}$$

Although this reaction is endothermic, the temperature of the gas at these densities ($T \gtrsim 800\,K$; see Fig. 2) is high enough to make this mechanism significant in comparison to reactions RA18, DR4 and DR5, owing to the very low fractional ionization of the gas.

The third phase occurs at $n \sim 10^{10}\,cm^{-3}$ as the decline in the H_3^+ abundance is briefly halted by an increase in the H_3^+ formation rate. This is caused by the increase in the H_2 abundance at these densities, which itself is driven by the onset of efficient three-body formation of H_2.

Finally, at a density $n \gtrsim 10^{11}\,cm^{-3}$, the H_3^+ abundance decreases once more, owing to the rapid loss of the few remaining free H^+

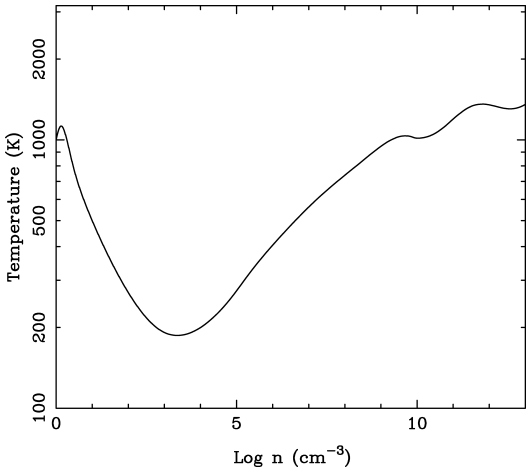

Figure 2. Temperature evolution as a function of gas density in our reference calculation, run REF.

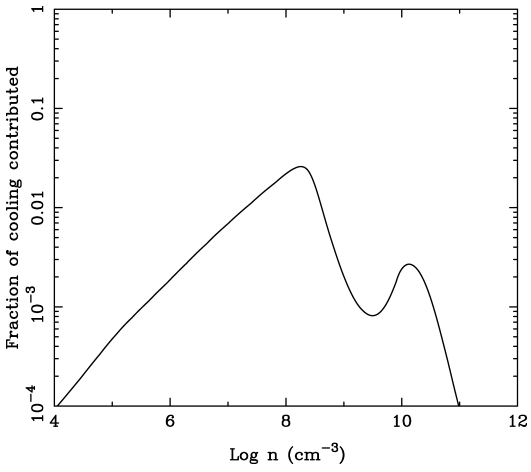

Figure 3. Ratio of the H_3^+ cooling rate to the total cooling rate, plotted as a function of density, for run REF.

ions from the gas, and the consequent disruption of the major H_3^+ formation mechanisms. The reaction responsible for this loss of H^+ ions is the same as the reaction driving the formation of H_3^+, namely RA18. If this were the only process operating, then it would convert all of the H^+ in the gas into H_3^+ in a time $t_{\rm conv}$, given approximately by

$$t_{\rm conv} \sim \frac{1}{k_{\rm RA18} n_{\rm H_2}}. \quad (96)$$

Comparing this time-scale with the free-fall time-scale, $t_{\rm ff} \simeq 1.4 \times 10^{15} n^{-1/2}$ s, and taking $k_{\rm RA18} = 10^{-16}$ cm^3 s^{-1}, we find that $t_{\rm conv} < t_{\rm ff}$ if $n > 50/x_{\rm H_2}^2$. For $x_{\rm H_2} \sim 10^{-3}$, this gives a critical density $n_{\rm conv} \sim 5 \times 10^7$ cm^{-3}. Therefore, in the absence of any other effects, conversion of H^+ to H_3^+ should occur rapidly once the number density exceeds $n_{\rm conv}$. In practice, however, a second effect intervenes. The steady increase in the gas temperature at these densities soon results in reaction TR17 becoming a major destruction mechanism for H_3^+, as noted above. Destruction of H_3^+ by reaction TR17 produces H_2^+ ions, most of which are then destroyed by reaction CT3

$$H_2^+ + H \rightarrow H_2 + H^+, \quad (97)$$

producing H^+ ions. Therefore, most of the H^+ ions that are removed from the gas by reaction RA18 are replaced by this chain of reactions. A net loss of H^+ from the gas occurs only if the H_3^+ ion produced by reaction RA18 is destroyed by dissociative recombination, rather than by reaction TR17. The proportion of the H_3^+ destroyed by dissociative recombination is given by

$$f_{\rm DR} \sim \frac{(k_{\rm DR4} + k_{\rm DR5}) n_{\rm e}}{(k_{\rm DR4} + k_{\rm DR5}) n_{\rm e} + k_{\rm TR17} n_{\rm H}}, \quad (98)$$

where we have assumed that dissociative recombination (reactions DR4 and DR5) and reaction TR17 are the only significant processes destroying H_3^+. Consequently, the net rate at which H^+ ions are removed from the gas is a factor $f_{\rm DR}$ slower than was assumed in our calculation of $t_{\rm conv}$ above, and hence the actual time-scale on which the majority of the H^+ ions are removed is given by

$$t_{\rm loss} = \frac{1}{f_{\rm DR}} t_{\rm conv}. \quad (99)$$

Now, $t_{\rm loss}$ depends on the electron density through $f_{\rm DR}$, and so as long as H^+ is the dominant source of free electrons, decreasing its abundance increases $t_{\rm loss}$, thereby preventing rapid removal of the H^+ ions from the gas. However, once the H^+ abundance falls below $\sim 10^{-11}$, it is singly ionized lithium, Li^+, that becomes the dominant positive ion. At this point, further decreases in $x_{\rm H^+}$ have very little effect on $t_{\rm loss}$. Taking $x_{\rm e^-} = 10^{-11}$ and $T = 1000$ K, and assuming that $(k_{\rm DR4} + k_{\rm DR5}) n_{\rm e} \ll k_{\rm TR17} n_{\rm H}$, we find that $f_{\rm DR} \simeq 10^{-4} x_{\rm H}^{-1}$, and hence $t_{\rm loss} \simeq 10^{20} x_{\rm H} / n_{\rm H_2}$ s. Thus, at the point at which Li^+ first becomes the dominant positive ion, which occurs around $n \sim 10^9$ cm^{-3} in our reference simulation, $t_{\rm loss} \gg t_{\rm ff}$. However, the wholesale conversion of H to H_2 by three-body reactions that begins to set in at around this density rapidly decreases $t_{\rm loss}$, and at $n \sim 10^{11}$ cm^{-3} it becomes shorter than the free-fall time-scale of the gas. At this point, most of the remaining H^+ ions are lost from the gas, following which H_3^+ formation largely ceases. Since the destruction of H_3^+ by reactions DR4, DR5 and TR17 is unaffected by the fall-off in the H^+ abundance, the end result is a very rapid fall-off in the H_3^+ abundance.

To determine whether the small amount of H_3^+ that forms in the gas is enough to significantly affect its thermal evolution, we have compared the H_3^+ cooling rate per unit volume to the total cooling rate per unit volume. The results are plotted in Fig. 3. We see that even at its moment of peak effectiveness, which occurs at $n \sim 10^8$ cm^{-3}, H_3^+ contributes no more than about 3 per cent of the total cooling rate. At lower densities, the H_3^+ ions, which are not yet in LTE, contribute less of the cooling because they undergo fewer collisions. At higher densities, on the other hand, the effectiveness of H_3^+ is reduced by the significant decrease in its chemical abundance, even though each individual H_3^+ ion contributes more cooling than at $n = 10^8$ cm^{-3}.

If H_3^+ is ineffective, then what about other potential coolants, such as LiH, H_2^+ and its deuterated counterparts, or other ions such as HeH^+ or H_2D^+? As far as LiH is concerned, Mizusawa et al. (2005) have already shown that far too little forms for it ever to be a significant coolant, a result which we confirm (cf. our Fig. 1d with their fig. 1b). The contributions made by the other possible coolants are assessed in Figs 4(a) and (b), where for convenience we plot only the sum of the contributions from two sets of species. For the ions in one of these sets (H_2^+, HD^+ and D_2^+; Fig. 4a), we have cooling functions that should be at least reasonably accurate; for those in the other set (H_2D^+, HD_2^+, D_3^+, HeH^+, HeD^+, He_2^+, LiH^+, LiD^+ and LiH_2^+; Fig. 4b), we use the highly

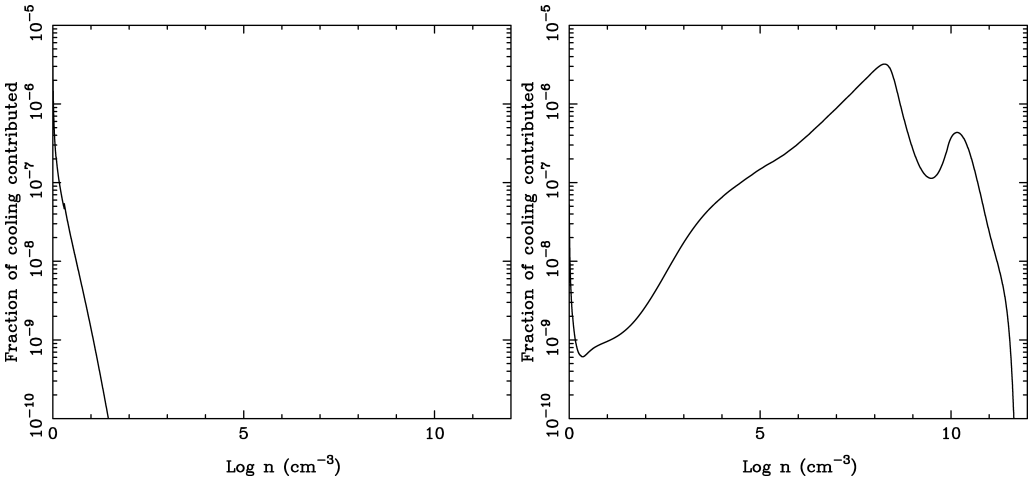

Figure 4. (a) As Fig. 3, but for cooling from H_2^+ and its deuterated counterparts. Note the difference in horizontal and vertical scales from Fig. 3. (b) As (a), but for the sum of the contributions of the minor coolants discussed in Section 4.6.

approximate treatment described in Section 4.6. It is clear from the figures that none of these species contribute significantly to the total cooling rate, which is unsurprising given their extremely small abundances throughout the range of densities examined here (see also Fig. 1).

5.2 Sensitivity to the choice of H_3^+ collision rate

As we saw in the previous subsection, one of the factors preventing H_3^+ from becoming a dominant coolant in our reference calculation is the fact that its abundance begins to decrease, owing to the increasing importance of destruction by collisions with hydrogen atoms, before its cooling rate has reached its LTE limit. If the H_3^+ ion were to reach LTE earlier than we have assumed – in other words, if the low-density limit of its cooling rate were to be larger – then H_3^+ cooling would have more effect. We have therefore explored the effect of altering C, the total H_3^+ collisional excitation rate coefficient that is the single free parameter in our treatment of H_3^+ cooling. The value of C in our reference model, hereafter $C_{\rm ref}$, is given by equation (77). Increasing it or decreasing it compared to this value has the effect of, respectively, increasing or decreasing the low-density H_3^+ cooling rate; or, equivalently, decreasing or increasing the critical density at which H_3^+ reaches LTE.

In Fig. 5, we show the effect that increasing or decreasing C by a factor of 10 has on the contribution made by H_3^+ to the total cooling rate. As one would expect, the result is rather dramatic. In particular, it is clear that if $C = 10\,C_{\rm ref}$, then H_3^+ cooling *does* contribute significantly to the total cooling rate around densities $n \sim 10^8$ cm^{-3}. However, such a large value for C seems unrealistic, given that in our expression for $C_{\rm ref}$, we are already assuming that collisions occur at the Langevin rate. Collisional excitation by electrons could in ideal circumstances give one a large value for C, but it is clear from Fig. 1 that the electron abundance is orders of magnitude too low in the present case for collisions with electrons to be important. Moreover, even if C were as large as $10\,C_{\rm ref}$, the extra cooling provided by the H_3^+ ions would have only a small effect on the temperature evolution, as Fig. 6 demonstrates.

On the other hand, if C is smaller than we have assumed, then H_3^+ cooling has even less effect. Therefore, despite the uncertainties in our treatment of H_3^+ cooling at low densities, our main result – that H_3^+ cooling is, in general, unimportant – seems robust.

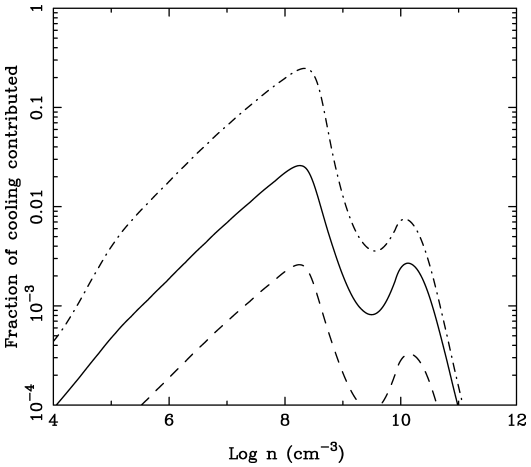

Figure 5. Ratio of the H_3^+ cooling rate to the total cooling rate, plotted as a function of density, for runs in which the total H_3^+ collision rate C was varied. Results are plotted for runs REF (solid line), C1 (dashed line) and C2 (dash–dotted line), corresponding to $C = C_{\rm ref}$, $0.1\,C_{\rm ref}$ and $10\,C_{\rm ref}$, respectively.

5.3 Influence of cosmic rays

In Section 5.1 we saw that a major reason for the dramatic decrease in the H_3^+ abundance at gas densities $n > 10^8$ cm^{-3} is the loss of the remaining H^+ ions from the gas. In the absence of any H^+ ions, H_3^+ can no longer be produced directly by reaction RA18 (formerly, the dominant production mechanism), while its production from reactions involving H_2^+ or HeH^+ is also disrupted, as the main formation routes for these species also depend upon the availability of H^+. Clearly, therefore, one way of significantly enhancing the abundance of H_3^+ at high densities would be to provide a source of H^+ ions at high densities. Alternatively, the H_3^+ abundance could also be enhanced if there were a suitable source of H_2^+ ions in dense gas.

One mechanism capable of producing both H^+ and H_2^+ ions in dense gas is the partial ionization of the gas by an external flux of cosmic rays. In view of the many uncertainties and unknowns regarding the composition, energy spectrum and energy density of the cosmic rays produced by the earliest supernovae, summarized

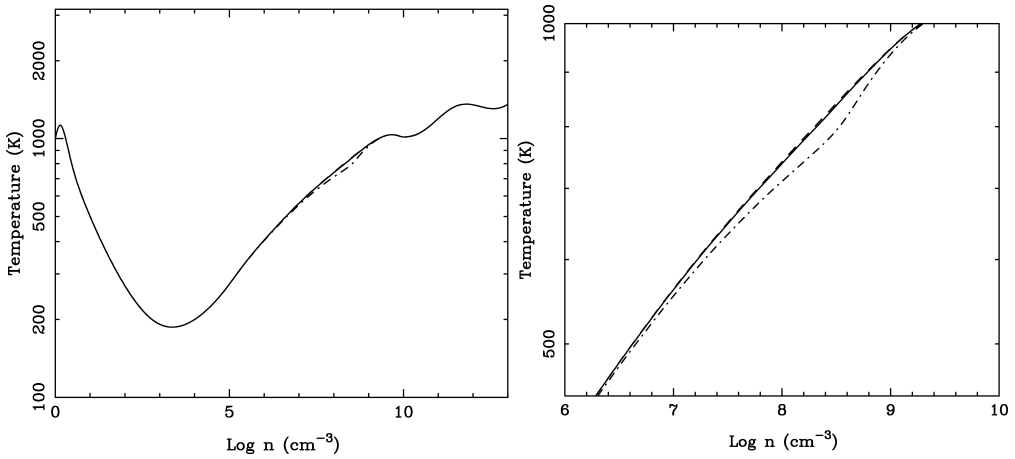

Figure 6. (a) Temperature evolution as a function of gas density for runs in which the total H_3^+ collision rate C was varied. Results are plotted for runs REF (solid line), C1 (dashed line) and C2 (dash–dotted line). Note that the solid and dashed lines are not distinguishable in this plot. (b) As (a), but focusing on a smaller range of densities and temperatures, to better show the difference between the runs. The results of runs REF and C1 remain barely distinguishable.

in Stacy & Bromm (2007) and Jasche, Ciardi & Ensslin (2007), we use a highly simplified treatment of their effects. We assume that all of the uncertainties can be folded into a single free parameter, $\zeta_{\rm H}$, the cosmic ray ionization rate of atomic hydrogen, and that the cosmic ray ionization rates of other atoms and molecules have the same scaling with $\zeta_{\rm H}$ as they are commonly assumed to have in the local ISM. Secondary effects resulting from the Prasad–Tarafdar mechanism are treated as outlined in Section 3.3; note that we assume in this first set of models that Lyα photons make a negligible contribution to the secondary photochemical rates.

In Fig. 7(a), we show how the temperature evolution of the gas changes as we increase $\zeta_{\rm H}$. We show in the figure results from five runs that included cosmic rays: CR1, CR2, CR3, CR4 and CR5, with $\zeta_{\rm H} = 10^{-20}$, 10^{-19}, 10^{-18}, 10^{-17} and $10^{-16}\,{\rm s}^{-1}$, respectively. We also plot the temperature evolution in our reference run REF, for the purposes of comparison. We see that as we increase the cosmic ray ionization rate, the gas gets colder. In particular, for $\zeta_{\rm H} \geq 10^{-18}\,{\rm s}^{-1}$, the gas is able to cool to $T < 100\,{\rm K}$, indicative of the fact that in these runs, HD becomes the dominant low-temperature coolant. This is a simple consequence of the ionization produced by the cosmic rays: the additional free electrons allow more H_2 to be produced than in our reference run (see Fig. 7b), and so the gas can cool to lower temperatures. Stacy & Bromm (2007) find a similar effect in their recent study of the effects of cosmic rays on primordial star formation, and also show that the effect of the cosmic rays on the temperature evolution becomes significant once $\zeta_{\rm H} \geq 10^{-19}\,{\rm s}^{-1}$; we find a slightly larger critical value here, possibly due to the differences in our treatment of H_2 cooling.

In Fig. 7(c), we show how the increase in $\zeta_{\rm H}$ affects the contribution that H_3^+ cooling makes to the total cooling rate. We see that as the ionization rate increases, H_3^+ cooling becomes steadily less effective at low densities, particularly for $\zeta_{\rm H} \geq 10^{-18}\,{\rm s}^{-1}$, owing to the growing importance of HD cooling at these densities. Above $n \sim 10^8\,{\rm cm}^{-3}$, however, the contribution from H_3^+ cooling increases with increasing $\zeta_{\rm H}$. As Fig. 7(d) illustrates, this is a consequence of a significant increase in the high-density H_3^+ abundance in these runs compared to run REF, which is an expected consequence of the greater availability of H^+ and H_2^+ at high densities in the runs with non-zero $\zeta_{\rm H}$.

Fig. 7(c) also demonstrates that if $\zeta_{\rm H} \geq 10^{-18}\,{\rm s}^{-1}$, then H_3^+ is responsible for >10 per cent of the total cooling over several orders of magnitude in gas density. Moreover, if $\zeta_{\rm H} \geq 10^{-17}\,{\rm s}^{-1}$, then there is a brief period in which it provides >50 per cent of the total cooling. Thus, for cosmic ray ionization rates of this order of magnitude, H_3^+ cooling is clearly significant and H_3^+ may even be the dominant source of cooling at densities $n \sim 10^{10}$–$10^{11}\,{\rm cm}^{-3}$.

How plausible is it that the cosmic ray ionization rate in primordial gas will be as large as $10^{-17}\,{\rm s}^{-1}$? This value is comparable with the standard estimates for the cosmic ray ionization rate in dense gas in the local ISM (see e.g. Bergin et al. 1999; van der Tak & van Dishoeck 2000), and lower than recent estimates of the rate in diffuse gas (see e.g. McCall et al. 2003), and so this value is not *prima facie* unreasonable. However, our requirement that the cosmic rays penetrate to very high gas densities means that they must be highly energetic. If we use the same simple model for our collapsing protostellar core as in Section 4.2, then at $n \sim 10^{10}\,{\rm cm}^{-3}$, the core radius is $r \sim 10^{15}\,{\rm cm}$, and the column density of the core is $N \sim 10^{25}\,{\rm cm}^{-2}$. To penetrate to this depth, the cosmic rays must have energies of at least 100 MeV (Stacy & Bromm 2007), which means that given reasonable assumptions regarding the shape of the cosmic ray energy spectrum, the main contribution to the cosmic ray ionization rate will come from cosmic rays with roughly this energy. Following Stacy & Bromm (2007), we can estimate the required energy density in 100 MeV cosmic rays as

$$U_{\rm CR,100MeV} \simeq 4 \times 10^{-13} \left(\frac{\zeta_{\rm H}}{10^{-17}\,{\rm s}^{-1}} \right)\,{\rm erg\,cm}^{-3}. \quad (100)$$

If we further assume that most high-redshift cosmic rays are produced in the supernova remnants left by pair-instability supernovae (Heger & Woosley 2002), then Stacy & Bromm (2007) show that the total cosmic ray energy density $U_{\rm CR}$ is related to the cosmological star-forming rate per unit comoving volume, Ψ_*, by

$$U_{\rm CR}(z) = 2 \times 10^{-15}\,{\rm erg\,cm}^{-3} \left(\frac{p_{\rm CR}}{0.1} \right) \left(\frac{E_{\rm SN}}{10^{52}\,{\rm erg}} \right) \left(\frac{1+z}{21} \right)^{3/2} \times \left(\frac{f_{\rm PISN}}{2 \times 10^{-3}\,{\rm M}_\odot^{-1}} \right) \left(\frac{\Psi_*}{2 \times 10^{-2}\,{\rm M}_\odot\,{\rm yr}^{-1}\,{\rm Mpc}^{-3}} \right), \quad (101)$$

where $p_{\rm CR}$ is the fraction of the supernova explosion energy, $E_{\rm SN}$, that is used to accelerate cosmic rays, and $f_{\rm PISN}$ is the number of pair-instability supernovae per solar mass of stars formed. Given

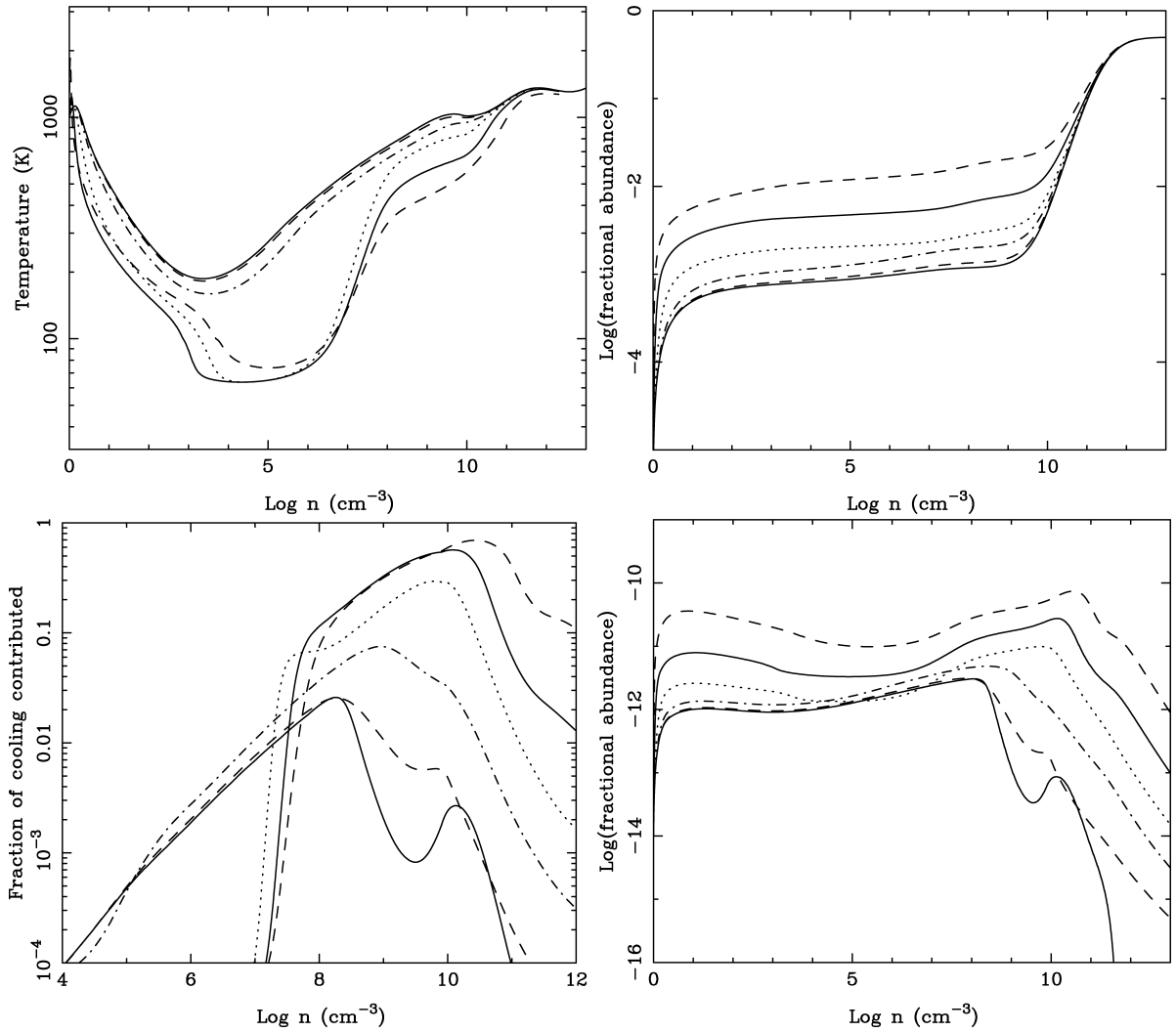

Figure 7. (a) Temperature evolution as a function of gas density for runs in which the cosmic ray ionization rate $\zeta_{\rm H}$ was varied. Results are plotted for runs REF (upper solid line), CR1 (upper dashed line), CR2 (dash–dotted line), CR3 (dotted line), CR4 (lower solid line) and CR5 (lower dashed line), corresponding to $\zeta_{\rm H} = 0.0$, 10^{-20}, 10^{-19}, 10^{-18}, 10^{-17} and $10^{-16}\,{\rm s}^{-1}$, respectively. (b) As (a), but showing the evolution of the H_2 abundance with density in the same set of runs. Note that in this plot the lower solid and dashed lines correspond to runs REF and CR1, respectively, while the upper solid and dashed lines correspond to runs CR4 and CR5, respectively. (c) As (b), but showing the ratio of the H_3^+ cooling rate to the total cooling rate. The lower solid and dashed lines on the right-hand side of the plot correspond to runs REF and CR1, respectively, the dash–dotted and dotted lines to runs CR2 and CR3, respectively, and the upper solid and dashed lines on the right-hand side of the plot to runs CR4 and CR5, respectively. (d) As (c), but showing the evolution of the H_3^+ abundance with density in the same set of runs.

reasonable values for $p_{\rm CR}$, $E_{\rm SN}$ and $f_{\rm PISN}$, this relationship implies that to produce a cosmic ray energy density of the order of $10^{-13}\,{\rm erg\,cm^{-3}}$, we require a star formation rate per unit volume of the order of $1\,{\rm M_\odot\,yr^{-1}\,Mpc^{-3}}$, two to three orders of magnitude larger than current estimates of the Population III star formation rate (Yoshida et al. 2003; Bromm & Loeb 2006). Moreover, this estimate assumes that essentially all of the cosmic ray energy density is in 100 MeV cosmic rays; if we allow for a significant fraction of cosmic rays with smaller energies, as are required to produce the ionization in low-density gas in our simplified model, then the required cosmic star formation rate increases still further.

From this argument, we can conclude that any extragalactic cosmic ray background will be too small to produce the effect that we desire. How about local sources of cosmic rays? Stacy & Bromm (2007) show that much higher energy densities can be produced close to individual supernova remnants, but to get an energy density of $10^{-13}\,{\rm erg\,cm^{-3}}$ one would have to be within $\sim$10 pc of the remnant, near enough that the gas would have been strongly processed by the UV radiation of the supernova progenitor (Glover & Brand 2001; Whalen, Abel & Norman 2004; Susa 2007). Consequently, this scenario for producing a high cosmic ray ionization rate also does not appear promising.

Furthermore, even if we assume that it is possible to maintain a large $\zeta_{\rm H}$ at high densities, and that H_3^+ cooling does briefly become dominant, it is possible to show that its effects on the temperature evolution of the gas remain small. In Fig. 8, we compare the temperature evolution in runs CR5 and CR6. In both runs, we have set $\zeta_{\rm H} = 10^{-16}\,{\rm s^{-1}}$, but in run CR6 we have artificially disabled H_3^+ cooling. We see that at densities $10^8 \lesssim n \lesssim 10^{12}\,{\rm cm^{-3}}$ the temperature in run CR5 is smaller than the temperature in run CR6, as expected. However, the difference is relatively small, and the temperature evolution is qualitatively similar in both cases.

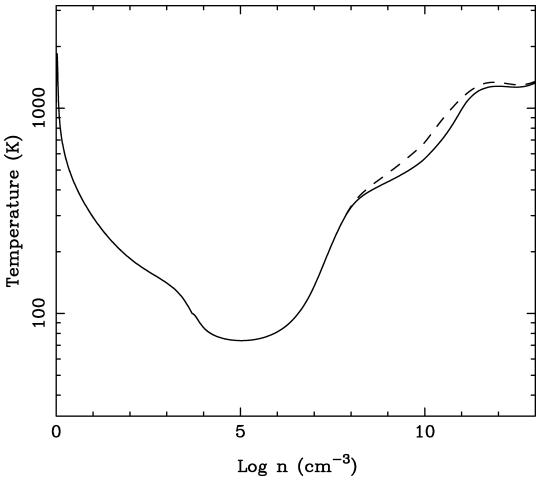

Figure 8. Temperature evolution as a function of gas density in runs CR5 (solid line) and CR6 (dashed line). Both runs share the same set of input parameters, including a cosmic ray ionization rate $\zeta_{\rm H} = 10^{-16}\,{\rm s}^{-1}$, but in run CR6, H_3^+ cooling has been artificially disabled.

Finally, we have examined the importance of cosmic ray induced photoionization and photodissocation (the Prasad–Tarafdar mechanism, discussed in Section 3.3) by performing several additional simulations. In runs CR7, CR8 and CR9, we took $\zeta_{\rm H} = 10^{-20}$, 10^{-18} and $10^{-16}\,{\rm s}^{-1}$, respectively, but neglected the effects of the Prasad–Tarafdar mechanism completely. In runs CR10, CR11 and CR12, we adopted the same cosmic ray ionization rates, but maximized the effects of the Prasad–Tarafdar mechanism by assuming that the Lyα photons produced by secondary excitations of atomic hydrogen could propagate freely into the core of the protogalaxy, and could contribute to the total secondary photoionization and photodissociation rates there (cf. our standard treatment, where we assume that the Lyα photons are unable to penetrate into the core).

In Fig. 9(a) we compare the temperature evolution of the gas in these six runs with the evolution in runs CR1, CR3 and CR5, which have the same values of $\zeta_{\rm H}$, but which include the effects of cosmic ray induced photoprocesses using our standard treatment. In Fig. 9(b), we show a similar comparison of the ratio of H_3^+ cooling to total cooling in these runs.

Below $n = 10^8\,{\rm cm}^{-3}$, the Prasad–Tarafdar mechanism has no discernable effect on the evolution of the gas. At higher densities, however, its effect is to suppress H_3^+ cooling. More specifically, cosmic ray induced photodissociation of H_2^+ (reaction CP3) reduces the amount of H_3^+ formed via reaction TR3, leading to a reduction in the H_3^+ abundance at these densities, and hence an overall reduction in the effectiveness of H_3^+ cooling. Nevertheless, the effect of the enhanced cooling in runs including its effects is slight, as can be seen from Fig. 9(a).

Fig. 9 also allows us to assess the impact of the inaccuracy in our treatment of the Lyα photons produced by secondary excitations of atomic hydrogen. Our results indicate that when $\zeta_{\rm H}$ is small, the Prasad–Tarafdar mechanism has little effect on the amount of H_3^+ cooling that occurs, and so any inaccuracies in our treatment of it are unimportant. In high-$\zeta_{\rm H}$ runs, the Prasad–Tarafdar mechanism is more important, but we find that we obtain very similar results with and without the inclusion of the Lyα photons, and so any inaccuracy in their treatment is again unimportant.

5.4 Influence of a radiation background

In most of our calculations, we have assumed that any external sources of radiation have a negligible effect on the evolution of our collapsing protogalactic gas. At the epoch corresponding to the formation of the very first stars, this assumption is well justified: the CMB does not significantly affect the gas chemistry at redshifts $z < 100$ and no other sources of radiation yet exist. Once Population III star formation begins, however, the situation changes. Radiation

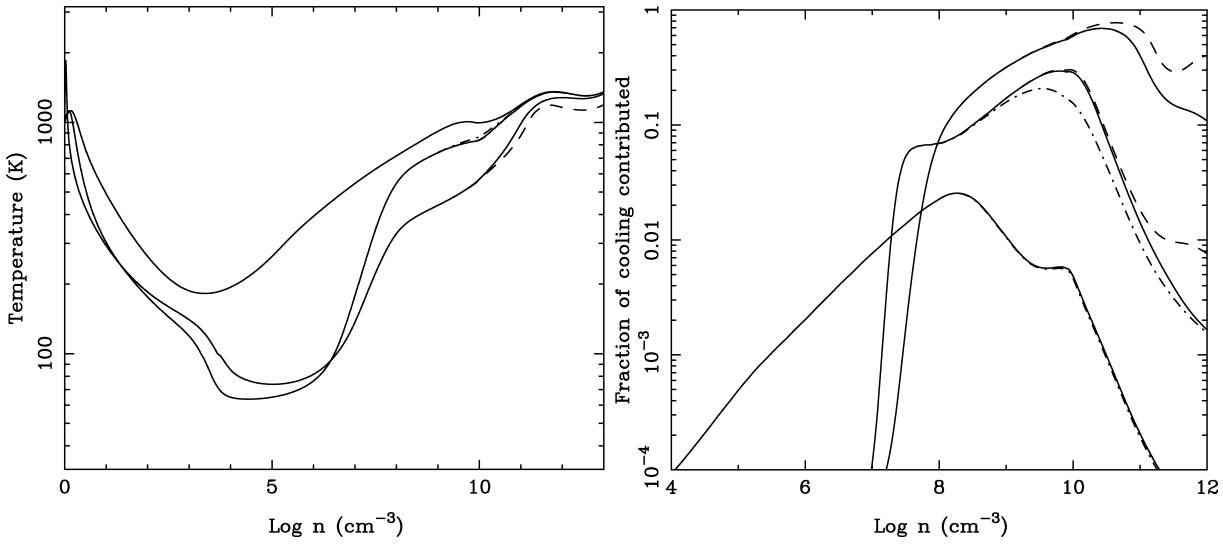

Figure 9. (a) Sensitivity of the temperature evolution to our treatment of the Prasad–Tarafdar mechanism. Solid lines correspond to runs using our default treatment, dashed lines to runs that neglect its effect entirely, and dash–dotted lines to runs that maximize its effects by including the effects of Lyα photons as if the gas were optically thin to them. The lower, middle and upper sets of curves correspond to runs with $\zeta_{\rm H} = 10^{-20}$, 10^{-18} and $10^{-16}\,{\rm s}^{-1}$, respectively. Note that many of the lines in this figure are indistinguishable. (b) As (a), but showing the ratio of the H_3^+ cooling rate to the total cooling rate in the same set of runs. The lower, middle and upper solid lines on the right-hand side of this plot correspond to runs CR1, CR3 and CR5, respectively, the lower, middle and upper dashed lines on the same side correspond to runs CR7, CR8 and CR9, and the lower, middle and upper dash–dotted lines on that side correspond to runs CR10, CR11 and CR12. (Note that the results of runs CR5 and CR12 are indistinguishable in the plot, as are the results of runs CR1, CR7 and CR10.)

from massive Population III stars or from their remnants can affect primordial gas through a variety of mechanisms, as discussed in detail in the recent reviews by Ciardi & Ferrara (2005) and Ciardi (2008). In this section, we explore how an external radiation field can influence the thermal evolution of primordial gas and affect the role of H_3^+ cooling.

5.4.1 Ultraviolet radiation

One of the most important forms of radiative feedback in the high-redshift universe is the build-up of a soft UV background at photon energies $h\nu < 13.6\,\mathrm{eV}$. Photons from this background that are absorbed in the Lyman and Werner band transitions of H_2 can cause photodissociation, and since these photons can propagate to large cosmological distances through the intergalactic medium, the strength of the background and the size of the associated photodissociation rate can both become considerable. This soft UV background is therefore expected to have a significant effect on the evolution of primordial gas within protogalaxies (Haiman, Rees & Loeb 1997; Haiman, Abel & Rees 2000; but see also Wise & Abel 2007 and O'Shea & Norman 2008 for evidence that the effects of the Lyman–Werner background may be less important than previously supposed).

To investigate the impact of such a UV background on our results, we have run several models with non-zero backgrounds: runs UV1, UV2, UV3, UV4, UV5 and UV6. As previously noted in Section 3.2, we assume that the spectral shape of the background is that of a diluted 10^5 K blackbody, with a sharp cut-off at 13.6 eV. The only free parameter is then the normalization of this spectrum. We choose to normalize it by specifying its strength at the Lyman limit. In runs UV1, UV2 and UV3, the field strength is $J_{21} = 10^{-4}$, 10^{-2} and 1.0, respectively, where J_{21} is the flux at the Lyman limit in units of $10^{-21}\,\mathrm{erg\,s^{-1}\,cm^{-2}\,Hz^{-1}\,sr^{-1}}$. In these three runs, we assume that self-shielding by H_2 and HD is not effective, and that the gas remains optically thin to the external radiation field throughout the simulation. In runs UV4, UV5 and UV6, the field strength is the same as in runs UV1, UV2 and UV3, respectively, but we assume that H_2 and HD self-shielding is so effective that the H_2 and HD photodissociation rates are negligible. The true behaviour of the gas lies between these two limiting cases.

In Fig. 10(a), we show how the gas temperature evolves in optically thin runs UV1, UV2 and UV3, as well as in run REF for comparison. The corresponding behaviour in runs UV4, UV5 and UV6 is shown in Fig. 10(b). In the optically thin runs, the effect of the UV background is to increase the temperature of the gas at early times; quite dramatically so in the case of run UV3, where the minimum temperature reached by the gas is $T \sim 900$ K, compared to only $T \sim 200$ K in our reference calculation. This temperature increase is an obvious consequence of the photodissociation of H_2 in low-density gas, as can be seen clearly by comparing these results with those from the runs in which H_2 photodissociation was assumed to be negligible.

As far as H_3^+ cooling is concerned, Fig. 11 demonstrates that it remains ineffective in both sets of runs. In the optically thin runs, H_2 dissociation at early times reduces the effectiveness of H_2 cooling, but also significantly reduces the H_3^+ abundance. The net effect is to reduce the amount of cooling coming from H_3^+ to below the level that it has in our reference run. At densities $n \gtrsim 10^9\,\mathrm{cm^{-3}}$, on the other hand, the effect of the UV background is to enhance cooling from H_3^+. This occurs because the H^+ abundance does not decline so quickly in the runs with the UV background, owing to the higher gas temperature, and so more free protons are available for making H_3^+ at very high densities. This effect boosts the contribution of H_3^+ to the cooling rate in run UV3 by about a factor of 4 compared to our reference run. Despite this, however, the contribution from H_3^+ remains unimportant.

In runs UV4, UV5 and UV6, the behaviour of the contribution from H_3^+ is somewhat different. The H_2 abundance in these runs evolves in almost the same manner as in run REF, as does the temperature. Therefore at early times, there is no difference in the H_3^+ contribution. At $n > 10^7\,\mathrm{cm^{-3}}$, however, a difference does become apparent between run REF and runs UV5 and UV6, with the H_3^+ contribution falling off faster the more the strength of the UV background is increased. This behaviour is again a result of a change

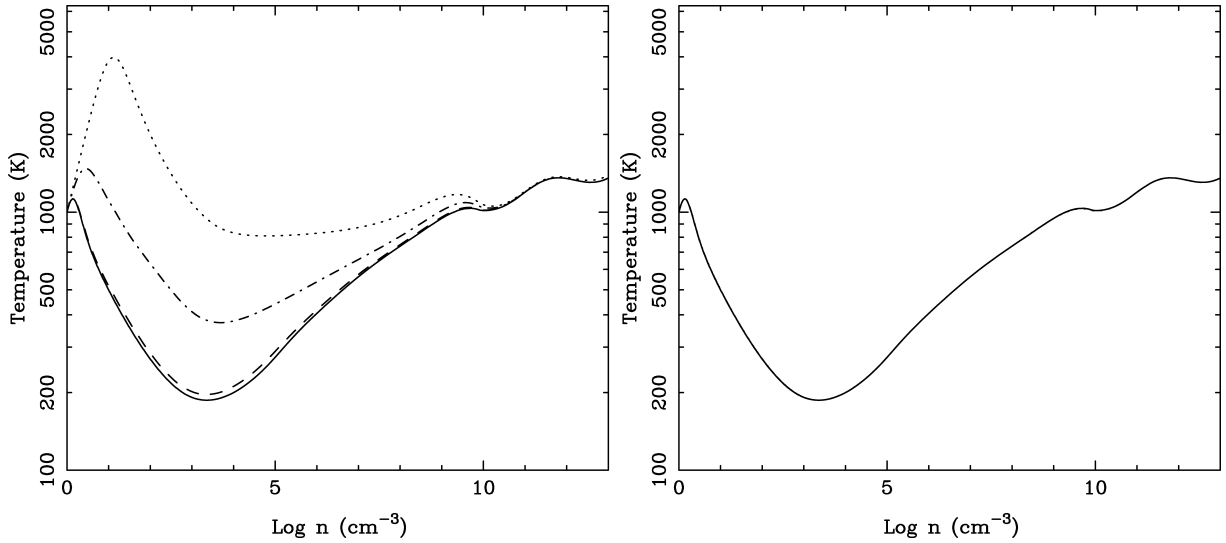

Figure 10. (a) Temperature evolution as a function of gas density in runs REF (solid line), UV1 (dashed line), UV2 (dash–dotted line) and UV3 (dotted line). The strength of the UV background in these runs was $J_{21} = 0.0$, 10^{-4}, 10^{-2} and 1.0, respectively, and the gas was assumed to remain optically thin throughout its evolution. (b) As (a), but for runs REF, UV4, UV5 and UV6. Runs UV4, UV5 and UV6 had the same UV background field strengths as runs UV1, UV2 and UV3, respectively, but in this case we assumed that the gas was optically thick in the Lyman–Werner lines of H_2 and HD. The results of the four runs are indistinguishable in the plot.

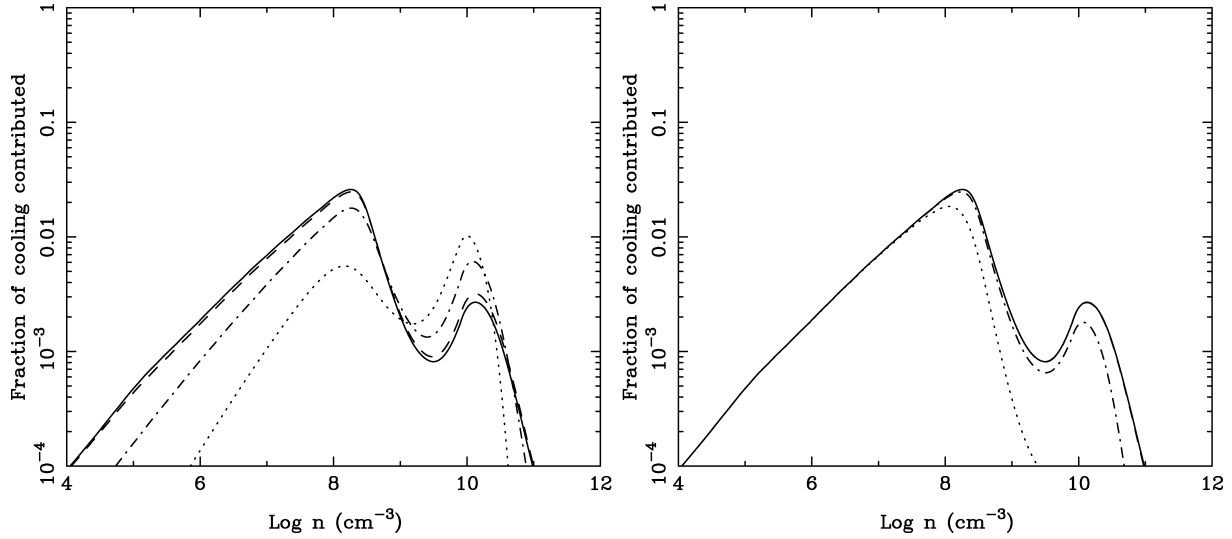

Figure 11. (a) Ratio of the H_3^+ cooling rate to the total cooling rate in runs REF (solid line), UV1 (dashed line), UV2 (dash–dotted line) and UV3 (dotted line). (b) As (a), but for runs REF (solid line), UV4 (dashed line), UV5 (dash–dotted line) and UV6 (dotted line).

in the behaviour of the H^+ abundance at high densities. In this case, the H^+ abundance falls off faster at high density when the UV field strength is increased. This occurs because the UV background maintains a higher Li^+ fraction in the gas than in our reference calculation. Because the Li^+ abundance is larger, it contributes more free electrons to the gas, and so the fraction of H_3^+ ions that are destroyed by dissociative recombination in the high-density regime becomes larger. Consequently, fewer of the H^+ ions destroyed by reaction RA18 are recycled by reaction TR17, and so the H^+ and H_3^+ abundances fall off more rapidly than in our reference model. A similar effect is not seen in the optically thin runs because it is more than offset by the effects of the higher gas temperature, which increases the rate of reaction TR17, thereby decreasing the fraction of H_3^+ ions that are destroyed by dissociative recombination.

5.4.2 X-rays

X-rays are another form of radiation that can affect the evolution of primordial gas. By providing an additional source of ionization in dense gas, they can promote H_2 formation (Haiman, Rees & Loeb 1997; Haiman, Abel & Rees 2000; Glover & Brand 2003; Machacek, Bryan & Abel 2003), in much the same manner as the cosmic rays considered in Section 5.3. However, just as in the case of cosmic rays, for X-rays to materially affect the importance of H_3^+ cooling, they must be able to penetrate deeply into the collapsing protostellar core, to densities $n \sim 10^{10}\,\mathrm{cm}^{-3}$ or more, corresponding to column densities $N \sim 10^{25}\,\mathrm{cm}^{-2}$ or more. As a core with this column density is opaque even to hard X-ray photons, the photon flux required to produce a significant photoionization rate is considerable.

Given reasonable assumptions regarding the shape of any high-redshift hard X-ray background, the dominant contribution to the photoionization rate at $n = 10^{10}\,\mathrm{cm}^{-3}$ comes from X-ray photons with energies $E \sim 3$ keV (Yan, Sadeghpour & Dalgarno 1998). The hydrogen ionization cross-section at this energy is approximately $10^{-24}\,\mathrm{cm}^2$, and so for a column density $N = 10^{25}\,\mathrm{cm}^{-2}$, the gas has an optical depth $\tau \sim 10$ for a 3-keV photon. Each of the photons that is absorbed is responsible for roughly 100 ionizations, once the effects of secondary ionization are taken into account (Dalgarno, Yan & Liu 1999). Therefore, a flux F_X of 3-keV photons incident on the cloud exterior produces an ionization rate R_X given approximately by

$$R_\mathrm{X} \sim 100 \left(10^{-24} F_\mathrm{X} \Delta\nu\right) \mathrm{e}^{-10}\ \mathrm{s}^{-1}, \\ \sim 1.1 \times 10^{-9} F_\mathrm{X}\ \mathrm{s}^{-1}, \quad (102)$$

where the second line follows if we assume that $\Delta\nu \sim 1\,\mathrm{keV}/h$. Inverting this expression, we obtain

$$F_\mathrm{X} \sim 9 \times 10^{-9} \left(\frac{R_\mathrm{X}}{10^{-17}\ \mathrm{s}^{-1}}\right) \text{photons s}^{-1}\,\mathrm{cm}^{-2}\,\mathrm{Hz}^{-1}. \quad (103)$$

This corresponds to an X-ray background field strength at $E = 3$ keV of

$$I_\mathrm{X} = 4.2 \times 10^{-17} \left(\frac{R_\mathrm{X}}{10^{-17}\ \mathrm{s}^{-1}}\right) \mathrm{erg\,s^{-1}\,cm^{-2}\,Hz^{-1}}, \quad (104)$$

which is orders of magnitude larger than any plausible range of values for the high-redshift X-ray background (see e.g. Glover & Brand 2003). We can therefore rule out an extragalactic X-ray background as the source of the required hard X-ray photons.

Furthermore, although higher X-ray fluxes can be maintained close to strong X-ray sources such as miniquasars (Haiman et al. 2000; Kuhlen & Madau 2005), even in this case it is difficult to produce a significant ionization rate. For example, the luminosity at 3 keV of the model miniquasars considered by Kuhlen & Madau (2005), assuming their hardest spectral model, is $L_\mathrm{X} \simeq 10^{22}\,\mathrm{erg\,s^{-1}\,Hz^{-1}}$. To see a flux $I_\mathrm{X} = 4.2 \times 10^{-17}\,\mathrm{erg\,s^{-1}\,cm^{-2}\,Hz^{-1}}$ from this miniquasar, one must therefore be within a distance

$$r \simeq \left(\frac{L_\mathrm{X}}{I_\mathrm{X}}\right)^{1/2} = 5.0\,\mathrm{pc} \quad (105)$$

of it. Gas this close to the miniquasar would have been strongly processed by the UV radiation of its progenitor, and is not a promising place to expect to find further star formation.

We therefore consider it likely that the hard X-ray flux seen by most collapsing protostellar cores will be far too small to significantly affect the production of H_3^+ at high densities. Moreover, even if somehow a sufficiently large flux was produced, we would expect its effects to be very similar to those of the cosmic rays considered in Section 5.3. Accordingly, we do not consider it necessary

or time-efficient to examine the effects of a hard X-ray flux in any greater detail.

5.5 Sensitivity to initial conditions

5.5.1 Altering the initial density and temperature

In order to verify that our main results are not sensitive to the initial temperature or density assumed in our models, we have performed several calculations with different initial densities or temperatures. In runs N1 and N2, we set $n_i = 0.03$ and $30\,\mathrm{cm}^{-3}$, respectively, while keeping all of the other input parameters fixed. The effect that this has on the thermal state of the gas is illustrated in Fig. 12(a), where we compare the temperature evolution in runs N1 and N2 with the evolution in our reference calculation, run REF. It is clear from the figure that the temperature evolution of the three runs is strongly convergent, in line with previous findings (see e.g. Palla et al. 1983; Omukai 2000). Consequently, it comes as no surprise to find that the contribution that H_3^+ makes to the cooling in the three runs is not greatly affected by the choice of n_i, as shown in Fig. 12(b).

In runs T1 and T2, we set $T_i = 100$ and 10 000 K, respectively, and performed a similar comparison, which is illustrated in Fig. 13. Again we find that the results of runs T1, T2 and our reference run REF converge well, although the differences in this case are slightly larger than those that occur when n_i is varied.

5.5.2 Altering the initial fractional ionization

We have also explored the effect of altering the initial fractional ionization of the gas. In runs X1, X2 and X3, we set the initial H^+

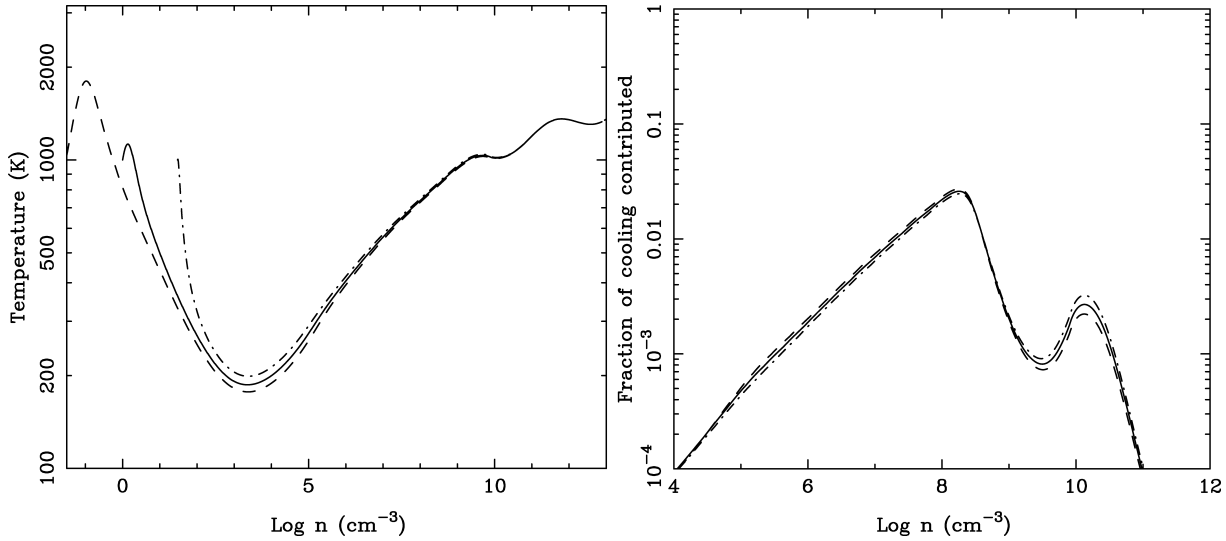

Figure 12. (a) Temperature evolution of the gas for various different initial densities. Results are plotted for runs REF, N1 and N2, which have initial densities $n_i = 1\,\mathrm{cm}^{-3}$ (solid line), $n_i = 0.03\,\mathrm{cm}^{-3}$ (dashed line) and $n_i = 30\,\mathrm{cm}^{-3}$ (dash–dotted line), respectively. (b) As (a), but showing the ratio of the H_3^+ cooling rate to the total cooling rate for the three different models.

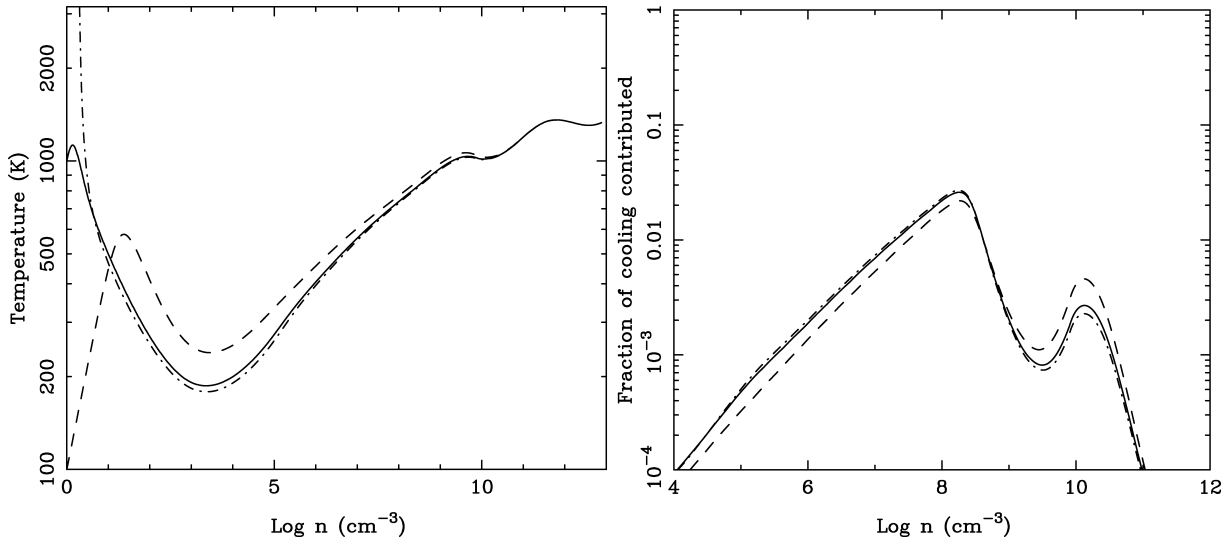

Figure 13. (a) Temperature evolution of the gas for various different initial temperatures. The results plotted are from runs REF, T1 and T2, which had initial temperatures of $T_i = 1000$ K (solid line), $T_i = 100$ K (dashed line) and $T_i = 10\,000$ K (dash–dotted line), respectively. (b) As (a), but showing the ratio of the H_3^+ cooling rate to the total cooling rate for the three different models.

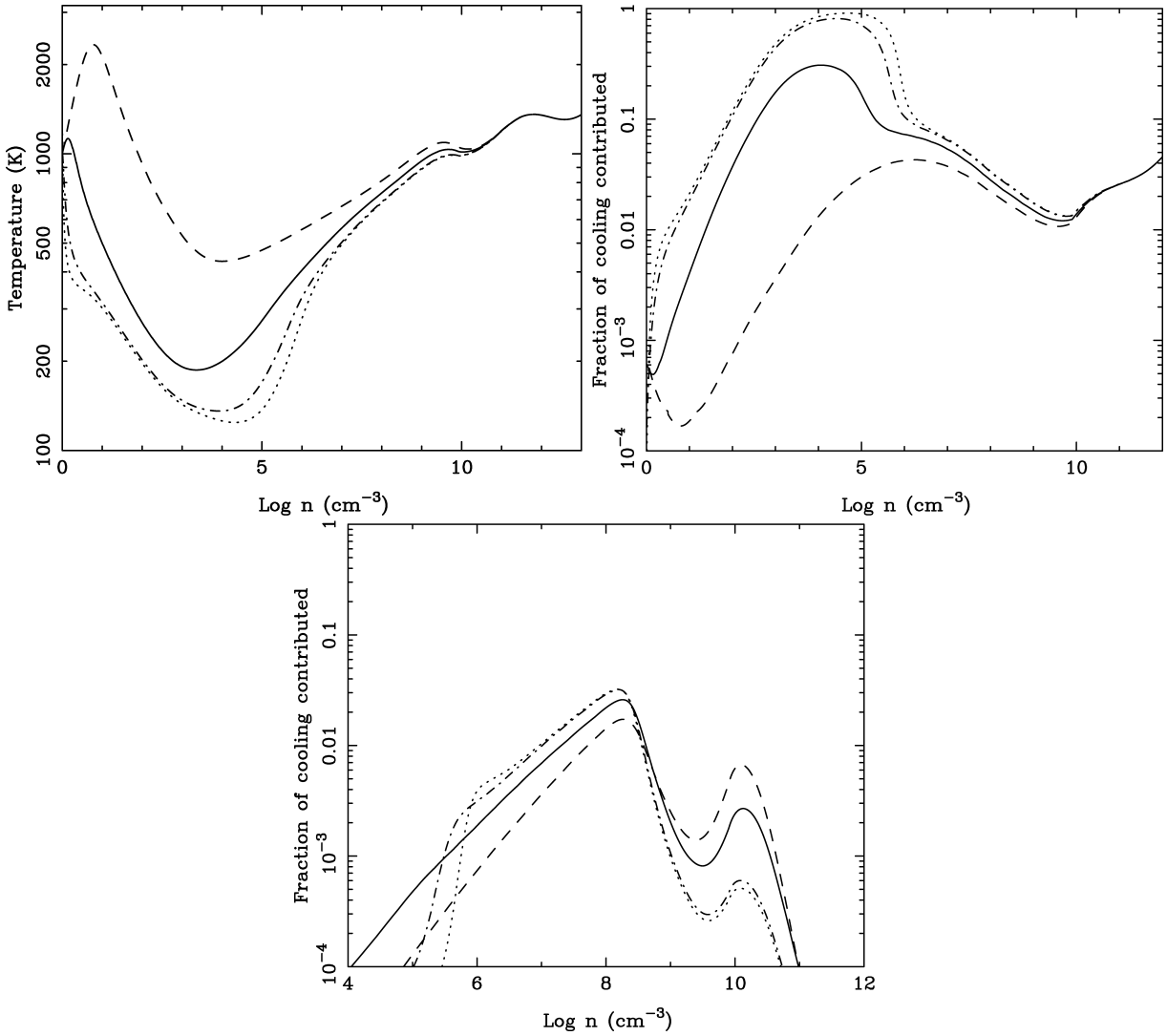

Figure 14. (a) Temperature evolution of the gas in runs REF (solid line), X1 (dashed line), X2 (dash–dotted line) and X3 (dotted line), which had initial H^+ abundances of $x_{H^+} = 2.2 \times 10^{-4}$, 10^{-6}, 10^{-2} and 1.0, respectively. (b) As (a), but showing the ratio of the HD cooling rate to the total cooling rate in these four runs. (c) As (b), but for the ratio of the H_3^+ cooling rate to the total cooling rate.

abundance to 10^{-6}, 10^{-2} or 1.0, respectively. We also rescaled the initial D^+ abundances by a similar amount. However, the initial He^+ abundance was not altered. As Fig. 14(a) demonstrates, altering the initial fractional ionization in this way has a dramatic effect on the temperature evolution of the gas. In run X1, the low abundances of free electrons and of H^+ delay the formation of H_2 and limit the amount that can form. The gas therefore undergoes a period of adiabatic heating that lasts for much longer than in our reference calculation. Furthermore, once enough H_2 has formed to cool the gas, the gas temperature remains significantly higher than in run REF. However, the two runs eventually converge at $n \sim 10^{10}\,\mathrm{cm}^{-3}$, as at this density three-body processes dominate the formation of H_2, and so the H_2 abundance, and hence the thermal evolution of the gas, are no longer sensitive to the fractional ionization.

In runs X2 and X3, on the other hand, the enhanced initial ionization has the effect of promoting the formation of H_2, and cooling the gas more than in our reference run. Moreover, the cooling provided by this extra H_2 is sufficient to lower the gas temperature to a level at which chemical fractionation between HD and H_2 becomes highly effective. The resulting boost in the HD abundance allows it to dominate the gas cooling and to cool the gas to a lower temperature than could be reached by H_2 cooling alone. Note, however, that in contrast to the results of previous studies (see e.g. Nakamura & Umemura 2002; Nagakura & Omukai 2005; Johnson & Bromm 2006; Yoshida et al. 2007), the gas does not reach the CMB temperature. This is a consequence of the relatively rapid rate of collapse assumed here (cf. Section 5.7) and of the revised treatment of H_2 cooling used in this paper, which tends to render H_2 cooling less effective, as explored in more detail in Glover & Abel (2008). In any case, the period of HD dominance lasts for only a short time, as illustrated in Fig. 14(b). As the HD level populations near their LTE values, HD cooling becomes less effective and the gas starts to warm. As it warms, chemical fractionation becomes less effective and the HD:H_2 ratio declines. Once the gas has warmed to $T \sim 200\,\mathrm{K}$, which occurs at a density between 10^5 and $10^6\,\mathrm{cm}^{-3}$, the amount of HD remaining in the gas is no longer sufficient to maintain HD as the dominant coolant; H_2 becomes dominant once more, with HD thereafter relegated to a minor role.

In Fig. 14(c), we show how the ratio of the H_3^+ cooling rate to the total cooling rate varies in these runs. We see that if the initial fractional ionization is lowered, the contribution of H_3^+ to the cooling is lowered at $n < 10^9\,\mathrm{cm}^{-3}$ and increased at $n > 10^9\,\mathrm{cm}^{-3}$ relative to our reference calculation. The lowered importance of H_3^+ cooling at low densities is a result of the higher gas temperature: the greater temperature sensitivity of the H_2 cooling rate compared to the H_3^+ cooling rate makes the former more effective in comparison to the latter as the temperature is raised. At high densities, the gas temperatures converge, and the difference between the runs has a different cause: the lower H_2 abundance (discussed at the beginning of this subsection) increases the time required to convert all of the H^+ to H_3^+. For this reason, the H^+ abundance in $n \sim 10^9$–$10^{10}\,\mathrm{cm}^{-3}$ gas in the low ionization run is higher than in the reference run, with the result that the H_3^+ abundance and the H_3^+ contribution to the cooling are also marginally higher.

If the initial fractional ionization is increased, an interesting effect occurs. The contribution of H_3^+ to the total cooling rate is considerably suppressed at densities $n < 10^6\,\mathrm{cm}^{-3}$ and $n > 10^{8.5}\,\mathrm{cm}^{-3}$ compared to the contribution in our reference run, but is slightly *enhanced* at densities $10^6 < n < 10^{8.5}\,\mathrm{cm}^{-3}$. The reduction in the effectiveness of H_3^+ at low densities in these runs is a result of the previously noted strong enhancement of the HD cooling rate at $n < 10^6\,\mathrm{cm}^{-3}$, as can clearly be seen by comparing Figs 14(b) and (c). On the other hand, the suppression of H_3^+ cooling at $n > 10^{8.5}\,\mathrm{cm}^{-3}$ results from the rapid loss of H^+ in the gas driven by reaction RA18, which occurs more rapidly than in the reference run owing to the greater H_2 abundance in these runs. Between these two density regimes, there is a small range of densities in which the H_3^+ : H_2 ratio remains relatively large, and where the gas temperature is ∼300–500 K. At these temperatures, the ratio of the H_3^+ to H_2 cooling rates is larger than at $T = 1000\,\mathrm{K}$, owing to the greater temperature dependence of the H_2 cooling rate, but the temperature is not low enough for the HD abundance to be significantly enhanced by chemical fractionation. These conditions are therefore close to ideal for H_3^+ cooling, and the fact that even in this case the H_3^+ contributes no more than a few per cent of the total cooling helps to strengthen our conclusion that it is generally of little or no importance.

5.5.3 *Changing the elemental composition*

Finally, we have examined the effect of changing the elemental composition of the gas by removing all of the deuterium (run EL1), lithium (run EL2) or both (run EL3). Although not physically realistic, these runs do provide a convenient way to examine the roles that the deuterium and lithium play in the overall thermal evolution of the gas. In Fig. 15, we show how the gas temperature evolves in run EL1 in comparison to our reference calculation, run REF. We see that the omission of deuterium has a noticeable effect on the temperature evolution at densities $10^3 < n < 10^6\,\mathrm{cm}^{-3}$, and a very slight effect on the temperature at densities $n > 10^{12}\,\mathrm{cm}^{-3}$. Examination of the contribution of HD cooling to the total cooling rate in run REF (plotted as the solid line in Fig. 14b) demonstrates that at these densities, HD contributes significantly to the total cooling rate; indeed, at its peak at $n \sim 10^4\,\mathrm{cm}^{-3}$, it contributes almost a third of the total cooling. At first sight, this result is rather surprising, as it is often assumed that HD cooling is unimportant in primordial gas unless the gas has a large initial fractional ionization, as in runs X2 or X3 discussed above. However, it appears that the conventional wisdom is wrong on this point; our results here are consistent with those of previous studies that have included HD (see e.g. Bromm et al. 2002; Mizusawa et al. 2005), and show that although HD is never the *dominant* coolant, it does contribute enough to the total cooling rate at densities $n \sim 10^4$–$10^5\,\mathrm{cm}^{-3}$ to warrant inclusion in future models of Population III star formation.

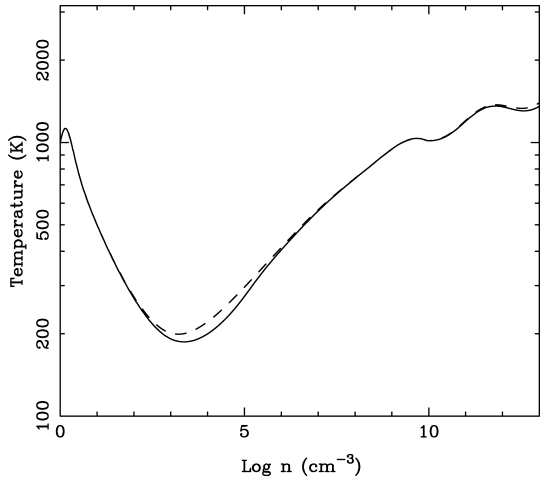

Figure 15. Temperature evolution as a function of density in runs REF (solid line), which had the standard cosmological deuterium abundance, and EL1 (dashed line), in which the deuterium abundance was set to zero.

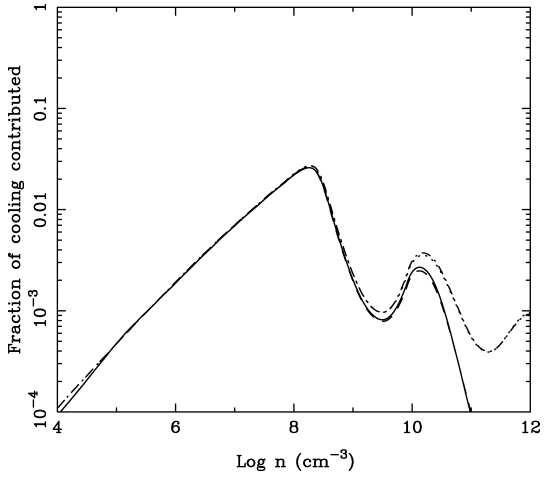

Figure 16. Contribution of H_3^+ cooling to the total cooling rate in runs with no deuterium (EL1; dashed), no lithium (EL2; dash–dotted) and no deuterium or lithium (EL3; dotted), along with the results of our reference run REF (solid) for comparison. Note that the dashed and solid lines are barely distinguishable from each other; similarly, the dotted and dash–dotted lines are not distinguishable in this plot.

In run EL2, the temperature evolution is essentially the same as in run REF, while in run EL3, the evolution is the same as in run EL1, indicating that lithium does not play a significant role in the cooling of the gas, in agreement with the results presented in Section 5.1; note that runs EL2 and EL3 are not plotted in Fig. 15, as they would not be distinguishable from the existing lines. In Fig. 16, we investigate the size of the contribution that H_3^+ makes to the total cooling rate in runs EL1, EL2 and EL3; we also plot the result from run REF for purposes of comparison. The most obvious point to note is that in the runs without lithium, namely EL2 and EL3, the H_3^+ contribution no longer falls off sharply at high densities, although it remains too small to be significant. This is easy to understand, given our

previous discussion of the chemistry of the gas at high densities and low fractional ionizations (see Section 5.1). As previously noted, in the absence of lithium, the net rate of removal of H^+ ions from the gas via reaction RA18 decreases as the fractional ionization decreases, since an increasing fraction of the H_3^+ created by reaction RA18 is converted back to H_2 and H^+ by reactions TR17 and CT3, instead of being destroyed by reactions DR4 and DR5. Therefore, the H^+ removal time-scale, $t_{\rm loss}$, remains longer than the free-fall time-scale throughout the simulation, and the H^+ abundance falls off gradually at high densities; the rapid fall-off that occurs in our reference run once $t_{\rm loss} < t_{\rm ff}$ does not take place. Consequently, the corresponding rapid fall-off in the H_3^+ abundance also does not occur, as the H_3^+ formation rate never becomes negligible.

Although the presence or absence of lithium does not affect the conclusions of our current study, as in either case cooling from H_3^+ is negligible, it is clear that if one is interested in determining the fractional ionization of the gas accurately at very high densities, it is vital to include Li and Li^+ in the chemical model (see also Maki & Susa 2004, who come to a similar conclusion).

5.6 Sensitivity to uncertainties in the chemical rate coefficients

5.6.1 Reaction RA18

As we have already discussed in Section 3, large uncertainties exist in the rate coefficients of a number of the processes included in our chemical model. Of particular relevance to this paper is the huge uncertainty that appears to exist in the value of the rate coefficient for reaction RA18, the formation of H_3^+ by the radiative association of H_2 with H^+. In Fig. 17, we compare the contribution of H_3^+ cooling in our reference calculation (solid line), in which we adopt the large Gerlich & Horning (1992) rate coefficient for reaction RA18, with the contribution of H_3^+ cooling in run RA, a similar calculation that adopts the smaller Stancil et al. (1998) rate coefficient (dashed line). We see that H_3^+ is less effective in the latter case, and that its effectiveness also peaks at a later point in the simulation.

However, the reduction in the H_3^+ contribution is less than one might expect given the very large difference in $k_{\rm RA18}$ between the two runs. The reason for this is that although the rate of H_3^+ formation by radiative association is strongly suppressed, other H_3^+ formation mechanisms remain unaffected. The H_3^+ formed in run RA is produced primarily by the familiar reaction

$$H_2^+ + H_2 \rightarrow H_3^+ + H, \tag{106}$$

with the necessary H_2^+ coming mainly from reaction RA3, namely

$$H + H^+ \rightarrow H_2^+ + \gamma. \tag{107}$$

The persistence of a significant H_3^+ contribution at later times in run RA than in run REF is a clear consequence of the fact that the rate at which H^+ ions are removed from the gas by reaction RA18 is smaller in the former run than in the latter. As a result, the familiar rapid fall-off in the H^+ abundance that occurs once the H^+ removal time-scale, $t_{\rm loss}$, becomes smaller than the free-fall time (see Section 5.1) takes place at a later time in run RA than in run REF, and hence the corresponding fall-off in the H_3^+ abundance also occurs at a later point in the evolution of the gas.

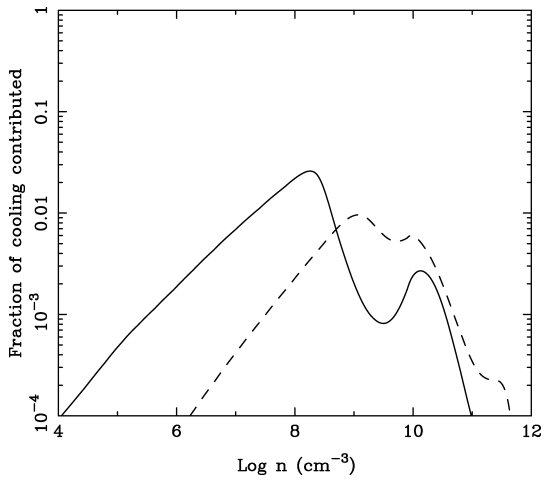

Figure 17. Ratio of the H_3^+ cooling rate to the total cooling rate in runs REF (solid line) and RA (dashed line). These runs used values for $k_{\rm RA18}$ that differed by four orders of magnitude, and that were taken from Gerlich & Horning (1992) and Stancil et al. (1998), respectively.

5.6.2 Reactions TB1 and TB2

Large uncertainties also exist in the rate coefficients for three-body H_2 formation (reactions TB1 and TB2). As illustrated in Fig. 18, these uncertainties significantly affect the temperature evolution of the gas at densities $n > 10^8$ cm^{-3}, particularly the uncertainty in the rate of reaction TB1. The use of larger values for the three-body reaction rates leads to faster production of H_2 at high densities, and hence a greater H_2 cooling rate. This has the effect of slowing the rise in the gas temperature at these densities, which may affect the ability of the gas to fragment at late times (see Clark, Glover & Klessen 2008). However, in the present context, the effect of the faster H_2 formation rates is to make cooling by H_3^+ even less effective at late times than in our reference calculation, as demonstrated in Fig. 19, where we examine the effect that varying the rate of both reactions has on the contribution that H_3^+ makes to the total cooling rate.

5.6.3 Reaction AD1

The uncertainty in the rate of reaction AD1 discussed in Glover et al. (2006) also affects the temperature evolution of the gas. We have examined two cases, runs AR1 and AR2. In run AR1, we use a rate coefficient $k_{\rm AD1} = 0.65 \times 10^{-9}$ cm^3 s^{-1} for reaction AD1, taken from Glover et al. (2006), which is a plausible lower limit on the rate coefficient. In run AR2, on the other hand, we use a rate coefficient $k_{\rm AD1} = 5.0 \times 10^{-9}$ cm^3 s^{-1} for reaction AD1, again taken from Glover et al. (2006), which is a plausible upper limit.

In Fig. 20(a), we show how the temperature of the gas evolves in these two runs, as well as in run REF for comparison. It is clear from the figure that the uncertainty in $k_{\rm AD1}$ has only a slight impact on the temperature evolution of the gas. In Fig. 20(b) we show a similar plot of the ratio of the H_3^+ cooling rate to the total cooling rate. Again, the rate coefficient uncertainty has only a small effect. This result is in line with previous work showing that these are unimportant when starting from cold, low ionization initial conditions (Glover et al. 2006). If, instead, we start with hot, ionized gas, then the effect of the uncertainties on the temperature evolution is much greater (Glover & Abel 2008). However, even in this case, the largest effects are seen at densities $n \lesssim 10^4$ cm^{-3}, far below the densities at which H_3^+ could conceivably become important, and so our basic conclusion regarding the unimportance of H_3^+ cooling remains unaffected.

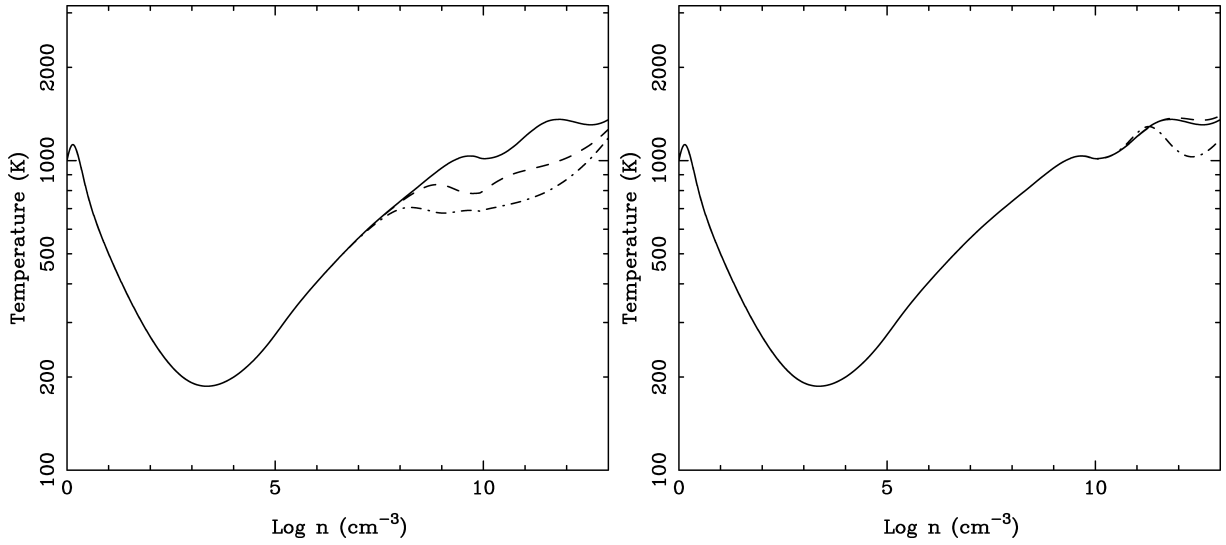

Figure 18. (a) Temperature evolution as a function of density, plotted for runs REF (solid line), 3B1 (dashed line) and 3B2 (dash–dotted line). We use different values for the rate of reaction TB1 in these three runs. In run REF, we use the rate coefficient from Abel et al. (2002), in run 3B1 the rate coefficient from Palla et al. (1983) and in run 3B2 the rate coefficient from Flower & Harris (2007). (b) As (a), but for runs REF (solid line), 3B3 (dashed line) and 3B4 (dash–dotted line). In these runs, the rate of reaction TB2 is varied. In run REF, we use the rate coefficient from Palla et al. (1983), while runs 3B3 and 3B4 use the rate coefficients from Cohen & Westberg (1983) and Flower & Harris (2007), respectively.

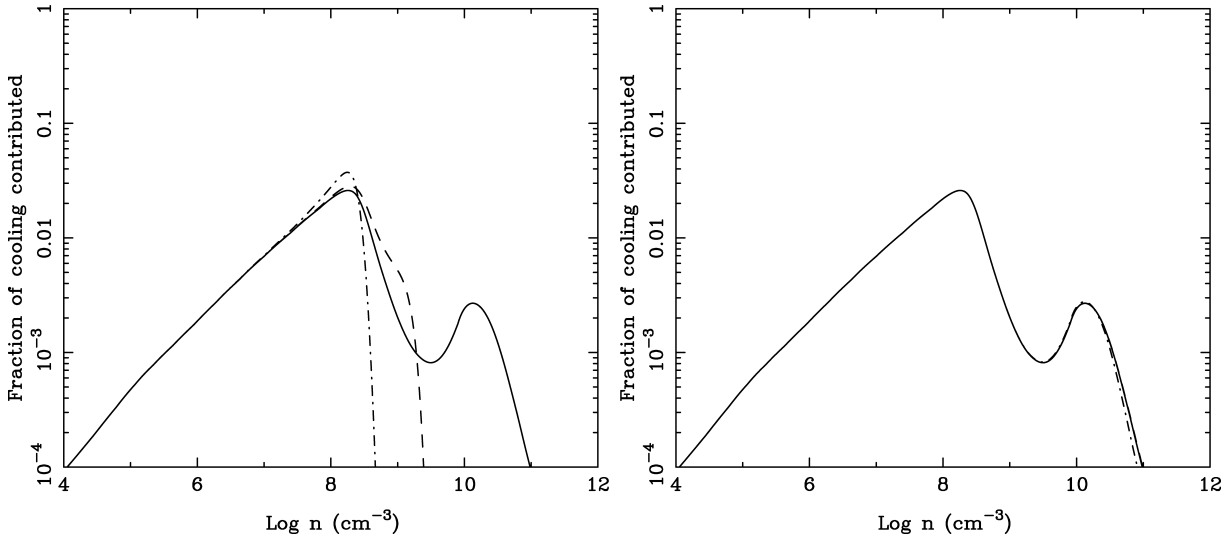

Figure 19. (a) Evolution of the ratio of the H_3^+ cooling rate to the total cooling rate in runs REF, 3B1 and 3B2. (b) As (a), but for runs REF, 3B3 and 3B4.

5.6.4 Reactions RA20 and CD26

Finally, we have investigated the effects of varying the rates of two of the key reactions involved in the LiH_2^+ chemistry: LiH_2^+ formation by radiative association of Li^+ and H_2 (reaction RA20) and the collisional dissociation of LiH_2^+ by H_2 (reaction CD26). As we have already discussed in Section 3.1.11, the rate coefficients for both of these reactions are unknown. In our reference model, we adopted values of $k_{\rm RA20} = 10^{-22}\,{\rm cm^3\,s^{-1}}$ and $k_{\rm CD26} = 1.0 \times 10^{-9}\exp(-3250/T)\ {\rm cm^3\ s^{-1}}$ for the rate coefficients; i.e. a small value for reaction RA20 and a large value for reaction CD26. These choices serve to minimize the role played by LiH_2^+ in the chemical evolution of the gas, and hence we considered them to be the most conservative options in the circumstances. In run LP1, we adopted instead a much larger value for the rate coefficient of reaction RA20, $k_{\rm RA20} = 10^{-17}\,{\rm cm^3\,s^{-1}}$, but kept the same value for $k_{\rm CD26}$ as in our reference model. In run LP2, we used our reference value for $k_{\rm RA20}$, but adopted a much smaller value for the rate coefficient of reaction CD26: $k_{\rm CD26} = 1.0 \times 10^{-13}\exp(-3250/T)\ {\rm cm^3\,s^{-1}}$. Finally, in run LP3, we altered both rate coefficients, using the larger value for $k_{\rm RA20}$ and the smaller for $k_{\rm CD26}$.

In Fig. 21, we show how the contribution of H_3^+ cooling to the total cooling rate varies with density in runs LP1, LP2 and LP3, along with run REF for comparison. It is clear that in runs LP1 and LP2, the behaviour is essentially the same as in our reference run. This can be understood if we consider the time-scale on which Li^+ ions are destroyed by the reaction sequence

$$Li^+ + H_2 \rightarrow LiH_2^+ + \gamma, \qquad (108)$$

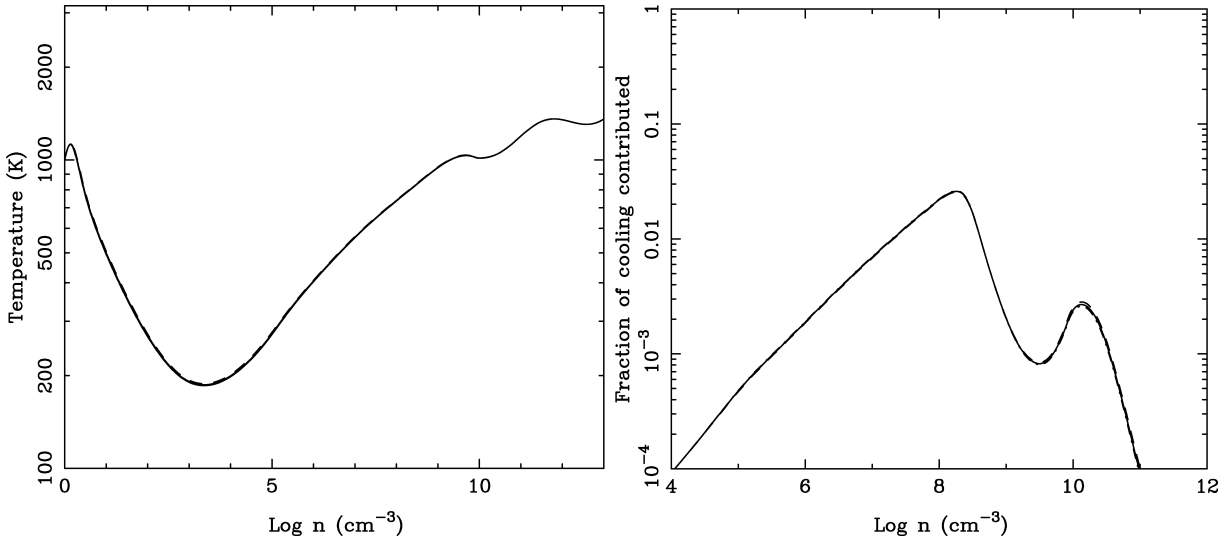

Figure 20. (a) Temperature evolution as a function of density in runs REF (solid line), AR1 (dashed line) and AR2 (dash–dotted line). In run AR1, the value for the rate coefficient of reaction AD1 is chosen so as to minimize H_2 production, while in run AR2, H_2 production is maximized, as discussed in more detail in the text. (b) As (a), but showing how the ratio of the H_3^+ cooling rate to the total cooling rate varies in these three models.

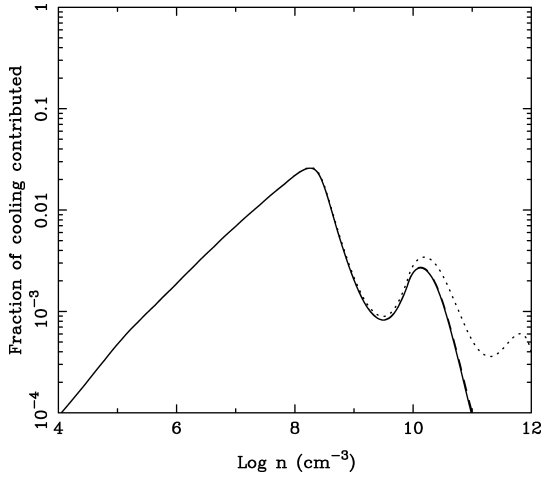

Figure 21. (a) Evolution of the ratio of the H_3^+ cooling rate to the total cooling rate as a function of density in runs REF (solid line), LP1 (dashed line), LP2 (dash–dotted line) and LP3 (dotted line); note that the first three of these lines are not distinguishable in the plot. In run LP1, the rate coefficient for reaction RA20 was increased by a large factor compared to our reference value, while in run LP2, the rate coefficient for reaction CD26 was decreased by a large factor. In run LP3, both changes were made.

followed by

$$LiH_2^+ + e^- \rightarrow \text{products}. \quad (109)$$

This sequence of reactions removes Li^+ on a time-scale

$$t_{\rm loss} = \frac{1}{k_{\rm RA20} n_{\rm H_2} f_{\rm DR}}, \quad (110)$$

where $f_{\rm DR}$ is given by

$$f_{\rm DR} = \frac{(k_{\rm DR19} + k_{\rm DR20} + k_{\rm DR21}) n_{\rm e^-}}{(k_{\rm DR19} + k_{\rm DR20} + k_{\rm DR21}) n_{\rm e^-} + k_{\rm CD26} n_{\rm H_2}}, \quad (111)$$

and represents the fraction of LiH_2^+ ions destroyed by dissociative recombination, rather than by collisional dissociation. In our reference run, at a gas density $n = 10^{10}\,{\rm cm^{-3}}$, the temperature $T \simeq 1000\,{\rm K}$ and the electron abundance $x_{\rm e^-} \simeq 5 \times 10^{-11}$, and hence $f_{\rm DR} \simeq 1.4 \times 10^{-7}$ and $t_{\rm loss} \simeq 1.4 \times 10^{19}\,{\rm s}$, many orders of magnitude longer than the dynamical time-scale. Thus, in our reference run, the LiH_2^+ chemistry has almost no effect on the Li^+ abundance. In run LP1, $k_{\rm RA20}$ is a factor of 10^5 larger than in our reference run, and in run LP2, $k_{\rm CD26}$ is a factor of 10^4 smaller, and so in both runs, $t_{\rm loss}$ is significantly reduced. However, it still remains far greater than the free-fall time-scale, which is $\sim 10^{10}\,{\rm s}$ at this density. Thus, in these runs, the LiH_2^+ chemistry still has almost no effect.

In run LP3, however, where we both increase $k_{\rm RA20}$ and decrease $k_{\rm CD26}$, $t_{\rm loss}$ is reduced by a factor of 10^9, making it $t_{\rm loss} \sim 1.4 \times 10^{10}\,{\rm s}$ at $n = 10^{10}\,{\rm cm^{-3}}$, of the same order of magnitude as the free-fall collapse time. Moreover, as $t_{\rm loss}$ scales with density as $t_{\rm loss} \propto n^{-1}$, while the free-fall time-scales as $t_{\rm ff} \propto n^{-1/2}$, $t_{\rm loss}$ becomes smaller than $t_{\rm ff}$ at densities not very much greater than $10^{10}\,{\rm cm^{-3}}$. Therefore, in this run, the LiH_2^+ chemistry does have a noticeable effect on the Li^+ abundance, reducing it by a factor of roughly 50 in comparison to the reference run by the end of the simulation. This reduction in the Li^+ abundance reduces the number of free electrons available for destroying H_3^+, and so limits the rate at which its abundance declines at very high densities, much as in runs performed without any lithium (cf. Section 5.5.3). Nevertheless, it is clear from Fig. 21 that this change in the lithium chemistry does not change our basic results: H_3^+ cooling remains ineffective, albeit somewhat less ineffective at high densities than in our reference run.

5.7 Sensitivity to the details of the dynamical model

A major limitation of our current study is the highly simplified dynamical treatment that we use in our one-zone model. In all of the calculations that we have presented so far, we have assumed that the gas is collapsing gravitationally at the free-fall rate. However, it is well known from more detailed three-dimensional hydrodynamical models (e.g. Abel et al. 2002; Yoshida et al. 2006) that in realistic primordial clouds, the collapse speed is significantly slower than the free-fall rate, owing to the non-negligible gas pressure. As a result, the gas takes longer to evolve than assumed here, and the

impact of compressional heating is also somewhat smaller. A crude way of taking this into account in a one-zone calculation is to artificially slow down the collapse of the gas. In other words, instead of assuming that the density evolves according to the standard free-fall relationship

$$\frac{\mathrm{d}\rho}{\mathrm{d}t} = \frac{\rho}{t_{\rm ff}}, \tag{112}$$

where $t_{\rm ff}$ is the free-fall time, we can instead assume that

$$\frac{\mathrm{d}\rho}{\mathrm{d}t} = \eta\frac{\rho}{t_{\rm ff}} \tag{113}$$

with $\eta < 1$. The effect of this change is to lengthen the time taken for the gas to collapse to any given density by a factor $(1/\eta)$.

In Fig. 22(a) we show the effect that slowing the collapse in this fashion has on the temperature evolution of the gas by comparing the results of three runs, DYN1, DYN2 and DYN3, with $\eta = 0.6$, $\eta = 0.3$ and $\eta = 0.1$, respectively, with the results of our reference run REF. We see that reducing η leads to a reduction in the temperature of the gas throughout the run, a simple consequence of the reduction in the compressional heating rate. Interestingly, in the $\eta = 0.3$ and 0.1 models, the reduced heating allows the gas to cool to temperatures low enough for chemical fractionation to strongly enhance the HD fraction, allowing HD cooling to further cool the gas down to temperatures close to $T_{\rm CMB}$. The fact that this effect is not seen in more realistic hydrodynamical models (e.g. Bromm et al. 2002) suggests that in these models we are overestimating the extent to which gas pressure slows the collapse, at least at early times.

In Fig. 22(b), we show how reducing η affects the contribution that H_3^+ cooling makes to the total cooling rate. In the $\eta = 0.6$ run, H_3^+ cooling is slightly more effective than in the reference run at densities $10^5 \lesssim n \lesssim 10^8\,\mathrm{cm}^{-3}$. This is a consequence of the slightly lower temperature of the gas at these densities in run DYN1 compared to run REF, which decreases the H_2 cooling rate more than the H_3^+ cooling rate. At lower densities, H_3^+ cooling in run DYN1 is slightly less effective than in run REF, as the lower gas temperature makes HD cooling more effective at these densities in the former run than in the latter. At higher densities, H_3^+ cooling becomes far less effective in run DYN1 than in run REF owing to a more rapid fall-off in the H_3^+ abundance, as illustrated in Fig. 22(c). As in earlier runs, the reason for this rapid fall-off is that the time-scale for the removal of H^+ from the gas by conversion to H_3^+ followed by destruction

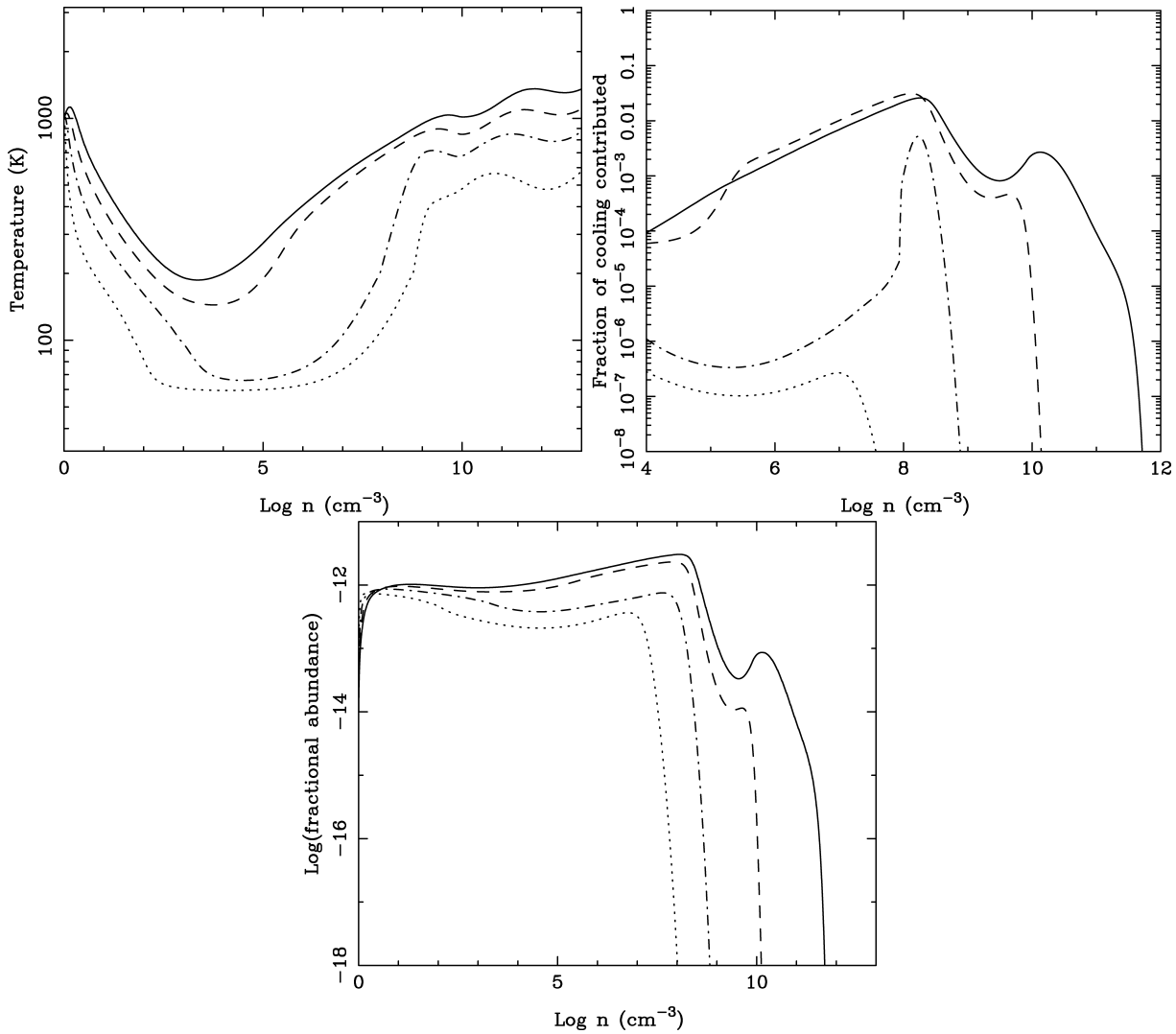

Figure 22. (a) Temperature evolution as a function of density in three runs in which the collapse parameter η was varied. Results are plotted for runs REF (solid line), DYN1 (dashed line), DYN2 (dash–dotted line) and DYN3 (dotted line), which had $\eta = 1.0$, 0.6, 0.3 and 0.1, respectively. (b) As (a), but showing the ratio of the H_3^+ cooling rate to the total cooling rate in the same three runs. (c) As (a), but showing the evolution of the H_3^+ abundance in the three runs.

of the H_3^+ by dissociative recombination, becomes shorter than the dynamical time-scale of the gas at these densities. In most of the runs that we have studied, the high gas temperature at these densities allows reaction TR17 to interfere with this process by converting most of the H_3^+ to H_2^+, following which reaction CT3 restores the original proton to the gas. As we saw in Section 5.1, the effect of this is to lengthen the time required to remove all of the H^+, which delays the precipitous fall-off until $n \sim 10^{11}\,\mathrm{cm}^{-3}$. However, in run DYN1, the lower gas temperature means that reaction TR17 is less effective, and so the delay is much shorter. Moreover, the dynamical time-scale itself is longer. Consequently, the rapid fall-off occurs at a lower density.

A similar kind of behaviour is seen in runs DYN2 and DYN3. However, in these runs the much lower temperature at low densities renders HD cooling dominant for significantly longer, while the lower temperature of the gas at high densities, plus the longer dynamical time-scale, allow the rapid fall-off in the H_3^+ abundance to occur sooner. Consequently, H_3^+ cooling never becomes significant in these runs.

6 CONCLUSIONS

We have examined the contribution that H_3^+ cooling makes to the total cooling rate of gravitationally collapsing primordial gas in a wide range of different models using a newly developed H_3^+ cooling function along with the most detailed model of primordial gas chemistry published to date. Our results demonstrate that in general H_3^+ cooling is not important, although it comes close to being so at densities $n = 10^7$–$10^9\,\mathrm{cm}^{-3}$, contributing at its peak a few per cent of the total amount of cooling. We come to this conclusion despite making several assumptions (regarding the collapse rate of the gas, the formation rate of H_3^+ by radiative association, and the collisional excitation rate of its excited vibrational states) that favour H_3^+ cooling, and thus we have confidence that our conclusion is robust.

As H_3^+ comes so close to being important, it is instructive to examine why it ultimately fails to dominate. This can be ascribed to a combination of two main effects. First, at high densities ($n \gtrsim 10^8\,\mathrm{cm}^{-3}$), the gas temperature becomes high enough to make the endothermic reaction TR17

$$H_3^+ + H \rightarrow H_2^+ + H_2 \qquad (114)$$

the most important H_3^+ destruction mechanism, which significantly suppresses the H_3^+ abundance at these densities. Secondly, the formation rate of H_3^+ is strongly suppressed by the rapid removal of H^+ from the gas at densities $n \gtrsim 10^{11}\,\mathrm{cm}^{-3}$. At these densities, the fractional ionization of the gas is so low that the main loss route for the H^+ is conversion to H_3^+, followed by H_3^+ dissociative recombination, and once the time-scale for H^+ removal via this combination of reactions becomes short compared to the free-fall time, the H^+ abundance decreases by orders of magnitude within a short space of time, effectively switching off the formation of H_3^+. Moreover, destruction of H_3^+ by dissociative recombination remains effective despite the fall-off in x_{H^+} thanks to the contribution of electrons from ionized lithium, Li^+, which for $n > 3 \times 10^8\,\mathrm{cm}^{-3}$ is the most abundant positive ion in the gas.

In our study, the only situation in which we found H_3^+ cooling to be important is if the gas is illuminated by a strong flux of cosmic rays or X-rays. If the incident flux is strong enough to produce an ionization rate $\gtrsim 10^{-18}\,\mathrm{s}^{-1}$ at densities $n \geq 10^{10}\,\mathrm{cm}^{-3}$, then the high-density H_3^+ abundance can be significantly increased, and H_3^+ can even become the dominant coolant. However, the necessary flux of cosmic rays or hard X-rays is difficult to produce in the high-redshift universe. As the estimates in Sections 5.3 and 5.4.2 demonstrate, the required flux is orders of magnitude greater than the size of any plausible extragalactic background, and will only be achieved within gas that is very close to a local source (i.e. within 5–10 pc). However, gas that is this close to a supernova remnant or miniquasar will have been strongly affected by radiative feedback from the progenitor star and so is not a promising place to expect to find ongoing Population III star formation.

Furthermore, even if the ionization rate is high enough to make H_3^+ an important or dominant coolant at high densities, the effect of H_3^+ cooling on the thermal evolution of the gas remains relatively small; the difference it makes to the temperature evolution at $n > 10^8\,\mathrm{cm}^{-3}$ is smaller than the error introduced by the uncertainty in the three-body H_2 formation rate (reaction TB1).

Finally, our model has also allowed us to explore the effects of cooling from the other minor ionic and molecular species present in the gas (e.g. H_2^+, H_2D^+, LiH, etc.). Despite making rather optimistic assumptions regarding the cooling from these species, we find that they are orders of magnitude less effective than H_3^+ at cooling high-density gas, and hence are never significant.

ACKNOWLEDGMENTS

The authors would like to thank P. C. Stancil for useful discussions regarding the rates of reactions involving deuterium, and C. Greene for providing us with an estimate of the LiH_2^+ dissociative recombination rate. DWS was supported in part by the NASA Astronomy and Physics Research and Analysis program and the NSF Astronomy and Astrophysics Grants programme.

REFERENCES

Abel T., Anninos P., Zhang Y., Norman M. L., 1997, New Astron., 2, 181
Abel T., Bryan G. L., Norman M. L., 2000, ApJ, 540, 39
Abel T., Bryan G. L., Norman M. L., 2002, Sci, 295, 93
Abgrall H., Roueff E., 2006, A&A, 445, 361
Abgrall H., Roueff E., Viala Y., 1982, A&AS, 50, 505
Badnell N. R., 2006a, A&A, 447, 389
Badnell N. R., 2006b, ApJS, 167, 334
Barlow S. G., 1984, PhD thesis, Univ. Colorado
Bautista M. A., Badnell N. R., 2007, A&A, 466, 755
Bennett O. J., Dickinson A. S., Leininger T., Gadéa F. X., 2003, MNRAS, 341, 361
Bergin E. A., Plume R., Williams J. P., Myers P. C., 1999, ApJ, 512, 724
Black J. H., 1978, ApJ, 222, 125
Black J. H., 1981, MNRAS, 197, 553
Black J. H., Dalgarno A., 1977, ApJS, 34, 405
Bodo E., Gianturco F. A., Martinazzo R., Raimondi M., 2001, Chem. Phys., 271, 309
Bromm V., Loeb A., 2006, ApJ, 642, 382
Bromm V., Coppi P. S., Larson R. B., 2002, ApJ, 564, 23
Brown P. N., Byrne G. D., Hindmarsh A. C., 1989, SIAM J. Sci. Stat. Comput., 10, 1038
Burton M. G., Hollenbach D. J., Tielens A. G. G. M., 1990, ApJ, 365, 620
Carata L., Orel A. E., Suzor-Weiner A., 1999, Phys. Rev. A, 59, 2804
Cen R., 1992, ApJS, 78, 341
Ciardi B., 2008, in O'Shea B., Heger A., Abel T., eds, First Stars III. Am. Inst. Phys., New York, p. 353
Ciardi B., Ferrara A., 2005, Space Sci. Rev., 116, 625
Clark P. C., Glover S. C. O., Klessen R. S., 2008, ApJ, 672, 757
Clegg R. E. S., 1987, MNRAS, 229, 31P
Cohen N., Westberg K. R., 1983, J. Phys. Chem. Ref. Data, 12, 531
Cojazzi P., Bressan A., Lucchin F., Pantano O., Chavez M., 2000, MNRAS, 315, L51

Croft H., Dickinson A. S., Gadea F. X., 1999, MNRAS, 304, 327
Cyburt R. H., 2004, Phys. Rev. D, 70, 023505
Dalgarno A., Lepp S., 1987, in Vardya M. S., Tarafdar S. P., ed., Astrochemistry. Reidel, Dordrecht, p. 109
Dalgarno A., McDowell M. R. C., 1956, Proc. Phys. Soc. London A, 69, 615
Dalgarno A., Kirby K., Stancil P. C., 1996, ApJ, 458, 397
Dalgarno A., Yan M., liu W., 1999, ApJS, 125, 237
Datz S., Sundström G., Biederman C., Broström L., Danared H., Mannervik S., Mowat J. R., Larsson M., 1995, Phys. Rev. Lett., 74, 896
Defazio P., Petrongolo C., Gamallo P., González M., 2005, J. Chem. Phys., 122, 214303
Dickinson A. S., 2005, J. Phys. B, 38, 4329
Dijkstra M., Haiman Z., Spaans M., 2006, ApJ, 649, 14
Dove J. E., Rusk A. C. M., Cribb P. H., Martin P. G., 1987, ApJ, 318, 379
Draine B. T., Bertoldi F., 1996, ApJ, 468, 269
Dunn G. H., 1968, Phys. Rev., 172, 1
Faure A., Tennyson J., 2003, MNRAS, 340, 468
Ferland G. J., Peterson B. M., Horne K., Welsh W. F., Nahar S. N., 1992, ApJ, 387, 95
Flower D. R., Harris G. J., 2007, MNRAS, 377, 705
Flower D. R., Le Bourlot J., Pineau des Forêts G., Roueff E., 2000, MNRAS, 314, 753
Flower D. R., Pineau des Forêts G., Walmsley C. M., 2004, A&A, 427, 887
Frommhold L., Pickett H. M., 1978, Chem. Phys., 28, 441
Fussen D., Kubach C., 1986, J. Phys. B, 19, L31
Galli D., Palla F., 1998, A&A, 335, 403
Galli D., Palla F., 2002, P&SS, 50, 1197
Gerlich D., 1982, in Lindinger W., Howorka F., Märk T. D., eds, Symposium on Atomic and Surface Physics. Kluwer, Dordrecht, p. 304
Gerlich D., Horning S., 1992, Chem. Rev., 92, 1509
Gianturco F. A., Gori Giorgi P., 1996, ApJ, 479, 560
Glassgold A. E., Langer W. D., 1973, ApJ, 186, 859
Glosík J., Plasil R., Pysanenko A., Novotný O., Hlavenka P., Macko P., Bánó G., 2005, J. Phys.: Conf. Ser., 4, 104
Glosík J. et al., 2008, J. Phys. B., 41, 191001
Glover S. C. O., 2008, in O'Shea B., Heger A., Abel T., eds, First Stars III. Am. Inst. Phys., New York, p. 25
Glover S. C. O., Abel T., 2008, MNRAS, 388, 1627
Glover S. C. O., Brand P. W. J. L., 2001, MNRAS, 321, 385
Glover S. C. O., Brand P. W. J. L., 2003, MNRAS, 340, 210
Glover S. C. O., Jappsen A.-K., 2007, ApJ, 666, 1
Glover S. C. O., Savin D. W., 2006, Phil. Trans. R. Soc. London A, 364, 3107
Glover S. C. O., Savin D. W., Jappsen A.-K., 2006, ApJ, 640, 553
Goldsmith P. F., Langer W. D., 1978, ApJ, 222, 881
Gredel R., Lepp S., Dalgarno A., Herbst E., 1989, ApJ, 347, 289
Guberman S. L., 1994, Phys. Rev. A, 49, R4277
Haiman Z., Rees M., Loeb A., 1997, ApJ, 476, 458; erratum ApJ, 484, 985
Haiman Z., Abel T., Rees M. J., 2000, ApJ, 534, 11
Heger A., Woosley S. E., 2002, ApJ, 567, 532
Hollenbach D., McKee C. F., 1979, ApJS, 41, 555
Huiszoon C., Briels W. J., 1993, Chem. Phys. Lett., 203, 49
Hummer D. G., Storey P. J., 1998, MNRAS, 297, 1073
Huq M. S., Doverspike L. D., Champion R. L., Esaulov V. A., 1982, J. Phys. B, 15, 951
Jacobs T. A., Giedt R. R., Cohen N., 1967, J. Chem. Phys., 47, 54
Jasche J., Ciardi B., Ensslin T. A., 2007, MNRAS, 380, 417
Janev R. K., Langer W. D., Evans K., Post D. E., 1987, Elementary Processes in Hydrogen–Helium Plasmas. Springer-Verlag, Berlin
Johnson J. L., Bromm V., 2006, MNRAS, 366, 247
Juřek M., Špirko V., Kraemer W. P., 1995, Chem. Phys., 193, 287
Karpas Z., Anicich V., Huntress W. T., 1979, J. Chem. Phys., 70, 2877
Karr J. Ph., Hilico L., 2006, J. Phys. B, 39, 2095
Kimura M., Lane N. F., Dalgarno A., Dixson R. G., 1993, ApJ, 405, 801
Kimura M., Dutta C. M., Shimakura N., 1994, ApJ, 430, 435
Kirby K., Dalgarno A., 1978, ApJ, 224, 444
Kokoouline V., Greene C. H., 2003, Phys. Rev. A, 68, 012703
Kraemer W. P., Špirko V., Juřek M., 1995, Chem. Phys. Lett., 236, 177
Krohn S. et al., 2001, Phys. Rev. Lett., 86, 4005
Krstić P. S., 2002, Phys. Rev. A, 66, 042717
Krstić P. S., Janev R. K., 2003, Phys. Rev. A, 67, 022708
Krstić P. S., Janev R. K., Schultz D. R., 2003, J. Phys. B, 36, L249
Kuhlen M., Madau P., 2005, MNRAS, 363, 1069
Larsson M. et al., 1996, A&A, 309, L1
Larsson M., Danared H., Larson Å., Le Padellec A., Peterson J. R., Rosén S., Semaniak J., Strömholm C., 1997, Phys. Rev. Lett., 79, 395
Latter W. B., Black J. H., 1991, ApJ, 372, 161
Launay J. M., Le Dourneuf M., Zeippen C. J., 1991, A&A, 252, 842
Le Teuff Y. H., Millar T. J., Markwick A. J., 2000, A&AS, 146, 157
Lepp S., Shull J. M., 1983, ApJ, 270, 578
Lepp S., Shull J. M., 1984, ApJ, 280, 465
Lepp S. H., Stancil P. C., Dalgarno A., 2002, J. Phys. B, 35, 57
Lenzuni P., Chernoff D. F., Salpeter E. E., 1991, ApJS, 76, 759
Linder F., Janev R. K., Botero J., 1995, in Janev R. K., ed., Atomic and Molecular Processes in Fusion Edge Plasmas. Plenum Press, New York, p. 397
Lipovka A., Núñez-López R., Avila-Reese V., 2005, MNRAS, 361, 850
McCall B. J. et al., 2003, Nat, 422, 500
McCall B. J. et al., 2004, Phys. Rev. A, 70, 052716
Machacek M. E., Bryan G. L., Abel T., 2003, MNRAS, 338, 273
Mac Low M.-M., Shull J. M., 1986, ApJ, 302, 585
Maki H., Susa H., 2004, ApJ, 609, 467
Maki H., Susa H., 2007, PASJ, 59, 787
Martin P. G., Schwarz D. H., Mandy M. E., 1996, ApJ, 461, 265
Martin P. G., Keogh W. J., Mandy M. E., 1998, ApJ, 499, 793
Mielke S. L., Peterson K. A., Schwenke D. W., Garrett B. C., Truhlar D. G., Michael J. V., Su M.-C., Sutherland J. W., 2003, Phys. Rev. Lett., 91, 063201
Mihalas D., Mihalas B. W., 1984, Foundations of Radiation Hydrodynamics. Oxford Univ. Press, New York
Millar T. J., Bennett A., Herbst E., 1989, ApJ, 340, 906
Miller S. et al., 2000, Phil. Trans. R. Soc., 358, 2485
Mizusawa H., Omukai K., Nishi R., 2005, PASJ, 57, 951
Moseley J., Aberth W., Peterson J. R., 1970, Phys. Rev. Lett., 24, 435
Moyano G. E., Collins M. A., 2003, J. Chem. Phys., 119, 5510
Nagakura T., Omukai K., 2005, MNRAS, 364, 1378
Naji A., Olamba K., Chenu J. P., Szücs S., Brouillard F., 1998, J. Phys. B, 31, 4887
Nakamura F., Umemura M., 2002, ApJ, 569, 549
Neale L., Miller S., Tennyson J., 1996, ApJ, 464, 516
Oka T., Epp E., 2004, ApJ, 613, 349
Omukai K., 2000, ApJ, 534, 809
Omukai K., Nishi R., 1998, ApJ, 508, 141
Omukai K., Tsuribe T., Schneider R., Ferrara A., 2005, ApJ, 626, 627
Orel A. E., 1987, J. Chem. Phys., 87, 314
Orel A. E., Schneider I. F., Suzor-Weiner A., 2000, Phil. Trans. R. Soc. London A, 358, 2445
O'Shea B. W., Norman M. L., 2008, ApJ, 673, 14
Osterbrock D. E., 1989, Astrophysics of Gaseous Nebulae and Active Galactic Nuclei. University Science Books, Mill Valley, CA
Palla F., Salpeter E. E., Stahler S. W., 1983, ApJ, 271, 632
Paul W., Lücke B., Schlemmer S., Gerlich D., 1995, Int. J. Mass Spec. Ion Proc., 149, 373
Peart B., Hayton D. A., 1994, J. Phys. B, 27, 2551
Peek J. M., Hashemi-Attar A.-R., Beckel C. L., 1979, J. Chem. Phys., 71, 5382
Pineau des Forêts G., Roueff E., Flower D., 1989, MNRAS, 240, 167
Posen A. G., Dalgarno A., Peek J. M., 1983, At. Data Nucl. Data Tables, 28, 265
Poulaert G., Brouillard F., Claeys W., McGowan J. W., Van Wassenhove G., 1978, J. Phys. B, 11, L671
Prasad S. S., Tarafdar S. P., 1983, ApJ, 267, 603
Ramaker D. E., Peek J. M., 1976, Phys. Rev. A, 13, 58
Ramanlal J., Tennyson J., 2004, MNRAS, 354, 161
Ramsbottom C. A., Bell K. L., Berrington K. A., 1994, J. Phys. B, 27, 2905

Rawlings J. M. C., Drew J. E., Barlow M. J., 1993, MNRAS, 265, 968
Ripamonti E., Abel T., 2004, MNRAS, 348, 1019
Ripamonti E., Haardt F., Ferrara A., Colpi M., 2002, MNRAS, 334, 401
Roberge W. G., Dalgarno A., 1982, ApJ, 255, 489
Roberts H., Herbst E., Millar T. J., 2004, A&A, 424, 905
Sarpal B. K., Tennyson J., 1993, MNRAS, 263, 909
Savin D. W., 2002, ApJ, 566, 599
Savin D. W., Krstic P. S., Haiman Z., Stancil P. C., 2004, ApJ, 606, L167; erratum ApJ, 607, L147
Schneider I. F., Dulieu O., Giusti-Suzor A., Roueff E., 1994, ApJ, 424, 983; erratum ApJ, 486, 580
Schulz G. J., Asundi R. K., 1967, Phys. Rev., 158, 25
Schwenke D. W., 1988, J. Chem. Phys., 89, 2076
Schwenke D. W., 1990, J. Chem. Phys., 92, 7267
Shapiro P. R., Kang H., 1987, ApJ, 318, 32
Shavitt I., 1959, J. Chem. Phys., 31, 1359
Shchekinov Y. A., Vasiliev E. O., 2006, MNRAS, 368, 454
Sidhu K. S., Miller S., Tennyson J., 1992, A&A, 255, 453
Smith D., Španel P., 1993a, Int. J. Mass Spectrom. Ion. Proc., 129, 163
Smith D., Španel P., 1993b, Chem. Phys. Lett., 211, 454
Stacy A., Bromm V., 2007, MNRAS, 382, 229
Stancil P. C., 1994, ApJ, 430, 360
Stancil P. C., Dalgarno A., 1997a, ApJ, 479, 543
Stancil P. C., Dalgarno A., 1997b, ApJ, 490, 76
Stancil P. C., Dalgarno A., 1998, Faraday Discuss., 109, 61
Stancil P. C., Zygelman B., 1996, ApJ, 472, 102
Stancil P. C., Babb J. F., Dalgarno A., 1993, ApJ, 414, 672
Stancil P. C., Lepp S., Dalgarno A., 1996, ApJ, 458, 401
Stancil P. C., Lepp S., Dalgarno A., 1998, ApJ, 509, 1
Sternberg A., Dalgarno A., Lepp S., 1987, ApJ, 320, 676
Stromhölm C., Schneider I. F., Sundström G. et al., 1995, Phys. Rev. A, 52, R4320
Suchkov A. A., Shchekinov Y. A., 1977, Sov. Astron. Lett., 3, 297
Suchkov A. A., Shchekinov Y. A., 1978, Sov. Astron. Lett., 4, 164
Sundström G. et al., 1994, Sci, 263, 785
Susa H., 2007, ApJ, 659, 908
Tegmark M., Silk J., Rees M., Blanchard A., Abel T., Palla F., 1997, ApJ, 474, 1
Thomas R. D. et al., 2006, in Proc. NASA LAW 2006. NASA Ames, California, p. 268
Trevisan C. S., Tennyson J., 2002a, Plasma Phys. Control. Fusion, 44, 1263
Trevisan C. S., Tennyson J., 2002b, Plasma Phys. Control. Fusion, 44, 2217
van der Tak F. F. S., van Dishoeck E. F., 2000, A&A, 358, 79
van Dishoeck E. F., 1988, in Millar T. J., Williams D. A., eds, Rate Coefficients in Astrochemistry. Kluwer, Dordrecht, p. 49
Verner D. A., Ferland G. J., 1996, ApJS, 103, 467
Voronov G. S., 1997, At. Data Nucl. Data Tables, 65, 1
Walkauskas L. P., Kaufman F., 1975, Symp. Int. Combust. Proc., 15, 691
Walmsley C. M., Flower D. R., Pineau des Forêts G., 2004, A&A, 418, 1035
Wang J. G., Stancil P. C., 2002, Phys. Scr., T96, 72
Whalen D., Abel T., Norman M. L., 2004, ApJ, 610, 14
Wise J. H., Abel T., 2007, ApJ, 671, 1559
Wishart A. W., 1979, MNRAS, 187, 59P
Wolniewicz L., Simbotin I., Dalgarno A., 1998, ApJS, 115, 293
Wrathmall S. A., Flower D. R., 2007, J. Phys. B, 40, 3221
Wrathmall S. A., Gusdorf A., Flower D. R., 2007, MNRAS, 382, 133
Wutte D., Janev R. K., Aumayr F., Schneider M., Schweinzer J., Smith J. J., Winter H. P., 1997, At. Data Nucl. Data Tables, 65, 155
Xu Y., Fabrikant I. I., 2001, Appl. Phys. Lett., 78, 2598
Yan M., Sadeghpour H. R., Dalgarno A., 1998, ApJ, 496, 1044
Yoshida N., Abel T., Hernquist L., Sugiyama N., 2003, ApJ, 592, 645
Yoshida N., Omukai K., Hernquist L., Abel T., 2006, ApJ, 652, 6
Yoshida N., Oh S. P., Kitayama T., Hernquist L., 2007, ApJ, 663, 687
Zemke W. T., Stwalley W. C., 1980, J. Chem. Phys., 73, 5584
Zygelman B., Dalgarno A., Kimura M., Lane N. F., 1989, Phys. Rev. A, 40, 2340
Zygelman B., Stancil P. C., Dalgarno A., 1998, ApJ, 508, 151

APPENDIX A: CHEMICAL NETWORK

In Tables A1–A14 we list the chemical reactions included in our model of primordial gas, along with the rate coefficients adopted and the references from which these rate coefficients were taken. Some of these reactions are discussed in more detail in Section 3.1. In these tables, T is the gas temperature in K, $T_3 = T/300$ K, and T_e is the gas temperature in units of eV. The full versions of the tables are provided as Supporting Information to the online version of this article.

Table A1. Chemical processes: collisional ionization (CI).

No.	Reaction	Rate coefficient ($cm^3\ s^{-1}$)	Reference
CI1	$H + e^- \rightarrow H^+ + e^- + e^-$	$k_{CI1} = \exp[-3.271\,396\,786 \times 10^1 + 1.353\,655\,60 \times 10^1 \ln T_e - 5.739\,328\,75 \times 10^0 (\ln T_e)^2 + 1.563\,154\,98 \times 10^0 (\ln T_e)^3 - 2.877\,056\,00 \times 10^{-1} (\ln T_e)^4 + 3.482\,559\,77 \times 10^{-2} (\ln T_e)^5 - 2.631\,976\,17 \times 10^{-3} (\ln T_e)^6 + 1.119\,543\,95 \times 10^{-4} (\ln T_e)^7 - 2.039\,149\,85 \times 10^{-6} (\ln T_e)^8]$	1
–	–	–	–

Note: T is the gas temperature in K, $T_3 = T/300$ K and T_e is the gas temperature in eV.
References: 1 – Janev et al. (1987); 2 – Voronov (1997).

Table A2. Chemical processes: photorecombination (PR).

No.	Reaction	Rate coefficient ($cm^3\ s^{-1}$)	Notes	Reference
PR1	$H^+ + e^- \rightarrow H + \gamma$	$k_{PR1} = 2.753 \times 10^{-14} \left(\frac{315\,614}{T}\right)^{1.500} \left[1.0 + \left(\frac{115\,188}{T}\right)^{0.407}\right]^{-2.242}$		1
PR2	$D^+ + e^- \rightarrow D + \gamma$	$k_{PR2} = k_{PR1}$		1
–	–	–	–	–

Note: T is the gas temperature in K. Note that the recently revised values for PR1 and for the radiative recombination portions of PR3 and PR4 presented by Badnell (2006b) do not differ from the older rate coefficients quoted here by more than a couple of per cent at the temperatures of interest in this study.
References: 1 – Ferland et al. (1992); 2 – Hummer & Storey (1998); 3 – Badnell (2006a); 4 – Verner & Ferland (1996); 5 – Bautista & Badnell (2007).

Table A3. Chemical processes: dissociative recombination (DR).

No.	Reaction	Rate coefficient ($cm^3\ s^{-1}$)	Notes	Reference
DR1	$H_2^+ + e^- \rightarrow H + H$	$k_{DR1} = 1.0 \times 10^{-8}$	$T \leq 617\,K$	1
		$= 1.32 \times 10^{-6} T^{-0.76}$	$T > 617\,K$	
DR2	$HD^+ + e^- \rightarrow H + D$	$k_{DR2} = 7.2 \times 10^{-8} T^{-0.5}$		2
DR3	$D_2^+ + e^- \rightarrow D + D$	$k_{DR3} = 3.4 \times 10^{-9} T_3^{-0.4}$		3
–	–	–	–	–

Note: T is the gas temperature in K and $T_3 = T/300\,K$.
References: 1 – Schneider et al. (1994); 2 – Stromhölm et al. (1995); 3 – Walmsley et al. (2004); 4 – McCall et al. (2004); 5 – Larsson et al. (1996); 6 – Roberts, Herbst & Millar (2004), based on Larsson et al. (1996); 7 – Larsson et al. (1997); 8 – Guberman (1994); 9 – Stancil et al. (1998), based on Guberman (1994); 10 – Carata, Orel & Suzor-Weiner (1999); 11 – Krohn et al. (2001); 12 – same as corresponding H reaction; 13 – Thomas et al. (2006), C. Greene (private communication).

Table A4. Chemical processes: charge transfer (CT).

No.	Reaction	Rate coefficient ($cm^3\ s^{-1}$)	Notes	Reference
CT1	$H + D^+ \rightarrow D + H^+$	$k_{CT1} = 2.06 \times 10^{-10} T^{0.396} \exp(-\frac{33}{T})$		1
		$+ 2.03 \times 10^{-9}\ T^{-0.332}$		
CT2	$H + D^- \rightarrow D + H^-$	$k_{CT2} = 6.4 \times 10^{-9}\ T_3^{0.41}$		2
CT3	$H + H_2^+ \rightarrow H_2 + H^+$	$k_{CT3} = 6.4 \times 10^{-10}$		3
–	–	–	–	–

Note: T is the gas temperature in K and $T_3 = T/300\,K$.
References: 1 – Savin (2002); 2 – Dalgarno & McDowell (1956), scaled by D reduced mass; 3 – Karpas, Anicich & Huntress (1979); 4 – same as corresponding H reaction; 5 – Zygelman et al. (1989); 6 – Estimate by Stancil et al. (1998), based on Stancil, Babb & Dalgarno (1993); 7 – Stancil et al. (1996); 8 – Zygelman et al. (1989), scaled by D reduced mass; 9 – As reference 6, but scaled by D reduced mass; 10 – Savin et al. (2004); 11 – Barlow (1984); 12 – estimate, based on low-energy extrapolation of cross-section in Wutte et al. (1997); 13 – total rate coefficient from Barlow (1984), branching ratios from Pineau des Forêts, Roueff & Flower (1989); 14 – Walmsley et al. (2004); 15 – Kimura et al. (1993); 16 – Kimura, Dutta & Shimakura (1994); 17 – Stancil & Zygelman (1996); 18 – Kimura et al. (1994), scaled by D reduced mass; 19 – Stancil & Zygelman (1996), scaled by D reduced mass; 20 – from detailed balance applied to inverse reaction; 21 – Bodo et al. (2001).

Table A5. Chemical processes: radiative attachment and radiative association (RA).

No.	Reaction	Rate coefficient ($cm^3\ s^{-1}$)	Notes	Reference
RA1	$H + e^- \rightarrow H^- + \gamma$	$k_{RA1} = \mathrm{dex}[-17.845 + 0.762 \log T + 0.1523(\log T)^2 - 0.032\,74(\log T)^3]$	$T \leq 6000\,K$	1
		$= \mathrm{dex}[-16.420 + 0.1998(\log T)^2 - 5.447 \times 10^{-3}(\log T)^4 + 4.0415 \times 10^{-5}(\log T)^6]$	$T > 6000\,K$	
RA2	$D + e^- \rightarrow D^- + \gamma$	$k_{RA2} = k_{RA1}$		1
–	–	–	–	–

Note: T is the gas temperature in K and $T_3 = T/300\,K$.
References: 1 – Wishart (1979); 2 – Ramaker & Peek (1976); 3 – Ramaker & Peek (1976) and Frommhold & Pickett (1978), scaled by D reduced mass; 4 – Dickinson (2005); 5 – Dalgarno & McDowell (1956); 6 – same as corresponding H reaction, but scaled by D reduced mass; 7 – Kraemer, Špirko & Juřek (1995); 8 – Dalgarno et al. (1996),Gianturco & Gori Giorgi (1996); 9 – Stancil et al. (1996), scaled by D reduced mass; 10 – Gerlich & Horning (1992); 11 – estimate, based on Gerlich & Horning (1992): highly uncertain; 12 – estimate, see also Section 3.1.11; 13 – Juřek, Špirko & Kraemer (1995); 14 – Stancil et al. (1993); 15 – Ramsbottom, Bell & Berrington (1994); 16 – Dalgarno et al. (1996); 17 – Bennett et al. (2003).

Table A6. Chemical processes: associative detachment, dissociative attachment and associative ionization (AD).

No.	Reaction	Rate coefficient ($cm^3\ s^{-1}$)	Notes	Reference
AD1	$H + H^- \rightarrow H_2 + e^-$	$k_{AD1} = 1.5 \times 10^{-9} T_3^{-0.1}$		1
AD2	$D + H^- \rightarrow HD + e^-$	$k_{AD2} = 1.5 \times 10^{-9} T_3^{-0.1}$		2
AD3	$H + D^- \rightarrow HD + e^-$	$k_{AD3} = 1.5 \times 10^{-9} T_3^{-0.1}$		2
–	–	–	–	–

Note: T is the gas temperature in K and $T_3 = T/300\,K$.
References: 1 – Launay et al. (1991); 2 – same as corresponding H reaction, but scaled by D reduced mass; 3 – Schulz & Asundi (1967); 4 – Xu & Fabrikant (2001); 5 – Poulaert et al. (1978); 6 – Naji et al. (1998); 7 – Stancil et al. (1996).

Table A7. Chemical processes: collisional detachment and collisional dissociation (CD).

No.	Reaction	Rate coefficient ($cm^3\ s^{-1}$)	Notes	Reference
CD1	$H^- + e^- \rightarrow H + e^- + e^-$	$k_{CD1} = \exp[-1.801\,849\,334 \times 10^1 + 2.360\,852\,20 \times 10^0 \ln T_e - 2.827\,443\,00 \times 10^{-1} (\ln T_e)^2 + 1.623\,316\,64 \times 10^{-2} (\ln T_e)^3 - 3.365\,012\,03 \times 10^{-2} (\ln T_e)^4 + 1.178\,329\,78 \times 10^{-2} (\ln T_e)^5 - 1.656\,194\,70 \times 10^{-3} (\ln T_e)^6 + 1.068\,275\,20 \times 10^{-4} (\ln T_e)^7 - 2.631\,285\,81 \times 10^{-6} (\ln T_e)^8]$		1
–	–	–	–	–

Note: T is the gas temperature in K and T_e is the gas temperature in eV. K is the equilibrium constant relating reactions TB1 and CD9, and reactions TB2 and CD10; its value is given in Section 3.1.5.
References: 1 – Janev et al. (1987); 2 – assumed same as corresponding H reaction; 3 – Huq et al. (1982); 4 – same as corresponding H reaction, but scaled by D reduced mass; 5 – Mac Low & Shull (1986); 6 – determined from three-body rate coefficient by detailed balance (see Section 3.1.7); 7 – Martin, Keogh & Mandy (1998); 8 – Dove et al. (1987); 9 – determined from the Walkauskas & Kaufman (1975) rate coefficient for reaction TB3 by detailed balance; 10 – Trevisan & Tennyson (2002a); 11 – Trevisan & Tennyson (2002b); 13 – estimate, see also Section 3.1.11.

Table A8. Chemical processes: mutual neutralization (MN).

No.	Reaction	Rate coefficient ($cm^3\ s^{-1}$)	Reference
MN1	$H^+ + H^- \rightarrow H + H$	$k_{MN1} = 2.4 \times 10^{-6} T^{-1/2}(1.0 + 5.0 \times 10^{-5} T)$	1
MN2	$D^+ + H^- \rightarrow D + H$	$k_{MN2} = 1.1 \times k_{MN1}$	2
MN3	$H^+ + D^- \rightarrow D + H$	$k_{MN3} = 1.1 \times k_{MN1}$	2
–	–	–	–

Note: T is the gas temperature in K and $T_3 = T/300$ K. Some of the mutual neutralization reactions listed here also include dissociation or transfer in the process.
References: 1 – Croft et al. (1999); 2 – same as corresponding H reaction, but scaled by D reduced mass; 3 – Dalgarno & Lepp (1987); 4 – Dalgarno & McDowell (1956); 5 – Le Teuff et al. (2000); 6 – same as 2, with the additional assumption of equally probable outcomes; 7 – Peart & Hayton (1994).

Table A9. Chemical processes: three-body association (TB).

No.	Reaction	Rate coefficient ($cm^6\ s^{-1}$)	Reference
TB1	$H + H + H \rightarrow H_2 + H$	See Section 3.1.7	–
TB2	$H + H + H_2 \rightarrow H_2 + H_2$	See Section 3.1.7	–
TB3	$H + H + He \rightarrow H_2 + He$	$k_{TB3} = 6.9 \times 10^{-32} T^{-0.4}$	1
–	–	–	–

Note: T is the gas temperature in K.
References: 1 – Walkauskas & Kaufman (1975); 2 – same as corresponding H reaction; 3 – Krstić, Janev & Schultz (2003); 4 – estimate; 5 – Gerlich & Horning (1992); 6 – Mizusawa et al. (2005).

Table A10. Chemical processes: isotopic exchange (IX).

No.	Reaction	Rate coefficient ($cm^3\ s^{-1}$)	Notes	Reference
IX1	$H_2^+ + D \rightarrow HD^+ + H$	$k_{IX1} = 1.07 \times 10^{-9} T_3^{0.062} \exp(-\frac{T}{41\,400})$		1
IX2	$H_2^+ + D \rightarrow HD + H^+$	$k_{IX2} = 1.0 \times 10^{-9}$		2
IX3	$HD^+ + H \rightarrow H_2^+ + D$	$k_{IX3} = 1.0 \times 10^{-9} \exp\left(-\frac{154}{T}\right)$		3
–	–	–	–	–

Note: T is the gas temperature in K and $T_3 = T/300$ K.
References: 1 – Linder, Janev & Botero (1995); 2 – estimate; 3 – Dalgarno & McDowell (1956), scaled as in Stancil et al. (1998); 4 – Walmsley et al. (2004); 5 – Gerlich (1982); 6 – our fits to cross-sections from Wang & Stancil (2002); 7 – our fits to Mielke et al. (2003); 8 – Shavitt (1959); 9 – Millar, Bennett & Herbst (1989); 10 – Pineau des Forêts et al. (1989); 11 – Moyano & Collins (2003); 12 – derived from forward reaction, using equilibrium constant from Ramanlal & Tennyson (2004); 13 – Flower, Pineau des Forêts & Walmsley (2004); 14 – derived from inverse reaction in Walmsley et al. (2004).

Table A11. Chemical processes: transfer reactions (TR).

No.	Reaction	Rate coefficient ($cm^3\ s^{-1}$)	Reference
TR1	$H_2^+ + H_2 \rightarrow H_3^+ + H$	$k_{TR1} = 2.24 \times 10^{-9} T_3^{0.042} \exp(-\frac{T}{46\,600})$	1
TR2	$H_2^+ + HD \rightarrow H_3^+ + D$	$k_{TR2} = 1.05 \times 10^{-9}$	2
TR3	$H_2^+ + HD \rightarrow H_2D^+ + H$	$k_{TR3} = 1.05 \times 10^{-9}$	2
–	–	–	–

Note: T is the gas temperature in K and $T_3 = T/300$ K.
References: 1 – Linder et al. (1995); 2 – Stancil et al. (1998); 3 – Walmsley et al. (2004); 4 – Sidhu, Miller & Tennyson (1992); 5 – estimate, based on Sidhu et al. (1992); 6 – Black (1978); 7 – Stancil et al. (1998), based on Black (1978); 8 – estimate, based on Black (1978); 9 – Linder et al. (1995), scaled as in Stancil et al. (1998); 10 – estimate, based on Stancil et al. (1998); 11 – same as corresponding H reaction, but scaled by D reduced mass; 12 – Stancil et al. (1996); 13 – Stancil et al. (1998), based on corresponding H reaction in Stancil et al. (1996); 14 – estimate, based on Stancil et al. (1996); 15 – Bodo et al. (2001); 16 – same as corresponding H reaction; 17 – Defazio et al. (2005).

Table A12. Chemical processes: background radiation induced photodetachment, photodissociation and photoionization (BP).

No.	Reaction	Rate (J_{21}^{-1} s^{-1})	Reference
BP1	$H^- + \gamma \rightarrow H + e^-$	$R_{BP1} = 1.36 \times 10^{-11}$	1
BP2	$D^- + \gamma \rightarrow D + e^-$	$R_{BP2} = 1.36 \times 10^{-11}$	2
BP3	$H_2^+ + \gamma \rightarrow H + H^+$	$R_{BP3} = 4.11 \times 10^{-12}$	3
–	–	–	–

Note: γ represents a photon from the external background radiation field. The listed reaction rates were computed assuming that this background has the spectrum of a 10^5 K diluted blackbody, cut-off above $h\nu = 13.6$ eV, as described in Section 3. With this spectrum, reactions with threshold energies greater than 13.6 eV do not occur and are not listed in the table. f_{sh,H_2} and $f_{sh,HD}$ are the self-shielding factors for H_2 and HD photodissociation, respectively (see e.g. Glover & Jappsen 2007). Note that in this paper, we consider only the limiting cases $f_{sh,H_2} = f_{sh,HD} = 0$ and $f_{sh,H_2} = f_{sh,HD} = 1$.
References: 1 – Wishart (1979); 2 – assumed same as for corresponding H reaction; 3 – Dunn (1968); 4 – total rate assumed same as for corresponding H reaction, individual outcomes assumed equally probable; 5 – Draine & Bertoldi (1996); 6 – Abgrall & Roueff (2006); 7 – estimate; 8 – van Dishoeck (1988); 9 – estimate, based on van Dishoeck (1988); 10 – Roberge & Dalgarno (1982); 11 – Stancil (1994); 12 – Verner & Ferland (1996); 13 – Galli & Palla (1998); 14 – Kirby & Dalgarno (1978).

Table A13. Chemical processes: cosmic ray ionization (CR).

No.	Process	Rate (ζ_i/ζ_H)	Reference
CR1	$H + CR \rightarrow H^+ + e^-$	1.0	–
CR2	$H_2 + CR \rightarrow H_2^+ + e^-$	2.09	1
CR3	$H_2 + CR \rightarrow H + H^+ + e^-$	0.09	1
–	–	–	–

Note: CR represents a cosmic ray. ζ_H, the cosmic ray ionization rate of atomic hydrogen, is an adjustable parameter in our models.
References: 1 – Walmsley et al. (2004); 2 – assumed same as corresponding H process.

Table A14. Chemical processes: cosmic ray induced photodetachment, photodissociation and photoionization (CP).

No.	Reaction	σ_{X,eff,H_2} (Mb)	$\sigma_{X,eff,H}$ (Mb)	Reference
CP1	$H^- + \gamma_{cr} \rightarrow H + e^-$	5.0	5.8	1
CP2	$D^- + \gamma_{cr} \rightarrow D + e^-$	5.0	5.8	2
CP3	$H_2^+ + \gamma_{cr} \rightarrow H + H^+$	5.0	6.6	3
–	–	–	–	–

Note: γ_{cr} represents a secondary photon, produced by cosmic ray induced excitation of H or H_2, as described in Section 3.3. The references listed are the sources from which we have taken our photodissociation or photoionization cross-sections. The emission probabilities $P_{H_2}(\upsilon)$ used to calculate σ_{X,eff,H_2} are rough estimates based on the emission spectra given in Sternberg et al. (1987) and are likely accurate only to within a factor of a few.
References: 1 – Wishart (1979); 2 – assumed same as for corresponding H reaction; 3 – Dunn (1968); 4 – Verner & Ferland (1996); 5 – order of magnitude estimate; 6 – estimate, based on Stancil (1994); 7 – rough estimate, based on thermal rate in Galli & Palla (1998).

SUPPORTING INFORMATION

Additional Supporting Information may be found in the online version of this article.

Table A1. Chemical processes: collisional ionization (CI).
Table A2. Chemical processes: photorecombination (PR).
Table A3. Chemical processes: dissociative recombination (DR).
Table A4. Chemical processes: charge transfer (CT).
Table A5. Chemical processes: radiative attachment and radiative association (RA).
Table A6. Chemical processes: associative detachment, dissociative attachment and associative ionization (AD).
Table A7. Chemical processes: collisional detachment and collisional dissociation (CD).
Table A8. Chemical processes: mutual neutralization (MN).
Table A9. Chemical processes: three-body association (TB).
Table A10. Chemical processes: isotopic exchange (IX).
Table A11. Chemical processes: transfer reactions (TR).
Table A12. Chemical processes: background radiation induced photodetachment, photodissociation and photoionization (BP).
Table A13. Chemical processes: cosmic ray ionization (CR).
Table A14. Chemical processes: cosmic ray induced photodetachment, photodissociation and photoionization (CP).

Please note: Wiley-Blackwell are not responsible for the content or functionality of any supporting materials supplied by the authors. Any queries (other than missing material) should be directed to the corresponding author for the article.

This paper has been typeset from a TEX/LATEX file prepared by the author.